Energy & Environmental Science

Accepted Manuscript

This article can be cited before page numbers have been issued, to do this please use: A. R. B. Mohd Yusoff, M. Vasilopoulou, D. Georgiadou, L. C. Palilis, A. Abate and M. K. Nazeeruddin, *Energy Environ. Sci.*, 2021, DOI: 10.1039/D1EE00062D.

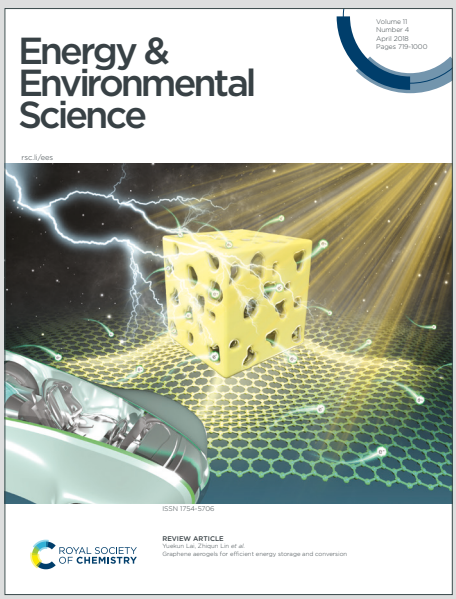

ROYAL SOCIETY OF CHEMISTRY

rsc.li/ees

View Article Online
DOI: 10.1039/D1EE00062D

Passivation and process engineering approaches of halide perovskite films for high efficiency and stability perovskite solar cells

Abd. Rashid bin Mohd Yusoff,[1,*] Maria Vasilopoulou,[2,*] Dimitra G. Georgiadou,[3,4] Leonidas C. Palilis,[5] Antonio Abate,[6,7,8,*] Mohammad Khaja Nazeeruddin[9,*]

[1]Department of Chemical Engineering, Pohang University of Science and Technology (POSTECH), Pohang, Gyeongbuk 37673, Republic of Korea

[2]Institute of Nanoscience and Nanotechnology, National Center for Scientific Research Demokritos, 15341 Agia Paraskevi, Attica, Greece

[3]Centre for Electronics Frontiers, Zepler Institute for Photonics and Nanoelectronics, University of Southampton, SO17 1BJ Southampton, United Kingdom

[4]Department of Physics, Imperial College London, SW7 2AZ London, United Kingdom

[5]Department of Physics, University of Patras, 26504 Patras, Greece

[6]Helmholtz-Zentrum Berlin für Materialien und Energie, Kekuléstraße 5, 12489 Berlin, Germany

[7]Department of Chemical, Materials and Production Engineering, University of Naples Federico II, Piazzale Tecchio 80, 80125 Fuorigrotta, Italy

[8]State Key Laboratory of Photocatalysis on Energy and Environment, Institute of Advanced Energy Materials, Fuzhou University, Fuzhou, Fujian, 350002 China

[9]Group for Molecular Engineering of Functional Mazterials, Institute of Chemical Sciences and Engineering, École Polytechnique Fédérale de Lausanne (EPFL), Rue de l'Industrie 17, CH-1951 Sion, Switzerland

View Article Online
DOI: 10.1039/D1EE00062D

Keywords: perovskite solar cells, high efficiency, environmental stability, thermal stability, reproducibility, molecular passivation of defect states, morphology and crystallinity control, additives, solvent annealing and solvent engineering, capping layer

Abstract The surface, interfaces and grain boundaries of a halide perovskite film carry critical tasks in achieving as well as maintaining high solar cell performance due to the inherently defective nature across their regime. Passivating materials and felicitous process engineering approaches have significant ramifications in the resultant perovskite film, and solar cell's overall macroscale properties dictate structural and optoelectronic properties. Herein, we exploit a vast number of defect engineering approaches aiming to increase the performance and the stability of perovskite solar cells, especially against humidity, continuous illumination, and heat. This review begins with the perovskite materials' fundamental structural properties followed by the advances made to induce higher stabilization in perovskite solar cells by fine-tuning material chemistry design parameters. We continue by summarizing defect passivation strategies based on molecular entities' application, including suitable functional groups that enable sufficient surface, bulk and grain boundaries passivation, morphology, and crystallinity control. We also present methods to control the density of defects through the variation of processing conditions, solvent annealing and solvent engineering approaches, gas-assisted deposition methods, use of self-assembled monolayers, as well as colloidal engineering and coordination surface chemistry. Finally, we give our perspective on how a combined understanding of material chemistry aspects and passivation mechanisms will further develop high-efficiency and stability perovskite solar cells.

View Article Online
DOI: 10.1039/D1EE00062D

1. Introduction

The quest to develop alternative renewable energy sources that can deliver high electrical power at low fabrication cost has fuelled the research of emerging photovoltaic (PV) technologies, which bear the potential to disrupt the incumbent silicon (Si) PV market. Solar cells based on organic-inorganic halide perovskite absorbers (refered to as perovskite solar cells, PSCs) are among the most promising emerging PV technologies.[1-4] These cells benefit from superior features exhibited by the halide perovskite absorber, such as exceptionally high light absorption coefficient up to 10^5 cm^{-1} and ultra-long electron-hole diffusion length of the order of few micrometres (μm) in polycrystalline films.[5,6] Remarkably, within the last 10 years, their power conversion efficiency (PCE) has rapidly increased from 3.8% in 2009,[7] to 25.5% in single-junction and 29.5% in silicon/perovskite tandem cells.[8] This breakthrough became possible thanks to pioneering works by the Nam Gyu Park[9] and Snaith[10] groups in Korea and the UK, respectively, reporting almost simultaneously in 2012 solid-state PSCs with efficiencies exceeding 9%.

Apart from their performance merits, PSCs have manufacturing advantages. They can be processed using low-cost precursor materials and solution-based fabrication methods compatible with flexible substrates. Together with their semi-transparency, they hold promise for entering the PV market soon. However, the major hurdle still to be surpassed is the concomitant increase of performance and long-term stability, with the latter being a vital issue for commercialisation. In particular, PSCs tend to degrade when exposed to environmental oxygen and moisture, heating and light illumination, and mechanical stress.[9-20] The degradation of PSCs in a humid environment originates from the amine salt precursors' hygroscopic nature, such as methyl ammonium or formamidinium halides, used for the perovskite preparation.[21] These salts facilitate the adsorption of water molecules from the surrounding environment, resulting in hydrate products. On the other

View Article Online
DOI: 10.1039/D1EE00062D

hand, when perovskite films are exposed to light, relatively weak bonds in the perovskite layer can be broken to produce halide defects, such as halide vacancy-interstitial pairs.[22] The latter enable halides to either migrate or react with molecular oxygen forming reactive superoxides.[23] Moreover, heat can vaporise halide species that migrate towards metal contacts, while exposure to light increases mobility.[24] Halide reaction with metals constitutes an additional PSC degradation factor.[25] Perovskites may also undergo severe delamination due to stress caused by temperature changes because of their low fracture energy (lower than 1 J m^{-2}) and thermal expansion coefficient much larger than that of the commonly used glass substrates.[26] All factors above contribute to severe efficiency loss in PSCs. Addressing each of them individually or, more importantly, simultaneously is expected to lead to excellent and stable solar cells performance.

Efficiency stabilization has been heavily investigated in recent years, as proven by many research articles summarised in recently published reviews[6,9-21]. Device encapsulation sufficiently prevents environmental-induced degradation of the perovskite absorber or the electrodes. Replacement of metal electrodes with either carbon or indium tin oxide (ITO) can provide non-reactive alternatives that create a barrier for moisture and oxygen penetration while also preventing volatile components in the perovskite layer from escaping to the environment. Addressing the intrinsic perovskite instability is among the most critical factors determining whether PSCs will find their way to practical applications. To this end, a huge amount of strategies already exists. These include sophisticated interface engineering, compositional tuning of the absorber, and passivation of bulk, surface, and grain boundary defects.[27-32] The latter, when combined with regulation of morphology and crystallinity of the fabricated perovskite films, aim to impede or even prevent the formation of ionic defects, the migration of which is detrimental to device stability. Various passivation approaches, based on the application of functional molecules, post-

View Article Online
DOI: 10.1039/D1EE00062D

deposition treatments and colloidal chemistry engineering, have been recently introduced, as they represent effective and easy to implement methodologies for the simultaneous enhancement of the device efficiency and stability.[33-36]

This review summarises advances made with perovskite materials, thin films, and solar cells to achieve a higher level of device performance and efficiency stabilization. We explore fine-tuning material chemistry aspects through passivation approaches and routes towards optimizing the morphology and crystallinity of the deposited films. The most successful methodologies include surface, interface and additive engineering, the variation of processing conditions, solvent annealing and solvent engineering approaches, gas-assisted deposition methods, the use of self-assembled monolayers, the formation of wide-bandgap perovskite capping layers, colloidal engineering and coordination surface chemistry. The remaining challenges and additional limitations that need to be addressed before the PSCs enter the PV market are also discussed.

2. Fundamental material limitations-Tairoling of composition and dimensionality

Organic-inorganic halide perovskites are compounds of the chemical structure ABX_3; A is either organic, such as methylammonium ($CH_3NH_3^+$, MA^+), formamidinium ($CH_3(NH_2)_2^+$, FA^+) and guanidinium ($CH_6N_3^+$, GA^+), or inorganic, such as caesium (Cs^+) and rubidium (Rb^+) monovalent cation. B is a divalent metal cation, such as lead (Pb^{2+}), tin (Sn^{2+}), or germanium (Ge^{2+}) and X is a halogen anion (Cl^-, Br^-, I^-).[39] In this structure, a three-dimensional (3D) framework is produced by BX_6^- octahedra sharing corners in all three orthogonal directions, whereas the A cation fills the 12-fold coordinated cubo-octahedral space. In contrast, the divalent metal atoms B (which are smaller in size than A cations) sit at the centres of the octahedra (**Figure 1a**).[40-42] Several perovskite structures usually correspond to a specific composition, depending on the temperature

View Article Online
DOI: 10.1039/D1EE00062D

and preparation procedure. For example, the prototypical hybrid organic-inorganic metal halide perovskite, methylammonium lead triiodide ($MAPbI_3$), undergoes phase transformations from tetragonal to cubic at T = 54 °C and from tetragonal to orthorhombic at T = -111 °C during cooling.[42,43]

Perovskites with lower dimensionality, such as two- (2D) and one- (1D) dimensional bulk materials and zero- (0D) dimensional nanomaterials can also be produced (**Figure 1b**). For example, the 2D framework is based on inorganic monolayers formed by corner-sharing BX_6^- octahedra, sandwiched between layers composed of large organic molecules. These are also known as organic–inorganic Ruddlesden−Popper (RP) perovskite materials, and have been thoroughly reviewed recently.[44-48] The chemical formula of RP perovskites is $A_{n-1}A_2'B_nX_{3n+1}$, includes a large monovalent cation A such as butylammonium ($CH_3(CH_2)_3NH_3^+$, BA^+) or phenethylammonium ($C_6H_5(CH_2)_2NH_3^+$, PEA^+); A′ is the monovalent cation commonly forming the 3D perovskite structures. The long-chain alkylamines in the RP perovskites act as insulating buffers that prevent penetration of moisture into the crystal structure. As a result, PSCs based on RP perovskites are more stable than their 3D perovskite counterparts, albeit with lower efficiencies originated from the wider band gaps and lower carrier mobilities of the 2D structures. To prepare both efficient and stable PSCs by combining the advantages of 2D and 3D perovskites, strategies involving mixed phases of 2D/3D hybrid perovskites through efficient composition and structural engineering have been introduced and discussed below.

View Article Online
DOI: 10.1039/D1EE00062D

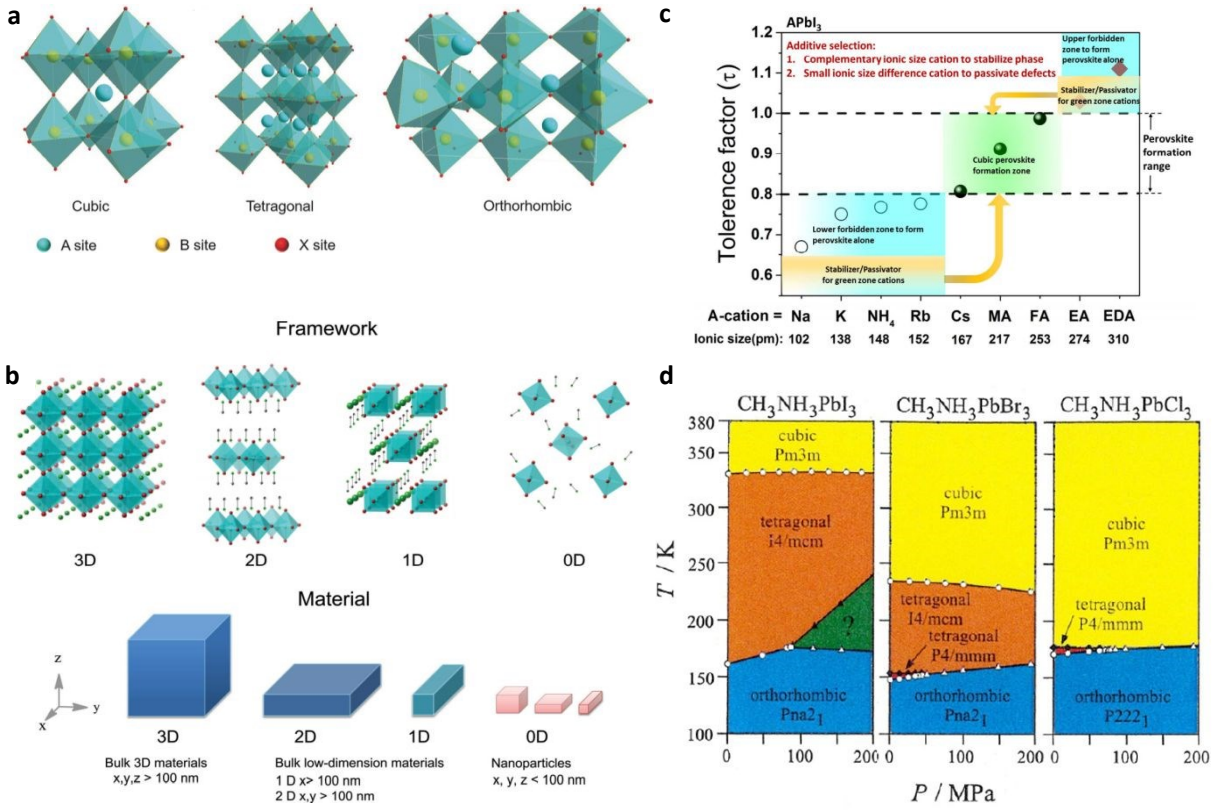

Figure 1. (a) Crystal structures of the three different $MAPbI_3$ phases: (left) cubic, (middle) tetragonal, and (right) orthorhombic. The crystal structures of the three phases differ by rotation of the inorganic octahedral cages. Reproduced with permission from ref. 42. Copyright 2017 John Wiley and Sons. (b) Schematic representation of perovskite frameworks with different dimensionalities (from left to right: 3D, 2D, 1D, and 0D). Reproduced with permission from ref. 41. Copyright 2015 John Wiley and Sons. (c) Calculated tolerance factors in $APbI_3$ perovskites including different A cations. The green color in the figure indicates the ideal cubic phase ($0.8 < t < 1$) which is formed for Cs, MA and FA cations only. Reproduced with permission from ref. 63. Copyright 2018 American Chemical Society. (d) Pressure-temperature phase diagrams of $MAPbX_3$, (X = Cl, Br, I) crystals. Effect of halide ratio variation on optical and transport properties of $MAPbX_3$ and $FAPbX_3$ perovskites. Reproduced with permission from ref. 93. Copyright 1992 Elsevier.

In general, the stability of PSCs critically depend on structural stability of the perovskites absorber, which can be predicted theoretically by calculating the tolerance factor,[49] *t*, a geometrical parameter introduced in 1926 by V. M. Goldschmidt:[50]

$$t = \frac{r_A + r_X}{\sqrt{2}(r_B + r_X)} \quad (1)$$

View Article Online
DOI: 10.1039/D1EE00062D

with r_A, r_B and r_X being the radii of A, B (generally, $r_A > r_B$) and X ions in the perovskite ABX_3. The tolerance factor assesses whether the large A cation can fit within the space between BX_6-octahedra in the perovskite framework.[51] When the tolerance factor is unity, a perfect fit is expected. For $0.8 < t < 1$ a stable perovskite phase is generally formed; compounds with a tolerance factor of $0.9 < t < 1$ tend towards forming an ideal cubic structure, but for t close to 0.8 distorted perovskite structures with tilted octahedra (usually orthorhombic) are generally obtained. It is common in halide perovskite literature to denote the phase with cubic structure as α-phase and the phase with non-perovskite structures as δ-phase.[40] If $t > 1$, the A cation is too large to fit within the framework and precludes the formation of stable perovskite phases. Finally, for $t < 0.8$, the A cation is too small, leading to alternative non-perovskite structures. Based on the above considerations, only three A cations known to date, namely Cs^+, MA^+ and FA^+ (**Figure 1c**), give tolerance values between 0.8 and 1 and are able to form a stabilized perovskite phases, either for Pb^{2+} or Sn^{2+} in the B site. Noatbly, Pb^{2+} perovskites are generally more stable than Sn^{2+} ones; the latter tend to oxidize even in the dark due to oxidation of Sn^{2+} to the Sn^{4+} state.[52-62]

Alkali metal cations (Na^+, K^+, Rb^+) and NH_4^+ have a $t<0.8$ thus not forming perovskite structures. However, all these cations in the "forbidden zones" (light blue areas in **Figure 1c**) can serve as low concentration additives into the perovskite phases formed by MA, FA and Cs cations, aiming to achieve phase stabilization and defect passivation. To serve as perovskite phase stabilizers, these cations should posses large ionic size difference compared to the parent perovskite cations.[63] However, for effective defect passivation small ionic size difference between these cations and perovskite ones is preferential. Moreover, intermixing different cations has be proven beneficial for the device performance and stability.[64] The addition of MA^+ to the FA^+ dipping bath prevented the undesirable formation of the δ-phase and at the same time retained the

View Article Online
DOI: 10.1039/D1EE00062D

bandgap edge of $FAPbI_3$ adequately red-shifted.[65-67] Caesium is the only inorganic elemental cation that it is large enough (r_{Cs+} = 167 pm) to sustain the perovskite structure. Moreover, it has a considerably smaller ionic radius than MA^+ and FA^+ to enable its intermixing with FA^+, which results in PSCs with enhanced photo- and moisture stability.[68-71] The triple-cation perovskite films are thermally more stable and less affected by temperature, solvent vapours or heating during processing protocols. Cs^+ increases the thermal stability for a fixed halide ratio, while increased Br^- content also contributes considerably to thermal stability. Furthermore, incorporation of small amounts of Rb^+ in mixed-cation perovskites leads to small photovoltage losses and stable device performance.[72,73]

Strategies to improve the performance and stability of PSCs also include substitution in the halide anion X^- position. With this approach effective bandgap tuning can be achieved. The compounds with I^- have the smallest bandgap (1.55-1.61 eV); perovskites with Br anions exhibit modest bandgap (2.0-2.44 eV), while those with Cl anions exhibit the highest bandgap (2.88-3.13 eV).[74-78] The higher band gap, along with higher effective mass and lower charge carrier mobility of Br^- and Cl^- perovskites impede charge carrier transport in the perovskite film and, consequentrly, decrease the device performance. However, more stable structures were obtained through I substitution with smaller Br anions in mixed halide perovskites.[79,80] An implication presented by mixed halide perovskites, however, is their photo-instability and the low obtained photovoltage.[81] These were attributed to halide segregation under illumination, which results in the formation of two crystalline phases, namely iodide-rich minority and bromide-enriched majority domains. The emission from the minority domains with the high iodide content dominate the photoluminescence spectra of the mixed halide perovskite films even at low volume fractions. This is because the photogenerated carriers relax from the high energy states of the higher bandgap

View Article Online
DOI: 10.1039/D1EE00062D

Br-rich majority domains into the lower energy states of the I-rich minority domains, where emission ultimately takes place. In the PSC devices, these domains may act as photogenerated carrier traps, facilitating non-radiative electron-hole recombination that induces voltage loss, while also has implications in the photostability of such devices. A more unconventional approach towards increased moisture stability involved replacement of two iodides with pseudohalide thiocyanate ions (SCN^-) in $MAPbI_3$.[82] Comparing the spherical shape of I^- ions with the linear shape of SCN^- ions, the lone pairs of electrons from the S and N atoms in SCN^- can interact strongly with the Pb^{2+} ion, which in turn stabilizes the frame structure of $MAPb(SCN)_2I$, making it harder for water to form a hydrate phase in this crystal structure.[83,84]

Besides chemical composition, environmental factors such as water and oxygen molecules, concentrated light and heat represent notorious degradation factors of perovskite absorbers.[85-92] Pressure-temperature phase transitions of $MAPbX_3$ (where X = Cl, Br, I) crystals have been also investigated through applying high pressure in the range between 0.1 Pa and 200 MPa.[93] A triple point was found in each compound for pressures lower than 100 MPa ($MAPbCl_3$: 75.1 MPa, 175.7 K, $MAPbBr_3$: 43.2 MPa, 152.9 K, $MAPbI_3$: 84.8 MPa, 176.2 K, **Figure 1d**). The low-pressure phases of Cl^- and Br^- perovskites disappeared upon increasing pressure to the triple point, while a new phase appeared in the I^- perovskite.

3. Perovskite defects and passivation approaches

Even though theoretical calculations predict highly ordered perovskite structures, in reality, even perovskite films of high quality possess significant intrinsic disorder mainly due to their relatively soft crystal structure.[69] Moreover, due to their ionic character and the generally low defect formation energies, halide perovskites exhibit a wide variety of defects that are accommodated on

View Article Online
DOI: 10.1039/D1EE00062D

the surface and at grain boundaries (GB) of the standard polycrystalline films.[94] Also, ion migration within the perovskite film contributes to the formation of parasitic non-radiative recombination centres.[69,95] Several types of defects are identified for the perovskite materials, divided into intrinsic and extrinsic defects. The former is also termed as native point defects and are always present in the perovskite framework and are commonly related to both the defective and incomplete lattice sites. These point defects can be summarized as follows for an ABX_3 perovskite: vacancy defects V_A, V_B, V_X, interstitial defects A_i, B_i, X_i and several types of substitutions (also known as antisites A_B, A_X, B_A, B_X, I_A, I_B), under-coordinated Pb^{2+}, cation (such as MA^+ and FA^+) and mobile halide and MA species, metallic Pb, halide-excess and Pb-halogen antisites.[96] Point defects can be combined to generate charge-neutral defect pairs such as Frenkel and Schottky defects. The former consists of a vacancy and an interstitial pair, whereas the latter consists of two vacancies of opposite charges. There are also 1D defects when lattice periodicity is discontinuous along a line, 2D surface defects and grain boundaries and 3D voids. For example, twelve types of intrinsic point defects have been reported for the prototypical $MAPbI_3$ perovskite; these are MA, Pb and I vacancies (denoted as V_{MA}, V_{Pb} and V_I), interstitial MA, Pb and I (denoted as MA_i, Pb_i and I_i), and six substitutions, in particular, MA substituting Pb (MA_{Pb}), Pb replacing MA (Pb_{MA}) MA and Pb substituting I (MA_I, Pb_I) and I substituting MA and Pb (I_{MA} and I_{Pb}). **Table 1** summarizes the most prevalent point defects in the lead and some in the tin halide perovskite films.

View Article Online
DOI: 10.1039/D1EE00062D

Table 1 Defect traps for representative thin-film perovskites (theoretical calculations and experimental measurements) and associated trap densities.[88,97-114]

Perovskite	**Traps origin**	**Trap density (cm^{-3}) (experimental method)**	**Ref.**
$MAPbI_3$	Intrinsic (bulk) defects (V_I, I_{MA}, V_{Pb}, MA_I, I_i, Pb_i) Surface defects	$1.6x10^{17}$ $2.5x10^{17}$ 10^{17}-10^{18} $6.7x10^{17}$ (PL) 10^{15}-10^{17} 10^{18}-10^{19} (TAS) $1.22x10^{16}$ (SCLC) 10^{21} (TSC) $9.2x10^{14}$ (DLCP)	97 98 99 100 101 102 103 104 105
$FAPbI_3$	FA_I, I_{FA}	$5.28x10^{14}$ (DLTS) 10^{17} (PL)	106 98
$Cs_{0.05}FA_{0.70}MA_{0.25}PbI_3$	V_I, I_{FA}	$4.3x10^{14}$ (DLCP)	105
$Rb_{0.05}Cs_{0.05}$ $FA_{0.75}MA_{0.15}Pb(I_{0.95}Br_{0.05})_3$	V_I, V_{Br}, I_{FA}, I_{MA}	$5.7x10^{14}$ (DLCP)	105
$FA_{0.92}MA_{0.08}PbI_3$	V_I, I_{FA}, I_{MA}	$7.9x10^{14}$ (DLCP)	105
$Cs_{0.05}FA_{0.8}MA_{0.15}$ $Pb_{0.5}Sn_{0.5}(I_{0.85}Br_{0.15})_3$	V_I, V_{Br}, V_{Sn}, I_{FA}, I_{MA}	$1.2x10^{15}$ (DLCP)	105
$CsPbI_2Br$	V_{Sn}, V_I, I_{FA}, V_{Br}	$(8x10^{16})$ 10^{15}-10^{16} (SCLC)	107 108,109
$FA_{0.75}MA_{0.25}SnI_3$	V_{Sn}	$5.8x10^{22}$ (TSC)	110
$FA_{0.75}MA_{0.25}Sn_{1-x}Ge_xI_3$	V_{Sn}	10^{8}-10^{14} (TSC)	111,112
$MAPbI_{3-x}Cl_x$	Bulk defects (V_I, I_{MA}, V_{Pb}, MA_I, I_i, Pb_i) Surface defects	 $3.2x10^{15}$-$1.1x10^{16}$ (PL) $7.7x10^{16}$-$1.2x10^{17}$ (PL)	113 113
$FAPbBr_3$	V_{Pb}, V_{Br}, FA_I, Br_i, Pb_i	$6.1x10^{18}$ (PL)	114
$Rb_xFA_{1-x}PbBr_3$	V_{Pb}, V_{Br}, FA_I, Br_i, Pb_i	$8.4x10^{18}$ (PL)	114
$MASnI_3$	V_{Sn}, V_I	$1.8x10^{14}$ (SCLC)	88
$CsGeI_3$	V_{Ge}, V_{Cs}, V_I,	-	

View Article Online
DOI: 10.1039/D1EE00062D

The calculated relative energies for most point defects in perovskites are very close to the band edges or even inside them. This indicates that perovskite materials are not prone to forming midgap states that are detrimental to the PSC. They act as Shockley-Read-Hall (SRH) non-radiative recombination sites, causing a significant reduction in photogenerated carrier lifetimes and concomitant drop of open-circuit voltage (V_{OC}).[115] Shallow trap states are most likely to be formed; they, however, induce reduced trapping times. The origin of such defect tolerance of perovskites is strongly related to the anti-bonding character of the molecular orbitals that constitute the bands' extrema (mostly Pb 6*p* orbitals in the conduction band minimum and X *p*-Pb 6*s* in the valence band maximum).[116] Typically, vacancies of any type represent shallow defects, while interstitials and antisites form deep traps with increasing formation energy.[117] For example, substantial non-radiative recombination losses have been determined in $MAPbI_3$ that arise from the more profound defects in the perovskite bandgap, including interstitial Pb (Pb_i) and antisite defects (MA_I, Pb_I, I_{MA}, and I_{Pb}). All these defects and the associated trap states exhibit a wide profile concerning their spatial and energetic distribution and densities. They are considered highly detrimental to PSC performance.[118] Even shallower defects may act as useful, unintentional, doping sites, contributing to photocurrent hysteresis. Besides the anomalous hysteresis in current density-voltage characteristics, they are also the cause of phase segregation and long-term instability issues. By introducing compositional engineering and appropriate passivation methodologies, including surface and bulk passivation using additive engineering, solution chemistry engineering, colloidal and coordination chemistry approaches and post-deposition treatments, the number of in-depth and shallow defects can be effectively reduced.

Extrinsic point defects are caused by the perovskite dangling bonds on the surface and the

View Article Online
DOI: 10.1039/D1EE00062D

surrounding environment; they can be categorized as surface and grain boundary defects. They represent a significant concern in the commonly used solution-processable grainy and polycrystalline halide perovskite films where trap densities of the order of 10^{16}–10^{17} cm^{-3} (for $MAPbI_3$) have been estimated, much higher than those of the ones found in single crystals (10^{9}–10^{10} cm^{-3}).[100] Defects at grain boundaries and the interfaces also present degradation sites as they serve as infiltration paths for moisture while also providing charge accumulation sites.[119] Furthermore, the halide-terminated surfaces of those films usually form traps that usually provide favourable paths for halide ions' migration due to reduced steric hindrance.[105] Surface and grain boundary defect passivation are of paramount importance to optimise and stabilise the device efficiency.[120]

Surface and interface passivation approach using small molecules (i.e., amine and carboxylic acids, Lewis bases and acids, porphyrins, pyridines, halide salts, electrolytes, multifunctional molecular modulators), self-assembled monolayers (SAMS), low dimensional perovskites and capping layers represent effective routes that aim to decrease defect density and charge trapping therein. Cross-linking of perovskite grains using organic small molecules or polymers and regulating perovskite film morphology and crystallinity using appropriate additives or post-treatment methods can synergistically contribute to a decrease in both intrinsic and extrinsic defect density, reduce charge accumulation and trapping and prevent the moisture attack effectively. In this review, we summarize and discuss recent achievements that have been made in the field of defect passivation approaches in perovskite films, including efforts on the surface and interface modification, modulation of grain boundaries, morphology and crystallinity control, and post-treatments leading to perovskite solar cells with improved performance attributes and stability. **Figure 2** illustrates intrinsic and extrinsic defects in the perovskite bulk and surface, as well as

View Article Online
DOI: 10.1039/D1EE00062D

several successful passivation approaches discussed in this review.

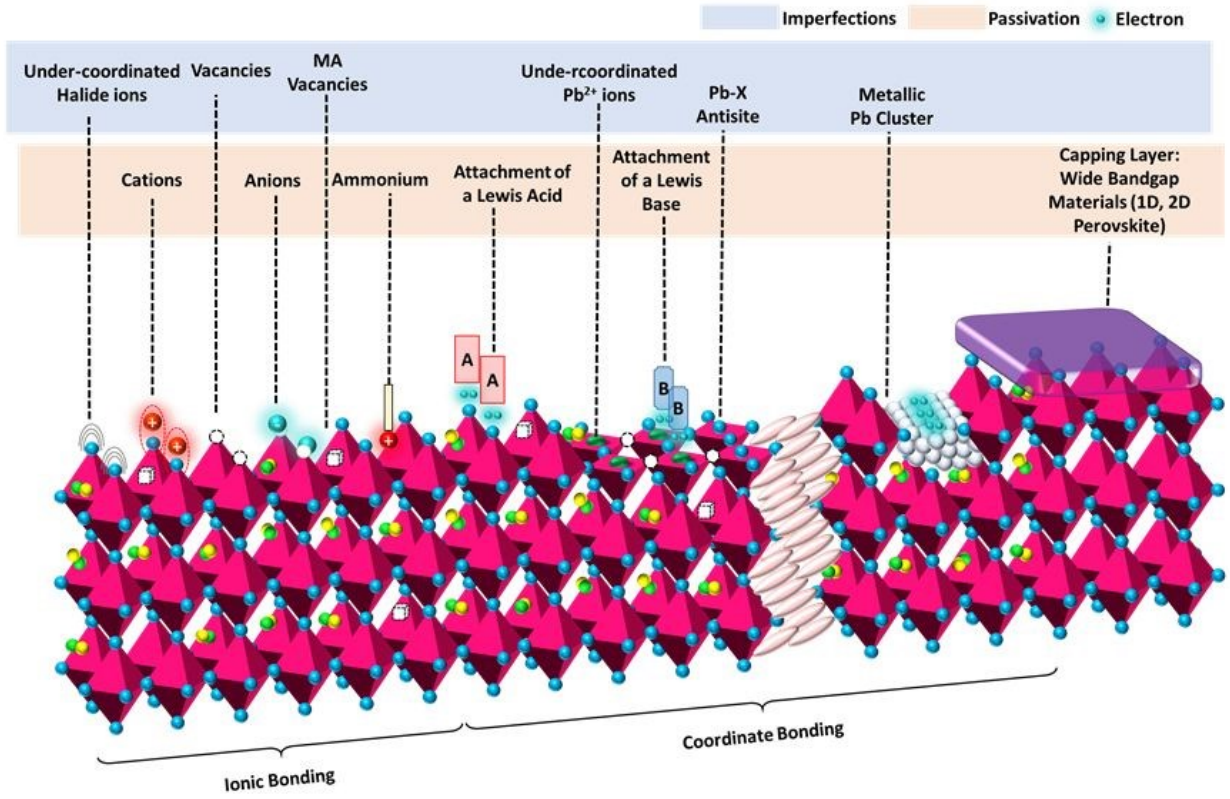

Figure 2. Intrinsic and extrinsic defects in halide perovskite film and several passivations approaches ionic or coordinate bonding using ammonium salts, Lewis acids and bases, organic halide salts, etc.; surface passivation with a low dimensional (wide bandgap) perovskite; suppression of ion migration at grain boundaries using molecular modulators.[28] Copyright 2019, the Royal Society of Chemistry.

3.1 Surface and interfacial defect passivation

The most crucial factor that dictades perovskite soalr cells performance is the adopted procedure for the growth of perovskite thin films. The soft lattice of halide perovskites presents both unique challenges and opportunities in thin film fabrication. Many methods have already been developed for their efficient synthesis and processing, which can be divided to vacuum deposition methods, such as thermal evaporation, pulse laser deposition, chemical vapor deposition etc., and solution-

View Article Online
DOI: 10.1039/D1EE00062D

based techniques, such as spin-coating, drop casting, solvothermal and hydrothermal synthesis, solid-state reaction, precipitation reaction and so on. However, the current review focuses on the passivation and process engineering methods of the already deposited film and reviewing the large field of thin film growth methods is beyond the scope of this work. The reader can refer to the already published review papers that summarize recent approaches on the synthesis of perovskite films as well as advantages and obstacles encountered with each of these approaches.[121-123]

3.1.1 Organic small molecule induced passivation. A wide variety of organic small molecular materials combined with different strategies and processes have been applied to effectively passivate defects and trap states present in perovskite films' surface and interfaces. They generally adopt passivation schemes based on effective coordination or ionic bonding within the perovskite framework. To do so, they bear appropriate functional groups such as amines, carboxylates, halides, basic and acidic ones, and large aliphatic chains or hydrophobic moieties to render the perovskite film surface more resilient to water penetration. Small molecules, including carboxylate groups, possess the intrinsic tendency to coordinate with under-coordinated lead cations strongly.[124] The binding interaction can be further strengthened in donor-π-acceptor (D-π-A) structures. An increase in electron density in carboxylate is obtained via an electron donor unit such as N,N-dibutylaminophenyl with superior donating ability.[125] Non-volatile small molecules with aromatic mono-, di- and tri-carboxylic acid groups, such as benzoic acid (BA), *p*-phthalic acid (PTA), and trimesic acid (TA), respectively, are also found to coordinate with Pb and passivate surface traps effectively.[126] The reduction in the density of defects and the concomitant decrease in carrier recombination therein by small-molecule coordination to perovskite led to higher device performance for all these molecules but to a different extent which was related to

View Article Online
DOI: 10.1039/D1EE00062D

the −COOH content.

Amines were also useful in passivating surface defects in perovskite films. For example, N^2,N^2,N^8,N^8-tetrakis(4-(methylthio)phenyl)dibenzo[*b,d*]thiophene-2,8-diamine (abbreviated as DBTMT) interacted with $MAPbI_3$ at the interface through the sulphur atoms in DBTMT to passivate surface and interface defects, improve the crystallinity and the Pb:I ratio, leading to a higher PCE and enhanced stability in planar p-i-n PSCs.[127] Amines with long alkyl chains have demonstrated improved defect passivation ability and enhanced and stabilised device efficiency.[128] Furthermore, the inclusion of hydrophobic entities in the passivation molecule further boosts the device resilience against moisture-induced degradation. A series of new organic molecules with strong hydrophobic nature synthesised by Zhao *et al.* were employed as surface passivation molecules in PSCs.[129] Among them, N-((4-(N,N,N triphenyl)phenyl)ethyl)ammonium bromide (TPA-PEABr) demonstrated the highest passivation effectiveness, as verified by the reduced surface defect density and a significantly improved efficiency and stability. Another hydrophobic tetratetracontane organic small molecule (TTC, $CH_3(CH_2)_{42}CH_3$) incorporated at the fullerene/perovskite interface of planar p-i-n PSCs reduced the surface and interface traps. It suppressed charge recombination, resulting in enhanced device performance and increased long-term stability.[130] Fluorinated compounds, such as the polyfluoro organic compound tris(pentafluorophenyl)boron (TPFPB), played multiple roles in passivating surface defects, reducing surface defect densities, yielding large grains, increasing surface hydrophobicity and improving charge transport.[131] The effective surface passivation of the perovskite absorber was also proven beneficial for device stability. PSCs with the TPFPB passivation retained a more considerable degree of their initial performance when exposed to ambient air and illumination with a xenon lamp. Furthermore, bidentate organic small molecules bearing hydrophobic moieties, such

View Article Online
DOI: 10.1039/D1EE00062D

as pyrazines and porphyrins, have been proven capable of passivating surface defect states in the perovskite film through either a monodentate or a bridging bidentate bonding with under-coordinated Pb^{2+} ions while also acting as protecting buffers against moisture penetration.[132,133]

Besides instability issues, a significant concern in PSC technology is their low reproducibility which highly hampers their practical application. Effective passivation of defects in the perovskite film can also lead to repeatable performance attributes in the respective devices. A π-conjugated small molecule embedding bilateral carboxyl and thiophene groups, namely 2,5-di(thiophene-2-yl)terephthalic acid (DTA), effectively passivated perovskite defects which led to a significant performance, an improvement in environmental and thermal stability as well as increased device reproducibility with only small deviations from optimum device performance.[134] In a similar approach, simultaneous enhancement in the device long-term stability and reproducibility was achieved by introducing a hexamethylenetetramine (HMTA) into the precursor solution.[135] This enabled morphological and structural control of the fabricated films while also created a hydrophobic "encapsulation" network on the perovskite surface through effective coordination of HMTA with under-coordinated Pb ions, boosting, apart from efficiency, the device stability and reproducibility. Except for being coordinated to lead cations, a small molecule with appropriate functional groups can also passivate halide ions. An iodopentafluorobenzene (IPFB) additive, for example, was capable of strong supramolecular halogen bond formation, thus passivating perovskite trap states.[136] An ionic compound, namely 1-ethylpyridinium chloride (EPC), bearing nitrogen atom in the pyridine group, also acted as an effective surface defect passivation medium. The chlorine anions were also found to participate in the defect passivation process.[137] Concerning interfacial passivation, a polar non-conjugated small-molecule electrolyte, namely 4,4′-(((methyl(4-sulphonatobutyl)ammonio)bis(propane-3,1-diyl))bis(dimethyl

View Article Online
DOI: 10.1039/D1EE00062D

ammoniumdiyl))bis-(butane-1-sulfonate) (MSAPBS), initially introduced at the ITO/perovskite interface, was found not only to inhibit interface charge accumulation but also to passivate interfacial defects and suppress non-radiative recombination.[138] Multi-zwitterionic small-molecule electrolytes were also served as useful as surface defect passivation agents while also interacted with bulk/interface defects. Synergistically, this resulted in performance enhancement with suppressed hysteresis and enhanced stability.[139]

The insertion of appropriate bulky hydrophobic tertiary and quaternary alkyl ammonium cations within the perovskite material enabled the formation of a moisture-resistant layer and improved the fabricated stability devices.[140,141] The steric effects due to the bulky cations and the change of surface Pb_5 –I_{1c} bonds effectively hindered water adsorption on the Pb_{5c} sites. Various MA-based PSCs with the modified perovskite films yielded PCEs over 15% with excellent stability under very high RH (~90%) over 30 days.[140] Note that aprotic sulfonium cations have exhibited, apart from electrochemical, superior humidity stability than protic ammonium cations, emphasizing the cation basicity's role in PSC stability against moisture.[141] Meanwhile, the coating of evaporated $MAPbI_3$ thin films with different hydrophobic molecules, namely trioctyl phosphine oxide and tridodecyl methylammonium iodide, resulted in a remarkably mitigated degradation of $MAPbI_3$ and formation of PbI_2 and led to high efficiency and enhanced stability single-junction n-i-p PSCs.

To achieve the highest degree of defect passivation, multi-functional small molecular materials have recently been proposed as an effective means to passivate defects, regulate film crystallinity and enhance crystal grain size. A judiciously engineered bifunctional molecular modulator 3-(5-mercapto-1H-tetrazol-1-yl)benzenaminium iodide (SN), linking the mercapto-tetrazolium (S) and phenylammonium (N) moieties, was incorporated in formamidinium-caesium

View Article Online
DOI: 10.1039/D1EE00062D

lead iodide-based PSCs by Grätzel and co-workers aiming at passivating surface defects and inducing the formation of large grain crystals with superior quality.[142] As a result, a power conversion efficiency (PCE) exceeding 20% for $(FAI)_{0.9}Cs_{0.1}(PbI_2)_{1.05}$ PSCs with a large area (exceeding 1 cm^2) combined with high operational stability under ambient conditions was demonstrated. Moreover, a rationally designed multifunctional molecular modulator, 4-tert-butyl-benzylammonium iodide (tBBAI), with bulky tert-butyl groups, prevented aggregation by steric repulsion was recently applied as a surface modifier in PSCs. tBBAI significantly accelerated charge extraction, while it also retarded non-radiative charge carrier recombination by passivating interfacial defects.[143] Furthermore, the tert-butyl groups enhanced surface hydrophobicity. They protected the perovskite film from moisture, leading to excellent cell operational stability retaining over 95% of the initial PCE after 500 h continuous solar illumination.

A molecular passivation treatment for perovskite films, using multifunctional molecular entities consisting of a small-sized hydrophobic aromatic group, i.e. a benzene ring in a benzylamine functional molecule, was also proposed to be an effective method to passivate perovskite defects. Proper steric edge-on arrangement of the benzene rings on the perovskite surface was considered responsible for efficiency stabilization and moisture-resistance (>4 months in ambient air) of the treated $FAPbI_3$ PSCs.[144] Generally, control of the degree and depth of interaction between perovskite and the employed molecules could tune the effectiveness of defect passivation.[145] Understanding the underlying passivation mechanisms through interactions between the molecular functional groups and the perovskite defects can further advance this field. For example, a detailed study of passivation with caffeine, theophylline and theobromine treatment revealed that the primary passivation event, which is accomplished through C=O binding on antisite Pb defects, can be assisted hydrogen-bond formation between N-H and iodine anions.[146]

View Article Online
DOI: 10.1039/D1EE00062D

The addition of a Lewis base is well known to reduce trap density and enhance the electron diffusion length in perovskites.[147] Bifunctional group passivation with a hydrophobic molecule of thiosalicylic acid was recently demonstrated to double anchoring the acid functional groups to under-coordinated Pb ions.[148] Rationally designed Lewis base small molecules with electron-rich nitrile (C-N) groups effectively reduced trap density of the Pb-exposed surface through coordination bonds and, thus, suppressing non-radiative recombination, resulting in an improved photostability in an inverted p-i-n configuration.[149] Lewis acids and bases containing phosphorus, such as triphenylphosphine oxide (TPPO), tris(pentafluorophenyl) phosphine (TPFP)and tetraisopropyl methylenediphosphonate (TMPP), were also employed in multiple-cation lead mixed-halide perovskites to improve PSC efficiency and stability.[150,151] Different functionalities, including defect passivation and suppression of phase segregation, resulted in reduced charge recombination, enhanced PCE and moisture resistance (**Figure 3**).

View Article Online
DOI: 10.1039/D1EE00062D

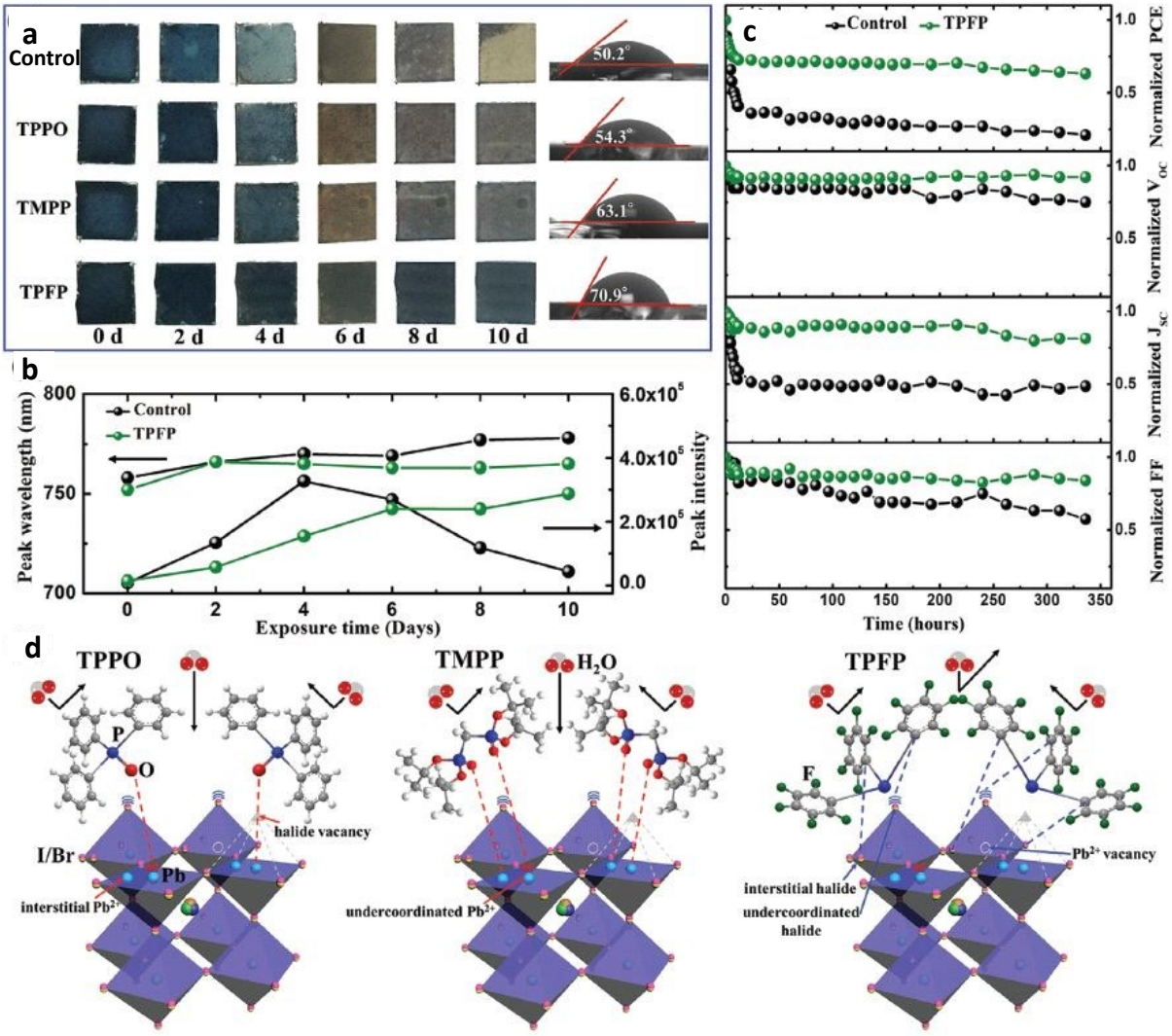

Figure 3. Moisture stability of control and phosphorus-containing Lewis acid and base molecule-treated multiple-cation lead mixed-halide perovskite films and unencapsulated devices. Molecules include triphenylphosphine oxide (TPPO), tetraisopropyl methylenediphosphonate (TMPP), and tris(pentafluorophenyl) phosphine (TPFP). (a) Photographs of perovskite films experiencing different exposure times under 85% relative humidity (RH) and their contact angles. (b) The evolution of photoluminescence (PL) peak wavelength and intensity of control and TPFP-perovskite films exposed under 85% RH for a different time. (c) Time-dependent normalized power conversion efficiency (PCE), open-circuit voltage (V_{OC}), short-circuit current (J_{SC}) and fill factor (FF) of control and TPFP-perovskite devices exposed under 75% RH. (d) Schematic illustration of molecule-induced surface passivation displaying six defect types, including Pb^{2+}/halide vacancies, interstitial Pb^{2+}/halides, and under-coordinated Pb^{2+}/halides and their interactions with the incorporated Lewis acid and base molecules.[150] Copyright 2020, John Wiley and Sons.

View Article Online
DOI: 10.1039/D1EE00062D

Non-fullerene acceptors (NFAs), such as a (3,9-bis(2-methylene-(3-(1,1-dicyanomethylene)-indanone))-5,5,11,11-tetrakis(5-hexylthienyl)-dithieno[2,3-d:2′,3′-d′]-s-indaceno[1,2-b:5,6-b′]dithiophene) (ITIC-Th) molecule,[152] have also been proven as an effective class of additive materials. Similarly, pristine or functionalized fullerenes acceptors (FAs), such as a cross-linkable [6,6]-phenyl-C_{61}-butyric styryl dendron ester (PCBSD), enabled effective surface and bulk passivation of perovskite films.[153] These molecules could simultaneously address the poor crystallization issue of perovskites, passivate defect states and enhanced electron extraction efficiency.[154] It was found that PSCs based on hybrid phenyl-C61-butyric acid methyl ester ($PC_{61}BM$):perovskite solids exhibited significantly reduced hysteresis and recombination losses.[155] They proposed that $PC_{61}BM$ molecules passivated PbI_3^- antisite defects during the perovskite self-assembly. A thin interfacial modification layer of $PC_{61}BM$ employed at the Al-doped ZnO/perovskite interface was also an effective interfacial defect passivation layer. It lowered the defect activation energy and reduced the trap density, improving the cells PCE with a significant reduction in their hysteresis.[156] Moreover, amino-functionalized PCBM has been very effective as passivation layer due to its electron-accepting ability that strongly inhibited ionic motion near the perovskite surface.[157] A pyridine-functionalized fullerene additive (C_{60}-PyP) also enabled coordination interactions with perovskite leading to passivated surface trap states, enlarged the grain size and improved film crystallization while also improved perovskite's resistance to degradation due to its hydrophobic nature.[158,159] **Table 2** includes the maximum PCE obtained with PSCs incorporating small organic molecules as passivation agents, while the device architecture is also presented.

.

View Article Online
DOI: 10.1039/D1EE00062D

Table 2. Performance of PSCs employing organic small molecular compounds and small molecule-based surface and interface passivation and cross-linking approaches for perovskite defect and GB passivation (PCEs denote champion values).

Organic Small Molecule (Passivation mechanism)	**PSC structure**	**PCE (%) Before/after passivation**	**Section**	**Ref.**
D-π-A SPs (binding with under-coordinated Pb^{2+} cations)	ITO/NiO_x/$MAPbI_3$-SP_3/PCBM/BCP/Ag	18.52/20.43	3.1.1	124
ABN (passivation of charged defects)	FTO/TiO_2/ABN-treated $Cs_{0.06}FA_{0.79}MA_{0.15}PbI_{2.55}Br_{0.45}$/Spiro-OMeTAD/Ag	20.22/21.02	3.1.1	125
DBTMT (interface interaction with perovskite)	ITO/DBTMT/$MAPbI_3$/C_{60}/BCP/Ag	-/21.12	3.1.1	127
UAA (unilateral alkylamines) (surface and GB passivation)	ITO/PTAA/UAA-modified $Cs_{0.05}$ $FA_{0.70}MA_{0.25}$ PbI_3/C_{60}/BCP/Cu	18.40/21.50	3.1.1	128
TPA-PEABr (surface passivation)	ITO/SnO_2:Li/$FA_xMA_{1-x}Pb(I_{1-y}Br_y)_3$/TPA-PEABr/Spiro-OMeTAD/Au	16.69/18.15	3.1.1	129
$CH_3(CH_2)_{42}$ CH_3 (TTC) (reduction of interfacial traps)	ITO/PTAA:F_4TCNQ/$MAPbI_3$/TTC/C_{60}/BCP/Ag	17.34/20.05	3.1.1	130
TPFPB (surface defect passivation)	FTO/TiO_2/$FA_{0.85}MA_{0.15}PbI_3$/TPFPB/Spiro-OMeTAD/Au	19.55/21.60	3.1.1	131
Pyrazine (Pyr) (bonding with under-coordinated Pb^{2+} ions)	ITO/SnO_2/(FAMA)$PbI_xBr_yCl_{3-x-y}$/Pyr/Spiro-OMeTAD/Au	19.14/20.58	3.1.1	132
Zinc Porphyrin (YD2-o-C8) (anchor with under-coordinated Pb^{2+} defects)	ITO/SnO_2/(CsFAMA)PbI_xBr_{3-x}/YD2-o-C8/Spiro-OMeTAD/Au	18.50/20.50	3.1.1	133
DTA (coordinate with unsaturated Pb^{2+} cations)	ITO/PTAA/DTA-treated $MAPbI_{3-x}Cl_x$/C_{60}/BCP/Ag	19.10/21.45	3.1.1	134
IPFB (halogen bond passivation)	FTO/TiO_2/Al_2O_3/$MAPbI_{3-x}Cl_x$/IPFB/Spiro-OMeTAD/Ag	13.00/15.70	3.1.1	136
EPC (multiple defect	FTO/TiO_2/$(FAPbI_3)_{0.95}(MAPbBr_3)_{0.05}$/EPC/Spiro-OMeTAD/Au	19.52/21.19	3.1.1	137

View Article Online
DOI: 10.1039/D1EE00062D

passivation)				
SN (multifunctional surface defect passivation)	FTO/TiO_2/SN-modified $FA_{0.9}Cs_{0.1}PbI_3$/SN/ Spiro-OMeTAD/Au	19.40/20.90	3.1.1	142
tBBAI (interface passivation)	FTO/TiO_2/$CS_{0.05}FA_{0.85}MA_{0.10}Pb(I_{0.97}Br_{0.03})_3$/tBBAI/Spiro-OMeTAD/Au	20.00/23.50	3.1.1	143
Phenylalkylamines (coordination with the Pb^{2+} ions or hydrogen bonding with the iodide ions)	FTO/TiO_2/Benzylamine-modified $FAPbI_3$/ Spiro-MeOTAD/Au	14.20/19.20	3.1.1	144
D-4-tert-butylphenylalanine (D4TBP) (healing of charged defects via electrostatic interactions)	ITO/PTAA/$CS_{0.05}FA_{0.81}MA_{0.14}PbI_{2.55}Br_{0.45}$/ D4TBP/$C_{60}$/BCP/Cu	19.10/21.40	3.1.1	145
Theophylline (bonding to surface iodide)	ITO/SnO_2/$(FAPbI_3)_x(MAPbBr_3)_{1-x}$/Theophylline / Spiro-OMeTAD/Ag	21.00/23.48	3.1.1	146
Urea ($CO(NH_2)_2$) (increase the optical path length)	ITO/SnO_2/Urea treated-$Cs_{0.05}FA_{0.81}MA_{0.14}PbI_{2.55}Br_{0.45}$/ Spiro-OMeTAD/$MoO_3$/Ag	-/19.40	3.1.1	147
6TIC-4F (defect passivation)	ITO/NiO_x/$CsPbI_xBr_{3-x}$/6TIC-4F/ZnO/C_{60}/Ag	13.90/16.10	3.1.1	149
TPFP (suppressed yellow phase formation)	ITO/SnO_2/$Cs_{0.05}FA_{0.8}MA_{0.15}Pb(I_{0.83}Br_{0.17})_3$/TPFP / Spiro-OMeTAD/Au	18.05/22.02	3.1.1	150
PEAI (Surface defect passivation)	ITO/SnO_2/$FA_{1-x}MA_xPbI_3$/PEAI/Spiro-OMeTAD/Au	20.95/23.32	3.1.4	185
CH_3O-PEAI (electrostatic interaction between the benzene ring and the undercoordinated Pb^{2+} ions)	ITO/SnO_2/$((FAPbI_3)_{1-x}(MAPbBr_{3-y}Cl_y)_x)$/$CH_3O$-PEAI/Spiro-OMeTAD/Au	19.98/22.98	3.1.4	189
$HA_2MAPb_2I_7$ (Interfacial passivation)	FTO/SnO_2/$CsFAMAPbI_xBr_{3-x}$/$HA_2MAPb_2I_7$/Spiro-OMeTAD/Ag	18.83/20.62	3.1.4	190
TMI (Surface passivation)	FTO/SnO_2/$(FAPbI_3)_{0.97}(MAPbBr_3)_{0.03}$/TMI/ Spiro-OMeTAD/Ag	18.01/18.93	3.1.4	192
Acids				

View Article Online
DOI: 10.1039/D1EE00062D

Trimesic acid (TA) (coordination between the carboxylic acid groups and Pb)	FTO/SnO_2/TA doped $MAPbI_3$/ Spiro-OMeTAD/Ag	12.52/15.81	3.1.1	126
MSAPBS (Interfacial and bulk defect passivation)	ITO/SnO_2/MSAPBS/$Cs_{0.05}FA_{0.81}MA_{0.14}PbI_{2.55}Br_{0.45}$/Spiro-OMeTAD/Au	18.95/21.18	3.1.1	139
Thiosalicylic acid (TSA) (anchoring of functional groups to uncoordinated lead ions)	FTO/TiO_2/$MAPbI_3$/TSA/Spiro-OMeTAD/Ag	16.24/18.07	3.1.1	148
PCBM (passivation of PbI_3^- antisite defects)	FTO/TiO_2/PCBM/$MAPbI_3$/Spiro-OMeTAD/Au	9.50/14.40	3.1.1	155
PCBM (Interfacial modification)	ITO/AZO/PCBM/$MAPbI_3$/ Spiro-MeOTAD/MoO_x/Al	13.00/16.90	3.1.1	156
$C_{60}NH_2$ (Interfacial passivation)	FTO/TiO_2/$C_{60}NH_2$/$MAPbI_3$/Spiro-OMeTAD/Au	17.33/18.34	3.1.1	157
PCBM:4,4′-bipyridine (Interfacial passivation)	ITO/NiO_x/$CsPbI_2Br$/4,4′-bipyridine/PCBM/$Zr(acac)_4$/Ag	10.96/12.09	3.1.1	159
PCBM:4,4′-bipyridine (Interfacial passivation)	ITO/NiO_x/$CsFAMAPbI_xBr_{3-x}$/4,4′-bipyridine/PCBM/$Zr(acac)_4$/Ag	15.92/16.67	3.1.1	159
Thioctic acid (TA) (Passivation of under-coordinated Pb^{2+} in $MAPbI_3$ and Ti^{4+} in TiO_2)	FTO/TiO_2/TA/$MAPbI_3$/Spiro-OMeTAD/Au	17.40/20.40	3.1.2	170
Quaternary Ammonium Halides ($NR_4^+X^-$) - Choline Chloride (ChCl)) (Passivation of ionic defects)	ITO/PTAA/$MAPbI_3$/ChCl/C_{60}/BCP/Cu	17.10/20.00	3.1.3	175
ChCl (Passivation of ionic defects)	ITO/PTAA/$FA_{0.85}MA_{0.15}Pb(I_{0.85}Br_{0.15})_3$/ChCl/$C_{60}$ /BCP/Cu	19.20/21.00	3.1.3	175
$C_4H_{12}IN$ (n-BAI) (Double-sided	FTO/TiO_2/PMMA:PCBM/n-BAI/$Cs_{0.07}Rb_{0.03}FA_{0.765}$ $MA_{0.135}PbI_{2.55}Br_{0.45}$/n-	19.65/22.77	3.1.3	181

View Article Online
DOI: 10.1039/D1EE00062D

surface passivation)	BAI/Spiro-OMeTAD/Au			
PFAI (Formation of surface patches)	FTO/SnO_2/$Cs_{0.05}Rb_{0.05}(FA_{0.83}MA_{0.17})Pb(I_{0.95}Br_{0.05})_3$/PFAI/Spiro-OMeTAD/Au	20.09/21.38	3.1.4	182
BBA_2PbI_4 (Formation of capping layer)	FTO/TiO_2/$Cs_{0.05}FA_{0.95}PbI_{2.7}Br_{0.3}$/$BBA_2PbI_4$/ Spiro-MeOTAD/Au	19.13/21.13	3.1.4	186
OLA ligand (Ligand capping of perovskite nanocrystals)	FTO/TiO_2/($FA_{0.83}MA_{0.12}Cs_{0.05}$ $PbI_{2.64}Br_{0.36}$)/ OLA/Spiro-OMeTAD/Au	19.48/21.50	3.1.5	203
DR3T (Passivation of GBs)	FTO/TiO_2/$MAPbI_3$/DR3T/Spiro-OMeTAD/Au	17.50/19.30	3.2.1	210
Aminoterephthalic acid (2AA) (Passivation of GBs)	ITO/SnO_2/$MAPbI_3$-2AA/Spiro-OMeTAD/Ag	19.13/21.09	3.2.1	211
DA_2PbI_4 (Defect and crystal growth modification)	ITO/TiO_x/$MAPbI_3$-DA_2PbI_4/ Spiro-OMeTAD/MoO_3/Ag	15.73/19.05	3.2.1	212
PTABr (Intarfacial and GB passivation)	ITO/SnO_2/PMMA:C_{60}/PTABr/$MAPbI_3$/PMMA/ Spiro-OMeTAD/Ag	-/18.99	3.2.1	213
PTABr (Intarfacial and GB passivation)	ITO/SnO_2/PMMA:C_{60}/PTABr/$Cs_{0.15}FA_{0.85}PbI_3$/ Spiro-OMeTAD/Ag	16.60/19.82	3.2.1	213
PTABr (Intarfacial and GB passivation)	ITO/SnO_2/PMMA:C_{60}/PTABr/ $Cs_{0.15}FA_{0.75}MA_{0.1}PbI_3$/Spiro-OMeTAD/Ag	16.60/21.41	3.2.1	213
C_{60} (Intarfacial and GB passivation)	ITO/BCP/C_{60}/$MAPbI_3$/Spiro-MeOTAD/Au	-/19.10	3.3.1	215
PFA (Surface and GB passivation)	FTO/TiO_2/$MAPbI_3$-PFA/Spiro-OMeTAD/Au	12.71/16.18	3.2.1	216
PFA (Surface and GB passivation)	FTO/TiO_2/$Cs_{0.05}(FA_{0.85}MA_{0.15})_{0.95}PbI_{2.55}Br_{0.45}$-PFA/Spiro-OMeTAD/Au	19.53/21.31	3.2.1	216
SY-2 (Interfacial passivation)	ITO/NiO_x/SY-2/$MAPbI_3$/$PC_{61}BM$/BCP/Ag	16.92/18.96	3.2.1	217
SQs (Passivation of GBs)	ITO/SnO_2/$MAPbI_3$/SQs/Spiro-OMeTAD/Au	15.77/18.83	3.2.1	218
TMTA (Passivation of GBs)	ITO/P3CT-N/$MAPbI_3$-TMTA/PCBM/C_{60}/BCP/Cu	19.08/19.26	3.2.3	226

View Article Online
DOI: 10.1039/D1EE00062D

PABAHI (Interact with the Pb-I framework via hydrogen bonds)	FTO/TiO_2/$MAPbI_3$-PABAHI/Spiro-OMeTAD/Au	16.40/17.40	3.2.3	227
Alkylamine ligands (AAMs) (Passivation of interfaces and GBs)	ITO/PTAA/$Cs_{0.05}(FA_{0.92}MA_{0.08})_{0.95}Pb(I_{0.92}Br_{0.08})$-OAM/$C_{60}$/BCP/Cu	20.50/23.00	3.2.3	228
VBA ligand (weak interwell van der Waals bonding between hydrophobic organic moieties of the ligands)	ITO/TiO_2/$(MAPbBr_3)_{0.15}(FAPbI_3)_{0.85}$/VBA/ Spiro-OMeTAD/Au	18.20/20.40	3.2.3	229
Methimazole (MMI) (Formation of GB patches)	ITO/SnO_2/$MAPbI_3$-MMI/Spiro-OMeTAD/Ag	17.00/20.10	3.2.4	233
Guanidinium Thiocyanate (GUTS) (Surface and GB passivation)	FTO/SnO_2/$MAPbI_3$/GUTS//Spiro-OMeTAD/Au	14.59/16.37	3.2.4	234

3.1.2 Polymer induced passivation. In addition to organic small molecules, conjugated or non-conjugated polymers have been recently applied to PSCs to function as passivation moieties for achieving improved and stabilized efficiencies. For example, donor-acceptor conjugated copolymers with carbazole and benzothiadiazole (BT) units bearing alkoxy side-chains in the BT unit were employed to function as perovskite surface passivation agents and dopant-free hole transport layers simultaneously. It was revealed that the methoxy side-chains on the BT unit introduced a surface defect passivation effect resulting in PSCs with superior PCE and stability compared to the Spiro-OMeTAD-based cells due to suppression of trap-induced recombination and cell degradation.[160] Mixing $MAPbI_xCl_{3-x}$ with a donor polymer [N-9''-hepta-decanyl-2,7-carbazole-alt-5,5-(4',7'-di-2-thienyl-2',1',3'-benzothiadiazole)] (PCDTBT),[161] which contains lone electron pairs due to the presence of S and N atoms, also proved a practical trap state

View Article Online
DOI: 10.1039/D1EE00062D

passivation approach. In contrast, the interaction between $MAPbI_xCl_{3-x}$ and PCDTBT led to a more ordered orientation and high-quality film morphology. As a result, PCDTBT-modified PSCs demonstrated an improved and stabilized PCE with enhanced stability. Similarly, thiazole-bridged diketopyrrolopyrrole (DPP)-based semiconducting polymers have been recently applied as passivation agents in PSCs leading to PCEs up to 20.30%.[162] A thin poly(3-hexylthiophene-2,5-diyl) (P3HT) layer deposited on top of an inorganic $CsPbI_2Br$ perovskite film was also found to effectively and reproducibly passivate surface defect states and significantly reduce electron-hole recombination within the perovskite.[163] A thin semiconducting poly(4-butylphenyldiphenylamine) polymer (PTPD) was also proved useful in interfacial passivation at the perovskite/HTL interface.[164]

Non-conjugated polymers, such as poly-vinylpyrrolidone (PVP), have also been applied as surface passivation layers in $CsPbI_3$-based PSCs.[165] Acylamino groups in PVP induced an electron cloud density enhancement on the perovskite surface due to chemical bonding between acylamino and $CsPbI_3$, lowering its surface energy and stabilising $CsPbI_3$ grains in the cubic phase. Similarly, poly-4-vinylpyridine (P4VP) effectively passivated the surface defects and grain boundaries upon coordination of lone pair electrons of nitrogen in pyridine with the under-coordinated Pb sites. The substantially reduced defect density led to reduced nonradiative recombination and extended electron diffusion length.[166] In particular, PSCs with P4VP incorporation exhibited significantly enhanced moisture and thermal stabilities. Self-assembled surface-passivated $FA_{0.8}Cs_{0.2}PbI_3$ perovskite thin films with a fluorinated polymer (FP) as an additive have also been incorporated in PCEs.[167] Upon separation and aggregation of the FP phase at the perovskite layer's top surface during film formation, FP acted as a passivation layer and improved the PCE from 17.2% to 19.1%. Notably, the passivation of the upper interface in PSCs might in principle be more efficient than

View Article Online
DOI: 10.1039/D1EE00062D

that of the lower interface. This hierarchy in interfacial passivation was attributed to the ‘‘reparation’’ effect of the utilized passivation medium on the perovskite layer, as it induced both ‘‘interfacial’’ and ‘‘bulk’’ effects by effectively filling the grain boundaries of the perovskite layer and reducing the trap state density in both the perovskite layer and the interface between it and the upper carrier transport layer.[168] A PCE of 19.55% and a V_{OC} of 1.133 V with negligible hysteresis and better long-term and thermal stability were achieved for the champion devices with an upper passivation layer of polystyrene (PS) or polymethyl methacrylate (PMMA). Moreover, an ultrathin passivation layer consisting of a PMMA:PCBM mixture was highly effective in passivating interfacial defects near the perovskite/TiO_2 interface, significantly suppressing interfacial recombination.[169] A crosslinkable organic small molecule thioctic acid (TA) has been coordinated to both TiO_2 and $MAPbI_3$ and then in situ crosslinked to form a polymer (Poly(TA)) network, which acted as bifacial passivation agent (**Figure 4**).[170] **Table 3** summarizes the perovskite passivation approaches using polymers and large molecular materials.

View Article Online
DOI: 10.1039/D1EE00062D

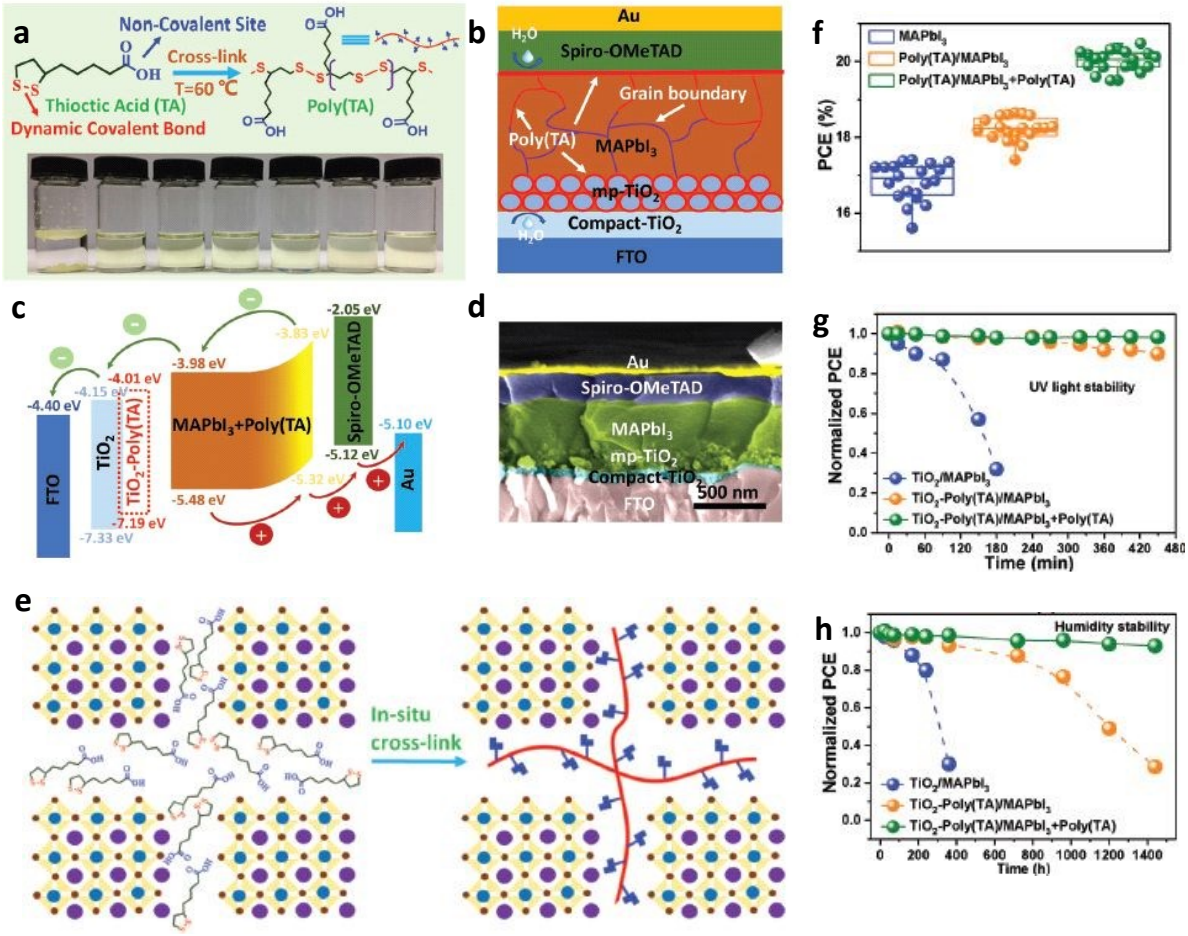

Figure 4. (a) Schematic representation of crosslinking polymerisation of organic small molecule thioctic acid **(**TA) under thermal conditions and photographs of TA dissolved (20 mg mL^{-1}) in different solvents, including water, ethanol, N,N-dimethylformamide (DMF), N-methyl pyrrolidone (NMP), dimethyl sulfoxide (DMSO), chlorobenzene (CB), and ethyl acetate (EA). (b) Schematic illustration of mesoporous perovskite solar cells with Poly(TA). (c) Photovoltaic device energy band diagram. (d) Cross-sectional SEM image of the solar cells with Poly(TA). (e) The working mechanism of crystal modification and trap passivation for Poly(TA) in perovskite solar cells. (f) Statistical distribution of PCE of devices assembled with $MAPbI_3$, Poly(TA)/$MAPbI_3$, and Poly(TA)/$MAPbI_3$ + Poly(TA). (g) The normalized PCE decay of PSCs based on $MAPbI_3$, Poly(TA)/$MAPbI_3$, and Poly(TA)/$MAPbI_3$ + Poly(TA) under UV irradiation. (h) Moisture stability upon exposure to air (50 ± 10% RH).[170] Copyright 2020, John Wiley and Sons.

View Article Online
DOI: 10.1039/D1EE00062D

Table 3. Performance of PSCs employing organic large molecular compounds (including polymers) and polymer-based cross-linking approaches for perovskite defect and GB passivation (PCEs denote champion values).

Polymer/Large Molecule (Passivation mechanism)	**PSC structure**	**PCE (%) Before/after passivation**	**Section**	**Ref.**
PCDTBT1 (Defect passivation)	ITO/TiO_2/$PC_{60}BM$/$MAPbI_3$/PCDTBT1/MoO_3/ Au	17.10/19.10	3.1.2	160
PCDTBT (Defect passivation)	ITO/PEDOT:PSS/$MAPbI_{3-x}Cl_x$/PCBM/BPhen/Ag	12.42/15.76	3.1.2	161
PTzDPPBTz (Passivation of the defects and vacancies created by under-coordinated Pb atoms)	ITO/PTAA/PTzDPPBTz/$MAPbI_3$/C_{60}/PEI/Ag	16.58/20.39	3.1.2	162
P3HT (Electronic passivation of surface defect states)	ITO/TiO_2/$CsPbI_2Br$/P3HT/Au	-/12.02	3.1.2	163
PTPD (Back contact passivation)	ITO/TiO_2/$Cs_{0.05}MA_{0.05}FA_{0.9}PbI_{2.85}Br_{0.15}$/PTPD/ Spiro-MeOTAD/Au	19.60/21.90	3.1.2	164
PVP (Surface passivation)	FTO/TiO_2/$CsPbI_3$/PvP/Spiro-OMeTAD/Au	-/10.74	3.1.2	165
P4VP (Interfacial and GB passivation)	ITO/PTAA/$MAPbI_3$/P4VP/PCBM/Al	17.46/20.02	3.1.2	166
P(VDF-TrFE) (Surface passivation)	FTO/TiO_2/$FA_{0.8}Cs_{0.2}PbI_3$/P(VDF-TrFE)/ Spiro-OMeTAD/Ag	17.20/19.10	3.1.2	167
PMMA (Surface passivation)	FTO/NiO_x/$MAPbI_3$/PMMA/PCBM/Ag	15.90/19.54	3.1.2	168
PMMA:PCBM (Passivation of defects at or near to the perovskite/TiO_2 i nterface)	FTO/TiO_2/PMMA:PCBM/$Cs_{0.07}$ $Rb_{0.03}$ $FA_{0.765}$ $MA_{0.135}$ $PbI_{2.55}$ $Br_{0.45}$/Spiro-OMeTAD/Au	18.40/20.40	3.1.2	169
PBTI (Passivation of GBs)	ITO/NiO_x/CSFAMAPbI_xBr_{3-x} /PBTI/PCBM/ZrAcac/Ag	18.89/20.67	3.2.2	223
PDMS	FTO/TiO_2/$FA_{0.15}MA_{0.85}PbI_3$/PDMS/	15.07/16.16	3.2.2	224

View Article Online
DOI: 10.1039/D1EE00062D

(Passivation of GBs)	Spiro-OMeTAD/Au			
Poly(propylene carbonate) (PPC) (bridge the perovskite grains)	ITO/SnO_2/$MAPbI_3$-PPC/Spiro-MeOTAD/Ag	18.77/20.06	3.2.3	225
PMMA (Passivation via Lewis-base electronic passivation of Pb^{2+} ions)	FTO/TiO_2/PMMA:PCBM/$Cs_{0.07}$ $Rb_{0.03}$ $FA_{0.765}$ $MA_{0.135}$ $PbI_{2.55}$ $Br_{0.45}$/PMMA/Spiro-OMeTAD/Au	19.50/20.80	3.2.4	230

3.1.3 Inorganic material induced passivation. Inorganic materials have also been investigated as passivation agents in perovskites owing to their robustness and ease of processing. Organophosphorus ligands, TOPO and TPPO,[148] have been used as passivation through interfacial modification of perovskite films upon Pb–O bonds forming under-coordinated Pb^{2+} ions.[171] Core/shell colloidal quantum dots (QDs) have also been applied as passivation layers on perovskite surfaces.[172] In particular, CdSe/ZnS QD layers decreased the surface trap density and stabilized the perovskite structure. Both surface and grain boundary defects were suppressed due to the Se^{2-} anions inducing van der Waals interactions between the perovskite's organic and inorganic components.

Another novel approach for interfacial passivation and suppressed carrier recombination was demonstrated by Chen *et al.* in all-inorganic caesium tin-germanium triiodide ($CsSn_{0.5}Ge_{0.5}I_3$) PSCs. They showed that the Sn-containing stable GeO_2 native-oxide layer that was spontaneously formed upon air exposure, fully covering the perovskite film, was highly effective in passivating the perovskite surface.[59] Defect passivation in inorganic perovskites using oxygen molecules and atoms was also identified as a remarkably effective strategy to suppress defect-assisted recombination.[173] Although oxygen molecule passivation occurs by physisorption on the perovskite's surface, oxygen atoms strongly interact with perovskites and provide enhanced

View Article Online
DOI: 10.1039/D1EE00062D

passivation compared to O_2. Significantly, dry-air processing conditions facilitate O_2 dissociation into O upon annealing, enhancing $CsPbI_2Br$-based PSCs efficiency and ambient stability.

In a similar approach, effective dual passivation of shallow and deep traps in an organic-inorganic hybrid perovskite and at the ETL/perovskite interface was achieved by an alkaline chloride (namely potassium chloride, KCl) interfacial modification, leading to state-of-the-art PSCs with a superior PCE of 22.6%, reduced hysteresis and excellent long-term stability in the air (**Figure 5**).[174] Dual passivation strategies have also been regularly employed in PSCs based on methylammonium and mixed cation perovskites.[196,197] Quaternary ammonium halides effectively passivated both positively charged cationic and negatively charged anionic defects, such as I^- and MA^+ vacancies, in several hybrid perovskites. Efficient defect healing reduced the charge trap density and elongated the carrier recombination lifetime, boosting the PCE to 20.59% and significantly enhancing ambient stability.[175] Similarly, inorganic binary alkaline halide salts with their cations and anions were found to passivate several types of ionic defects simultaneously and significantly suppress recombination at the SnO_2/perovskite interface, contributing to the elimination of hysteresis and a high PCE of 20.5% in PSCs that further retained 90% of their initial performance after 30 days storage.[176] Si *et al.* also demonstrated that incorporating ammonium chloride (NH_4Cl) could result in the simultaneous passivation of negative- and positive-charged ionic defects, reducing the perovskite defect density, prolonging the carrier lifetime, enhancing film crystallinity and boosting the PCE to 21.38% with enhanced long-term stability.[177] Lithium fluoride (LiF) is used for the passivation of interfaces of inverted perovskite solar cells and modules with a p-i-n structure.[178,179] The insertion of a thin LiF interlayer enabled PCE values of 14.1% for a unit cell and 8.7% for the module.[178] **Table 4** summarizes the inorganic molecular materials used as passivation agents in perovskite films.

View Article Online
DOI: 10.1039/D1EE00062D

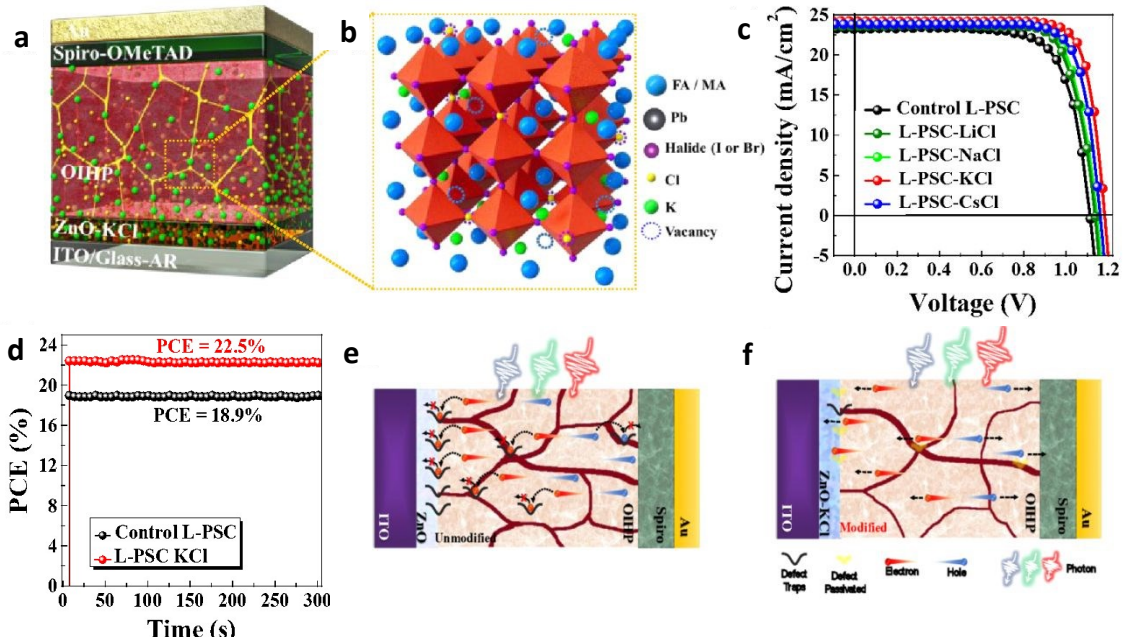

Figure 5. Performance of low temperature processed PSCs modified with alkaline chlorides. (a) The structure of the planar heterojunction PSCs. (b) Schematic illustration of the KCl passivation in organic-inorganic hybrid perovskite crystals. (c) The modified PSCs' J-V characteristics under AM 1.5G one sun illumination (100 mW cm^{-2}) under reverse scan. (d) The stabilized PCEs at maximum power point output (@0.89 V for the unmodified devices and @0.94 V for the KCl-modified devices). (e,f) Schematic illustration of charge traps at interfaces and in perovskite layer for the control and the modified PSCs.[174] Copyright 2020, Americal Chemical Society.

View Article Online
DOI: 10.1039/D1EE00062D

Table 4. Performance of PSCs employing inorganic molecular compounds for perovskite defect and GB passivation (PCEs denote champion values).

Inorganic Molecule (Passivation mechanism)	**PSC structure**	**PCE (%) (Before/after passivation)**	**Section**	**Ref.**
GeO_2 (Surface encapsulation and passivation)	FTO/PCBM/$CsSn_{0.5}Ge_{0.5}I_3$/GeO_2/ Spiro-OMeTAD/Ag	3.72/7.11	2	59
Alkanine Halides (KX) (Passivation of different types of ionic defects)	FTO/SnO_2/KCl/$CS_{0.05}FA_{0.81}MA_{0.14}PbI_{2.55}Br_{0.45}$/ Spiro-OMeTAD/Au	17.30/20.50	3.1.3	176
NH_4Cl (Simultaneous passivation of negative- and positive-charged ionic defects)	FTO/TiO_2/$MAPbI_3$-NH_4Cl/Spiro-OMeTAD/Au	18.03/21.38	3.1.3	177
KCl (Simultaneous contact and GB passivation)	ITO/SnO_2-KCl/$FAMAI_xBr_yCl_{3-x-y}$/ Spiro-OMeTAD/Au	20.20/22.20	3.2.4	235
Alkaline Chlorides (Passivation of shallow and deep traps)	ITO/ZnO/KCl/$MA_xFA_{1-x}Pb(I_xBr_{1-x})_3$/ Spiro-OMeTAD/Au	19.40/22.60	3.1.3	174
$PbCl_2$ (Frmation of a porous PbICl scaffold in the precursor film)	FTO/TiO_2/$PC_{61}BM$/$MAPbI_{3-x}Cl_x$/ Spiro-OMeTAD/Au	11.52/19.45	4.1.1	263
KI (Passivation of GBs and interfaces)	FTO/SnO_2/TiO_2/$(FA_{0.83}MA_{0.17})Pb(I_{0.83}Br_{0.17})_3$-KI/Spiro-OMeTAD/Au	17.3/19.50	3.2.1	214
Trichloro(octyl)silane (TC-silane) (Surface and GBs passivation)	FTO/SnO_2/$FAMAPbI_xBr_yCl_{3-x-y}$/TC-silane/ Spiro-OMeTAD/Au	17.01/20.03	3.2.1	219
NH_4SCN (Passivation of GBs)	ITO/PTAA/$FA_{0.7}MA_{0.2}Cs_{0.1}PbI_3$ /NH_4SCN/PCBM/PEI/Ag	-/19.68	3.2.4	232
TPPO (Passivation through antisolvent process for the interfacial modification)	FTO/TiO_2/$Cs_{0.05}FA_{0.79}MA_{0.16}Pb(I_{0.83}Br_{0.17})_3$ /TPPO/Spiro-MeOTAD/Au	17.24/18.29	3.1.3	171
CdSe/ZnS QDs (Surface defects passivation)	ITO/PEDOT:PSS/$MAPbI_{3-x}Cl_x$ /CdSe/ZnS/C_{60}/BCP/Ag	17.06/19.89	3.1.3	172

View Article Online
DOI: 10.1039/D1EE00062D

Oxygen (Atomic oxygen-induced passivation)	ITO/SnO_2/O-passivated $CsPbI_2Br$/ Spiro-OMeTAD/Au	13.32/15.17	3.1.3	173
LiF (Interfacial passivation)	ITO/PTAA/$MAPbI_3$/PCBM/LiF/Al	11.5/14.1%	3.1.3	178

3.1.4 Low-dimensional perovskites as passivating agents. It is commonly accepted that the perovskite film's surface is where defects are most easily formed. Therefore, the surface and interface defects' passivation is an important task to optimize PSCs' performance and stability. A distinct strategy was recently followed to passivate such defects that involved lower dimensionality perovskites as up-and-coming passivation agents in PSCs.[180] Two-dimensional (2D) wide-bandgap perovskites such as phenethylammonium lead iodide (PEA_2PbI_4) and butylammonium lead iodide (BA_2PbI_4) are insulated materials that have been employed to passivate bulk, surface and interface dangling bonds in the perovskite film by exploiting the associated intermolecular interaction. For example, a double-sided (bifacial) passivation of 3D perovskite films could be successfully implemented with thin, discontinuous, semi-insulating surface layers of bulky organic cation–based halide compounds forming 2D layered perovskites.[181] Highly efficient (22.77%) mixed-dimensional PSCs with a remarkable V_{OC} of 1.2 V are reported for a perovskite film with a bandgap of ~1.6 eV. Double-sided surface layers provide effective surface defect passivation and chemical passivation at both the ETL and HTL/perovskite interfaces, reducing surface recombination and suppressing interfacial charge recombination. 2D perovskites embedding phenylformamidinium (PFA) cations have been proven effective stabilizers of FA-based perovskites.[182] Also, a 2D/3D perovskite stacking layer was fabricated by in situ growth of a 2D PEA_2PbI_4 capping layer on top of the 3D triple cation (Cs/MA/FA) perovskite absorber to improve the stability of the ensuing PSCs.[183] Besides the remarkable efficiency stabilization of the fabricated cells that retained 90% of their initial PCE for more than

View Article Online
DOI: 10.1039/D1EE00062D

1,000 h of exposure in ambient air, high efficiency of 18.51% was also obtained in the 2D/3D PSCs (PCE of the control device 17.02%). The 2D perovskite capping layer application induced more extensive Fermi level splitting under light illumination in the 2D/3D structure, resulting in a higher V_{OC} than the pure 3D perovskite (1.11 versus 1.05 V). A record V_{OC} of 1.31 V was also demonstrated in PSC using a 2D/3D layered perovskite architecture where a n-butylammonium bromide layer was coated atop the double-action perovskite absorber layer.[184] The thin 2D perovskite layer mitigated non-radiative recombination in the absorber layer, enhancing V_{OC} by 80 mV. Jiang et *al*., developed a different strategy to convert PEAI into a 2D layered PEA_2PbI_4 perovskite for effective passivation of a 3D perovskite layer, in particular, $FA_{1-x}MA_xPbI_3$.[185] The perovskite film was deposited using a two-step spin-coating method. It then introduced the 2D perovskite passivation layer by spin-coating a PEAI salt solution onto the 3D perovskite surface. PEAI formed on the perovskite surface enabled higher solar cell efficiency by filling iodine vacancies on the surface and the grain boundaries, reducing defects density and suppressing non-radiative recombination.

Hydrophobic, halogenated, low-dimensional perovskite capping layers by employing different benzylammonium-based aromatic cations were used for surface and interface passivation at the perovskite/HTL interface.[186] Perovskite films with halogenated low-dimensional perovskite passivation layers displayed suppressed non-radiative recombination and reduced trap density, leading to significantly reduced voltage loss. As a result, optimal PSCs achieved a PCE as high as 21.13% with an enhanced V_{OC} of 1.14 V combined with outstanding long-term stability when exposed to moisture, heat and continuous UV irradiation. Nazeeruddin and co-workers have chosen PEA and [(4-fluorophenyl)ethyl]ammonium (FPEA) as 2D cations to formulate thin passivation layers of $(PEA)_2PbI_4$ or $(FPEA)_2PbI_4$ on top of the 3D perovskite.[187] The 2D perovskite

View Article Online
DOI: 10.1039/D1EE00062D

passivation layer neutralized surface defects of the 3D absorber, while also served as a protection layer of the latter preventing moisture penetration into it, demonstrating excellent device stability combined with an efficiency above 18%. 2-(4-fluorophenyl)ethyl ammonium iodide (FPEAI) was also used for the in situ growth of a 2D perovskite, in particular, $(p\text{-}FC_6H_4C_2H_4NH_3)_2[PbI_4]$ on top of a Cs/FA/MA triple-cation 3D perovskite with an excess of PbI_2.[188] The thin 2D perovskite layer facilitated interfacial charge transport, reducing the non-radiative recombinations, while also acted as a protective capping layer for the 3D perovskite film. Based on this 3D/2D perovskite layered structure, PSCs attained a high PCE of 20.54% combined with superior moisture stability maintaining 99% of their initial PCE over a considerable stability test period of 36 days. Furthermore, four organic phenethylammonium iodide salts with different functional groups directly linking to the benzene ring were introduced on the surface of $(FAPbI_3)_{1-x}(MAPbBr_{3-y}Cl_y)_x$ perovskite films. It was found that the electron density of the benzene ring significantly influences the interfacial passivation; only phenethylammonium iodides with electron-donating groups (methoxyl and methyl) were favourable for interfacial passivation, which was attributed to the electrostatic interaction between the benzene ring and the under-coordinated Pb^{2+} ions.[189] A remarkable PCE of 22.98% was achieved with a 1000 h stability under storage in dark ambient conditions. Besides, the chain length of organic ammonium iodide was found to affect the defect passivation effectiveness crucially. Compared to butylammonium iodide (BAI), hexylammonium iodide (HAI)-derived two-dimensional (2D) perovskite was more efficient in passivating interfacial defects, resulting in a notably enhanced photoluminescence lifetime and decreased interfacial charge recombination. Consequently, the ultimate PCE reached 20.62% compared to 18.83% for the reference cell. The long-term PSC durability against humidity and heat was simultaneously improved (**Figure 6**).[190] Substituted thiazolium iodide (TMI) passivating agents

View Article Online
DOI: 10.1039/D1EE00062D

were also employed to functionalize the perovskite surface and induce hydrophobicity.[190] TMI treatment resulted in V_{OC} and FF enhancement by reducing recombination paths at the perovskite/hole selective interface and by passivating shallow and deep bulk perovskite traps. As a result, a higher PCE was achieved, accompanied by remarkable long-term cell stability retaining ~95% of its initial efficiency after 800 h storage.

In an alternative approach, a trilayerd architecture consisting of a highly stable pure 2D (n=1) perovskite layer formulated on top of a quasi-2D (n=2) perovskite film capped a 3D perovskite absorber was demonstrated.[191] By precisely controlling the surface structure and thickness of the 2D perovskites, PSCs with an efficiency of 18.5% and excellent moisture stability were obtained. The wide-bandgap perovskite capping layer approach was also adopted to develop 3D/3D layered structures consisting of wider bandgap perovskites deposited onto lower bandgap ones. For example, compositionally engineered $FAPbBr_{3-x}I_x$ layer on top of the $(FAPbI_3)_{0.85}(MAPbBr_3)_{0.15}$ film could create a compositional gradient at the perovskite/HTL interface and was proven to function as an effective passivating layer, reducing interfacial charge recombination and resulting in a high PCE of 21.3%.[192]

View Article Online
DOI: 10.1039/D1EE00062D

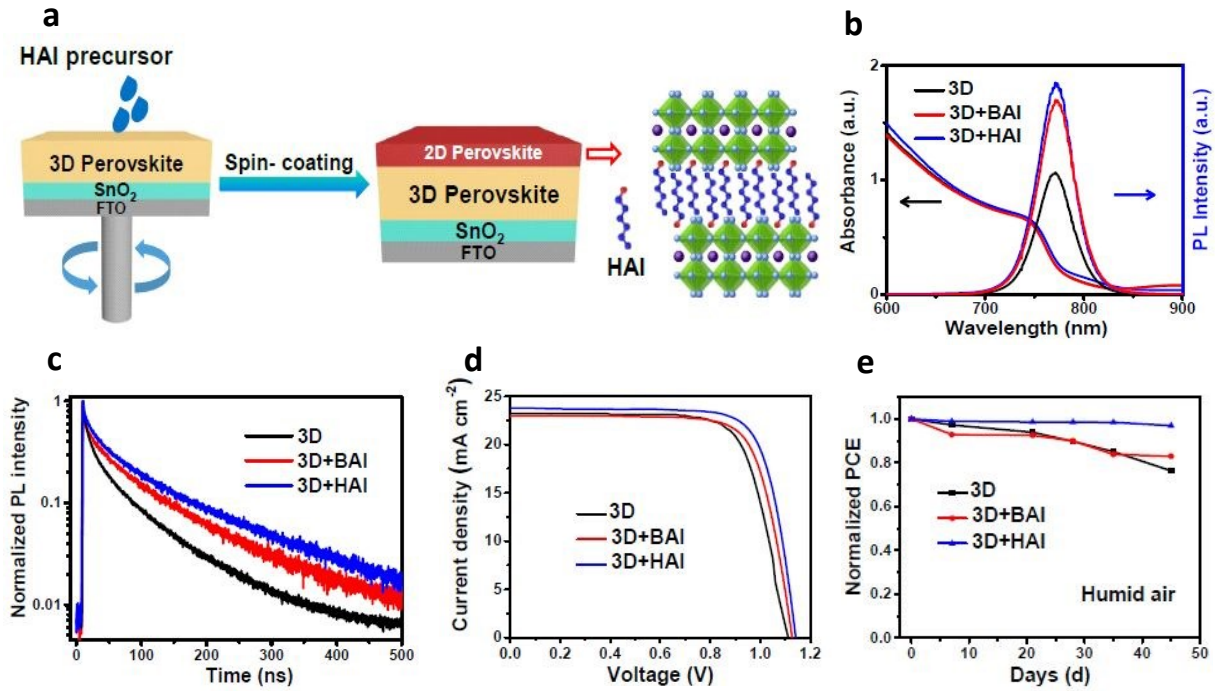

Figure 6. (a) Schematic diagram of the fabrication process of the 2D perovskite-based on HAI in the 2D/3D stacking structure. (b, c) Characterisation of 3D, 3D+BAI and 3D+HAI perovskite films samples: (b) UV–Vis absorption and photoluminescence (PL) spectra, (c) time-resolved PL (TR-PL) decay curves. (d) J-V curves of the champion PSCs based on 3D, 3D+BAI, and 3D+HAI. (e) Normalized PCE of the PSCs stored in an environment with a RH of 55%-75%, and a temperature of 25–40 °C.[190] Copyright 2020, American Chemical Society.

Besides 2D perovskite capping layers, 1D ones have also been developed atop or along with the 3D perovskite absorbers (forming a BHJ in the latter case) to function as thin surface passivation layers. Alkylammonium cations,[193] phenylalkylamines,[194] and pyrazolyl pyridine compounds[195] have been found to coordinate bonds with the perovskite through proton exchange effectively. A novel 1D-3D hetero-structure was formed in the entire volume of the perovskite film with relaxed lattice mismatch. In particular, 2-(1H-pyrazol-1-yl)pyridine (PZPY) was introduced into Pb halide 3D perovskites, readily allowing 1D–3D hybrid perovskite materials to be obtained (**Figure 7a**).[195] The intrinsically stable 1D–3D perovskites demonstrated a thermodynamic self-healing ability induced by blocking the migration channels of A-site ions by

View Article Online
DOI: 10.1039/D1EE00062D

the flexible 1D perovskite less densely close-packed structure. Moreover, they effectively passivated interfacial traps that could form during the crystal growth process, enabling a remarkably enhanced PL decay lifetime due to the suppressed carrier recombination compared to the 3D counterpart. The PSCs fabricated using these novel 1D-3D perovskites exhibited a higher reversible PCE under temperature cycling (25–85 °C) at 55% RH, mainly outperforming the pure 3D PSCs improved long-term stability. Another 1D perovskite, thiazole ammonium lead iodide ($TAPbI_3$), served as an effective capping layer on 3D perovskite. This capping layer passivated surface defects, promoted charge transport, prolonged carrier lifetime and prevented the migration of iodide anions within the 3D perovskite hence improving the overall PSC performance and ambient stability (**Figure 7b**).[196] Similarly, sulfonium-based ionic materials have also been applied as capping layers in perovskite films due to their higher electrochemical stabilities.[197,198]

2D perovskites based on a phenyltrimethylammonium (PTA) cation, namely $PTAMAPbI_4$, have also been applied as capping layers on the surface of MAPbI3 controllable PTAI intercalation via either spin-coating or soaking treatment. $PTAMAPbI_4$ not only passivated $MAPbI_3$ but also acted as an MA^+ locker to inhibit MAI extraction and significantly enhance stability, enabling a champion PCE of 21.16% with only a 7% decrease 500 h continuous illumination (**Figure 7c**).[199] Treating the perovskite film surface with (semi)conducting perovskite quantum dots (QDs) to form a capping layer has been well documented to improve PSC performance.[200] For example, a semiconducting diammonium porphyrin ($ZnPy\text{-}NH_3Br$) was employed to treat $CsPbBr_3$ nanocrystalline QDs coated a 3D perovskite film, thus constructing a stable 0D-2D perovskite capping layer (**Figure 7d**). That assembly strategy resulted in large-scale nanocube perovskite crystals, whereas the capping layer improved charge transport and separation. Optimized devices reached a PCE of 20.0%, compared to 19.5% for the QD-modified PSCs and 19.1% for the control

View Article Online
DOI: 10.1039/D1EE00062D

cells, which dropped by 15% and 35%, respectively when placed at 45% humidity (or illuminated for 450 h) and 85 °C for 1000 h.[200]

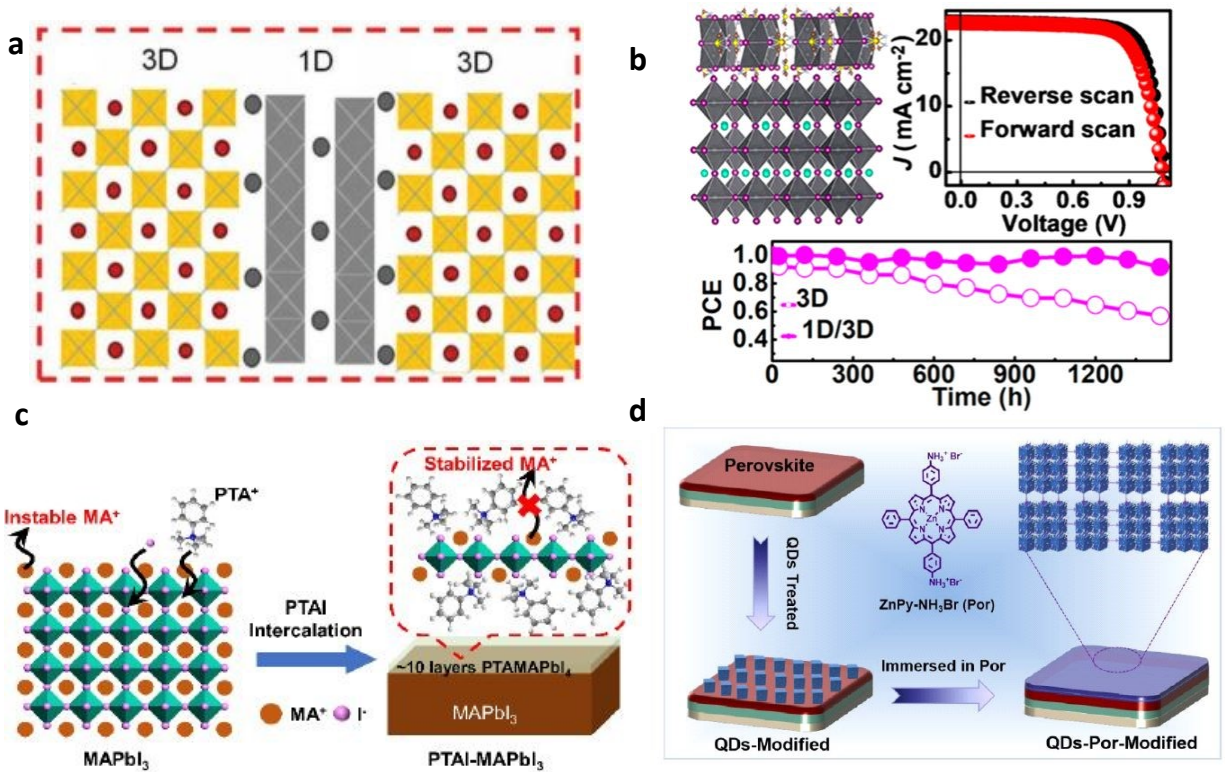

Figure 7. (a) Schematic illustration of the self-assembled 1D–3D perovskite film structure which was formed through blocking the ion-migration channels of A-site ions by the flexible 1D perovskite.195 Copyright 2018 John Wiley and Sons. (b) 1D capping layer strategy employing thiazole ammonium lead iodide ($TAPbI_3$): The crystal structure of a 1D/3D stacking perovskite (3D perovskite: $(MA,FA)PbI_3$), J−V curves of the best fabricated 1D/3D PSCs under reverse and forward scans and their stability performance.[196] Copyright 2019, American Chemical Society. (c) Illustrative scheme of PTAI intercalation induced formation of $PTA,MAPbI_4$ capping layer on $PTAIMAPbI_3$ as MA^+ locker to stabilize $MAPbI_3$.[199] Copyright 2020, John Wiley and Sons. (d) Schematic illustration of the fabrication process of perovskite 02-2D capping layer with zinc diammonium porphyrin ($ZnPy\text{-}NH_3Br$)-bridging $CsPbBr_3$ QDs.[200] Copyright 2020, American Chemical Society.

For example, a semiconducting diammonium porphyrin ($ZnPy\text{-}NH_3Br$) was employed to treat $CsPbBr_3$ nanocrystalline QDs coated on a 3D perovskite film, thus constructing a stable 0D-2D perovskite capping layer (**Figure 7d**). That assembly strategy resulted in the formation of large-

View Article Online
DOI: 10.1039/D1EE00062D

scale nanocube perovskite crystals, whereas the capping layer improved charge transport and separation. Optimized devices reached a PCE of 20.0%, compared to 19.5% for the QD-modified PSCs and 19.1% for the control cells, which dropped by 15% and 35%, respectively when placed at 45% humidity (or illuminated for 450 h) and 85 °C for 1000 h.[200]

3.1.5 Coordination surface chemistry-Use of self-assembled monolayers. Alternatively, surface ligand-modulation and treatment have been employed as surface passivation and trap density modification means in PSCs.[201,202] Addition of specific hydrophobic ionic organic surface ligands, such as cetyltrimethylammonium bromide (CTAB), cetyltrimethylammonium chloride (CTAC), octyltrimethylammonium bromide (OTAB), dodecyltrimethylammonium bromide (DTAB) and cetyldimethylethylammonium bromide (CDAB) modulated the shape and distribution of excess PbI_2 in perovskite films, leading to perovskite films with vertically distributed PbI_2 nanosheets between the GBs and, thus, reducing perovskite trap density and non-radiative recombination. Ligand-modulated devices exhibited a PCE increase from 20% to 22% and more extended stability, retaining 72% of their initial efficiency after 360 h constant illumination.[201] Surface ligands with different binding groups were found to either form a surface monolayer or penetrate the perovskite layer, depending on both the ligand tail and binding groups, as well as modulate the surface energetics, thus significantly impacting PSC characteristics, with increased performance demonstrated for ligands that create a more favourable energetic landscape for electron transfer from $MAPbI_3$ to a C_{60} ETL.[202] Surface treatment of perovskites by various nanocrystals (NCs) capped with oleylamine ligands was also found to be effective in lowering surface trap density and passivating trap states, upon forming a conformal coating on perovskite film, with its origin being oleylamine instead of the NCs.[203]

View Article Online
DOI: 10.1039/D1EE00062D

A common strategy to passivate/modify the interfaces between the perovskite absorber and the charge transporting layers to address both device stability and efficiency issues is incorporating suitable self-assembled monolayers (SAMs) at these interfaces.[204-209] Thiols were first proposed as effective SAMs to chemically modify the interface of $MAPbI_3$ with both a titanium dioxide (TiO_2) electron transporting layer (ETL) and different hole transporting layers (HTLs) leading to enhanced performance and stability of PSCs.[204] In particular, HOOC–Ph–SH thiol was incorporated at the TiO_2/perovskite interface to facilitate perovskite crystal growth and electron transfer from perovskite to TiO_2. A highly hydrophobic thiol, namely pentafluorobenzenethiol (HS-PhF_5), modified the spiro-OMeTAD/perovskite interface and remarkably improved device stability under storage and continuous illumination. Alternatively, hydrophobic small molecule-based SAMs have been effectively incorporated from solution in p-i-n or n-i-p planar heterojunction PSCs. For example, a novel small molecule V1036 without parasitic absorption was employed as a dopant-free hole-selective contact SAM in p–i–n PSCs.[205] Its formation was achieved by immersing the substrate into a solution that could simply bind to the ITO surface due to its phosphonic anchoring group. Devices with a PCE of up to 17.8% were demonstrated. A perfluorinated SAM (p-SAM) passivated the perovskite surface and, at the same time, also drastically improved the perovskite film stability.[206] As a result, p-i-n-type PSCs employing these SAM exhibited PCEs surpassing 21% with exceptional stability under elevated temperature or humid conditions (i.e. stable operation under standardized maximum-power point (MPP) operation at 85 °C in an inert atmosphere for more than 250 h and maintaining ~95% of the initial efficiency upon storage in humid air over ~3000 h).

Two other novel, versatile, hole-selective molecules based on carbazole bodies with phosphonic acid anchoring groups that can form SAMs on various oxides enabled conformal

View Article Online
DOI: 10.1039/D1EE00062D

coverage of arbitrarily formed metal oxide surfaces for p-i-n PSCs.[207] The SAMs created a favourable energy level alignment at the perovskite film interface without non-radiative losses. These SAMs were universally employed in three different perovskite compositions, to demonstrate interlayer-free PSCs with stabilized PCEs of up to 21.1% (**Figure 8**).

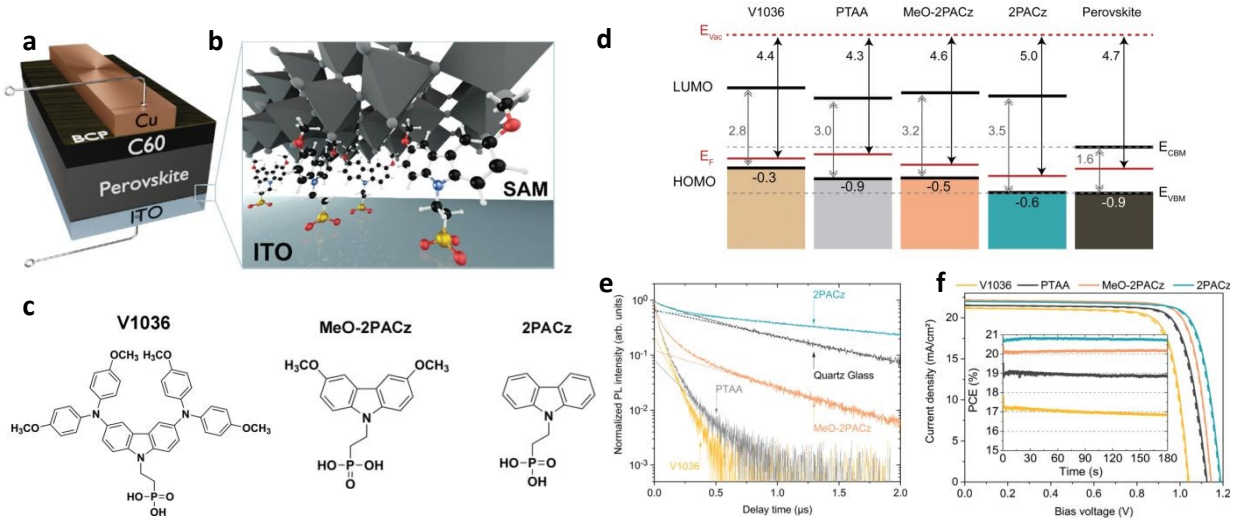

Figure 8. (a) Schematic of the PSC architecture with a triple cation perovskite absorber and SAMs as modifiers at the ITO/perovskite interface. (b) Visualizing how the proposed SAM molecules attach to the ITO surface enables the perovskite's hole selective contact. (c) Chemical structure of the SAM molecules V1036, MeO-2PACz and 2PACz. (d,e) Energetic alignment and Photoluminescence analysis on CsMAFA perovskite: (d) Schematic representation of the investigated SAMs' band edge positions based on UPS measurements values. The lowermost numbers indicate the difference between the Fermi level (E_F) of the ITO substrate and HOMO level or valence band maximum (VBM) (in eV). The energetic distance between conduction band minimum (CBM) or LUMO and VBM was estimated from the onset of optical absorption. The grey, dashed lines are guides to the eye that mark the CBM and VBM levels of the perovskite absorber. (e) PL transients of perovskite films deposited on the respective SAMs. The dotted lines are extrapolated fits to the transients' mono-exponential tail, from which the PL decay time values are obtained. (f) J–V curves under simulated AM 1.5G illumination in forwarding (J_{SC} to V_{OC}, dashed) and reverse scan (V_{OC} to J_{SC}, solid) with respective MPP tracks in the inset.[207] Copyright 2019, the Royal Society of Chemistry.

Acids such as 3-aminopropanoic acid have been explored as SAMs on a poly(3,4ethylenedioxythiophene):poly(styrenesulfonate) (PEDOT:PSS) HTL.[208] A much

View Article Online
DOI: 10.1039/D1EE00062D

smoother perovskite surface morphology with increased film crystallinity and coverage was achieved for $MAPbI_{3-x}Cl_x$, resulting in an enhanced stabilized PCE. Concerning the ETL/perovskite interface in n-i-p PSCs, a fullerene SAM (C_{60}SAM) was proposed to functionalize the interface between mesoporous TiO_2 and the perovskite $MAPbI_{3-x}Cl_x$.[209] C_{60}SAM acted as an efficient electron acceptor but inhibited electron transfer to TiO_2 due to energy level misalignment and low electronic coupling. However, thermalized electrons from C_{60}SAM could be transferred through the perovskite. The formed "mesoporous electron acceptor" could represent a versatile strategy, resulting in PCEs of up to 11.7%.

3.2 Passivation of grain boundaries

3.2.1 Organic and inorganic small molecules. Engineering of grain boundaries (GBs) in perovskite thin films is the most effective method to passivate defects present therein, contributing to efficiency stabilization. Several types of semiconducting small molecules with Lewis acid or base functional groups were exceptionally useful in the passivation of perovskite GBs. They can be easily attached to under-coordinated ions present therein.[210] Post-treatment of perovskite films with acids such as 2-aminoterephthalic acid produce efficient and stable PSCs with a remarkable PCE of 21.09% and improved stability. These improvements were attributed to the acid ability to act as a cross-linking agent that passivated the trap states at GBs thus inhibiting ion migration.[211] Although organic ammonium iodide could be used to effectively passivate surface defects and GBs in perovskite thin films by forming a thin 2D perovskite layer,[185,212] other organic[213] and alkaline[214] iodides were also explored for GB passivation. Phenyltrimethylammonium bromide (PTABr)[213] was universally useful in fine-tuning the perovskite film morphology upon enlarging its grain size and passivating grain boundaries. These led to a reduced trap density in the modified

View Article Online
DOI: 10.1039/D1EE00062D

perovskite film, negligible hysteresis and high-performance PSCs for various perovskites including $MAPbI_3$ and triple-cation perovskites.[213] On the other hand, potassium iodide (KI) incorporation into the perovskite absorber effectively passivated GBs and interfacial defects increased the crystal grain size and improved the film crystallinity.[214] As a result, charge trapping and bimolecular and trap-assisted recombination were suppressed, leading to an improved V_{OC} and FF and an optimized PCE.

Alternatively, small molecule (e.g. C_{60}) induced GB passivation, along with perovskite surface passivation and enhanced electron transport, improved the PCE of planar $MAPbI_3$ cells up to 19.1% and eliminated the photocurrent hysteresis.[215] Fluorocarbon based molecules were another example of highly effective passivation agents for surface defects and grain boundaries. A representative example was 1*H*,1*H*-perfluorooctylamine (PFA) with excellent surface and GBs co-passivation capability. This co-passivation strategy led to a 53.3% PCE enhancement in $MAPbI_3$ PSCs, with a champion PCE of 21.31% in CsFAMA-type PSCs, and exceptional stability with only 3% PCE loss after 2500 h of storage in 70% humidity.[216] Acceptor-donor-acceptor type small molecules with carbazole as the core moiety, ester/amide as the acceptor unit and extended π-conjugation achieved through phenylene thiophene units at the 3,6-positions of carbazole were found to passivate traps/defects at the perovskite grain boundaries and result in larger perovskite grains.[217] The multifunctional amide group exhibiting a Lewis base adduct character were attached to under-coordinated Pb^{2+} ions in the perovskite film, facilitating bifacial defect passivation and reducing the grain boundaries. The best performance was evidenced by a PCE of 18.96% which, after 1000 h storage in Ar atmosphere, retained 92% of the initial value.

Semiconducting squaraine molecules (SQ) with the zwitterionic structure were also demonstrated to interact with under-coordinated Pb^{2+} ions strongly. Simultaneous reduction of the

View Article Online
DOI: 10.1039/D1EE00062D

deep level traps and passivation of GBs enhanced PSCs' efficiency, which retained 90% of their initial PCE after 600 h storage.[218] Inorganic silanes constitute another excellent example for perovskite GB passivation. Trichloro(octyl)silane (TC-silane) modified the perovskite surface and passivated film GBs through cross-linking and forming a heat-resistive silicone layer, leading to a comprehensive improvement of PSC efficiency and stability against moisture and heat.[219] TC-silane passivated PSCs delivered a PCE of 20.03% with only a 20% loss after more than 800 h at ~75% RH in air and about 80 h under 85 °C thermal stress.

An approach to simultaneously control grain growth and passivate GBs in perovskite films was proposed by Lee *et al*. By adding the bifunctional non-volatile Lewis base additive urea (optimal concentration 4 mol.%) to the perovskite precursor solution, a significant enhancement of grain size and homogeneity, as well as reduction in defect density, was achieved due to the increase of the activation energy to slow down crystal growth and the subsequent (after crystal growth formation) precipitation at the GBs to passivate defects.[220] The high PL lifetime and elimination of trap mediated non-radiative recombination resulted in an improved PCE for $MAPbI_3$ PSCs. Similarly, the bifunctional additive, biuret, and multiple Lewis base groups were highly beneficial in regulating perovskite crystallisation and passivating GB defects.[221] Biuret interacted with under-coordinated Pb^{2+} and iodide ions from the iodoplumbate complex on two adjacent perovskite grains. The reader should also refer to recent articles that review the field of additive engineering of perovskite films and resultant solar cells.[222]

3.2.2 Polymer passivation. Conjugated or insulating polymers have also been applied to passivate GBs in perovskite thin films effectively. For example, a conjugated polymer additive, poly(bithiophene imide) (PBTI), was found to be effectively incorporated within GBs, resulting in

View Article Online
DOI: 10.1039/D1EE00062D

reduced defect density and hence suppressed ion migration combined with an improved perovskite film crystallinity (**Figure 9**).[223] The successful defect passivation by PBTI yielded reduced recombination losses and high PCE and improved PSC stability. Optimized cells exhibited a PCE of 20.67% compared to 18.89% for the control devices, and they retained over 70% of initial efficiency after 600 h under illumination.

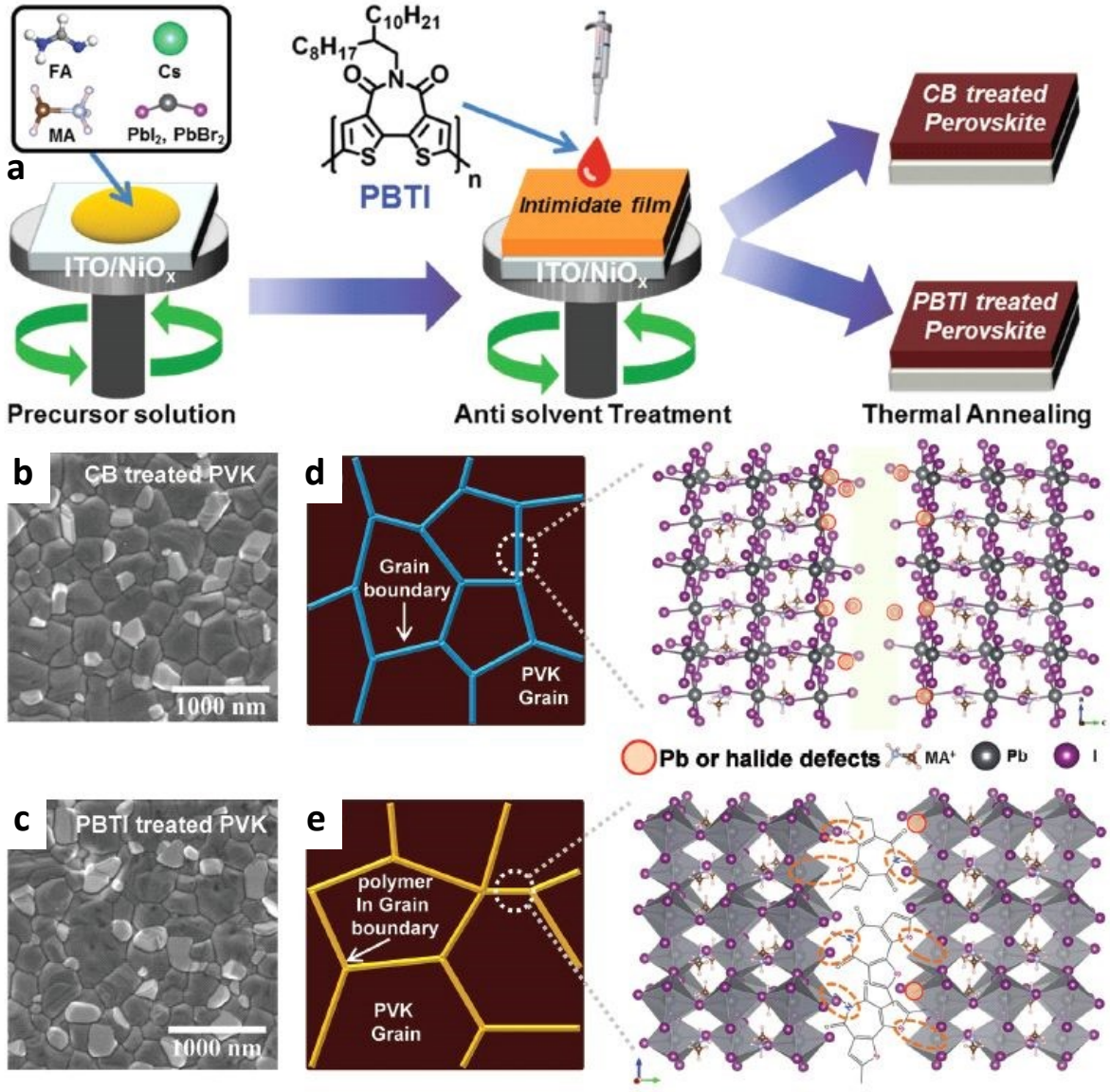

Figure 9. (a) Schematic diagram of the process of perovskite film fabrication (CB, chlorobenzene; PBTI, poly(bithiophene imide)); (b,c) SEM characteristics of CB- (b) and PBTI (c)-treated perovskite films; (d,e) schematic diagram of the grain boundary of CB- (d) and PBTI (e)-treated perovskite films and their defects.[223] Copyright 2019, John Wiley and Sons.

View Article Online
DOI: 10.1039/D1EE00062D

Polydimethylsiloxane (PDMS), a well known organosilicon polymeric compound, was recently introduced during perovskite spin-coating to passivate perovskite grains and adjacent GBs simultaneously.[224] It was found to promote the formation of lead oxide (PbO) bonding that prevented water reaction, while it simultaneously reduced the Pb defect density related to trap-assisted recombination. 0.04 wt.% PDMS-passivated mixed-cation PSCs notably enhanced their performance with an average PCE of 15.44% and a higher than 90% of the initial PCE sustained after 5000 h storage under 70% RH.

3.2.3 Cross-linking of perovskite grains. A different though effective strategy to passivate defects generated at grain boundaries is through the formation of polymer-perovskite composites. This can be accomplished by cross-linking between polymer chains and perovskite using polymeric Lewis acid or bases.[225] The non-radiative recombination centres present at the GBs are being passivated since the cross-linker acts as a bridge for the neighbouring perovskite grains. The resulting perovskite films and devices yield excellent environmental stability against moisture, light, and heat (**Figure 10 a,b**). Similar results can be obtained through the application of organic small molecules as cross-linkers. A representative example is the organic additive trimethylolpropane triacrylate (TMTA) which was chemically anchored to perovskite GBs, and then in-situ formed a robust continuous network polymer after thermal treatment.[226] This strategy enabled significant enhancement in the modified perovskite films' thermal, water and light-resisting properties (**Figure 10 c,d**). PSCs using TMTA cross-linked perovskite films exhibited exceptional performance combined with operational stability, retaining almost 80% of their efficiency after continuous illumination for 400 h at the MPP tracking. Besides, under moisture or thermal (85 °C) conditions, excellent stability was attained with over 90% of their initial efficiency to be preserved

View Article Online
DOI: 10.1039/D1EE00062D

after ageing for over 1000 h.

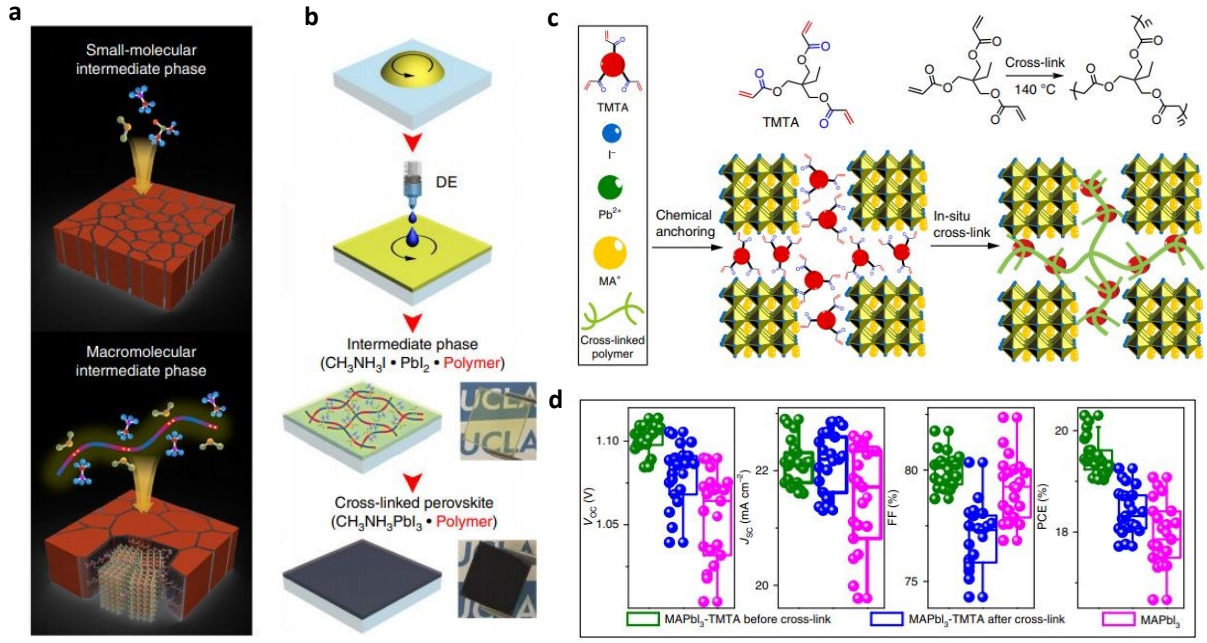

Figure 10. (a) Schematic illustrations of the perovskite film formation through cross-linking using small molecular (up) and macromolecular intermediate phase (bottom). (b) Fabrication steps for the cross-linked perovskite film and optical images of a transparent adduct film and the cross-linked perovskite film on the glass.[225] Copyright 2019, Springer Nature. (c) Schematic illustrations of in-situ cross-linked TMTA/perovskite films: TMTA chemically anchors to the grain boundaries of $MAPbI_3$ and then in-situ cross-links to a continuous network polymer. (d) The PSCs performance attributes: J-V metrics for PSCs based on TMTA/$MAPbI_3$ before, after cross-linking and control $MAPbI_3$.[226] Copyright 2018, Springer Nature.

The amino acid iodide salt-based molecular cross-linker *p*-aminobenzoic acid (PABA·HI), upon adding to a perovskite precursor solution, was demonstrated to effectively interact with the Pb-I framework *via* hydrogen bonds with enhanced cross-linking efficiency. Its rigid molecular structure originated this compared to freely rotating flexible molecular cross-linkers. Consequently, efficient GB passivation by PABA·HI was achieved, and the PABA·HI-added PSCs yielded a PCE of 17.4% and retained 91% of the initial PCE when stored for 312 h at an RH of 75%.[227] In a relevant approach, a trace amount of surface-anchoring alkylamine ligands (AALs) with different chain lengths were used as perovskite GB and interface modifiers in PSCs.[228] Long-

View Article Online
DOI: 10.1039/D1EE00062D

chain AALs added to the precursor solution resulted in a prominent (100) orientation, suppressed non-radiative recombination and improved the optoelectronic properties of mixed-cation mixed-halide perovskite films. The AAL modified films exhibited high carrier mobilities and long carrier diffusion lengths combined with suppressed surface and GB defects density. Their work function (W_F) was significantly decreased, indicating an effective n-doping process and more efficient electron transport due to the change of the perovskite's surface termination upon AAL modification. These led to a certified stabilized PCE of 22.3% (23.0% for lab-measured cells) and stable cell operation for over 1000 h.

Moreover, low-dimensional perovskites (e.g. perovskite quantum wells, PQWs) with organic ligands were also utilized to protect the perovskite from degradation and improve PSC stability. Instead of employing van der Waals bonding between hydrophobic organic moieties of short-chain ligands to stabilize PSCs' perovskite interfaces, a chemically reactive ligand, namely 4-vinylbenzylammonium, was used to create well-ordered PQWs atop a 3D perovskite layer.[229] The ligand's vinyl group was photochemically activated with UV light to form new covalent bonds among PQWs. UV-cross-linked 2D/3D devices showed improved operational stability and storage stability in the air with only a 10% loss of efficiency after 2300 h of dark ageing combined with an enhanced PCE of up to 20.4% and reduced hysteresis.

3.2.4 GB and surface co-passivation approaches. Simultaneous passivation of GBs and the fabricated perovskite films' surface is a practical approach that enables significant performance and stability enhancement in the perovskite solar cells. A universally applied double-side polymer-enabled GB defect passivation approach using ultrathin PMMA films resulted in exceptionally high-efficiency (~20.8%) PSCs with one of the highest V_{OC} (1.22 V).[230] This was attributed to

View Article Online
DOI: 10.1039/D1EE00062D

molecular interactions between different perovskites and PMMA, with the carbonyl (C=O) groups on PMMA being solely responsible for the excellent passivation *via* Lewis-base electronic interactions with Pb^{2+} ions and the significant concomitant reduction in non-radiative recombination.

In a different approach, the number of GBs could be effectively reduced by merely introducing an appropriate (10 mol%) concentration of formamidinium (FAI) and chloride ($PbCl_2$) ions into the $MAPbI_3$ precursor solution.[231] Inverted PSCs with larger grains and fewer GBs achieved a champion efficiency of 19.6% due to suppressing the rate of nonradiative recombination and lowering the trap state density. The synergy of the FA^+ and Cl^- ions led to a GB soldering process, which was highly beneficial to PCE enhancement. A similar strategy was followed by Xia *et al.*, who proposed a novel chemical sintering with an NH4SCN solution as a fast (<1 min) and effective process to substantially reduce GB defects in different films of different PbI_2-templated perovskites.[232] Optimal sintering yielded PSCs with PCE of 19.68% with a 20% loss over 720 h in ambient air. Liu *et al.* further advanced GB engineering by proposing the construction of surface "patches" formed at the GBs via in situ conversion of residual PbI_2 upon methimazole (MMI) treatment.[233] The MMI–PbI2 complex's working mechanisms were the effective suppression of ion migration and the resulting passivation of GBs accompanied by an improved film quality and enhanced carrier transfer. As a result, MMI-treated PSCs exhibited a PCE of 20.10% with negligible hysteresis and prolonged lifetime, retaining ~80% of the initial efficiency after 672 h continuous illumination. Concerning simultaneous GB and surface or interfacial defect passivation, recent efforts have focused on additive-based approaches. For example, GBs reduction and $MAPbI_3$ surface passivation could be induced by a guanidinium thiocyanate (GITC)-assisted Ostwald ripening post-treatment.[234] Formation of micron-sized grains

View Article Online
DOI: 10.1039/D1EE00062D

and an enhanced interfacial recombination resistance with one order of magnitude longer carrier lifetime along with a more favourable energy level alignment with the adjacent SnO_2 ETL led synergistically to PSCs with an enhanced PCE and mitigated hysteresis. Successful GB and interfacial defect passivation were alternatively realized by employing KCl as an additive in the SnO_2 ETL.[235] Specifically, K and Cl ions passivated the interfacial defects, whereas, meanwhile, K^+ ions diffused through the perovskite film and passivated the GBs. A notable enhancement of the PCE from 20.2% to 22.2% was readily achieved for the SnO_2-KCl modified PSCs.

Notably, compared with the widely applied polycrystalline perovskite thin films that need both GB and surface co-passivation approaches, single crystal perovskites present no GBs, indicating that they only require surface passivation methodologies.[236] As a result, despite having being recently investigated, they show great potential for solar cells with high efficiency and stability especially when successful surface passivation approaches are also applied.[237-239]

4. Morphology and crystallinity control

The morphology of the perovskite film largely dictates the optoelectronic properties and, therefore, the performance of the fabricated solar cells. Morphology control represents an effective way to passivate defect states by obtaining highly crystalline, compact, pinhole-free perovskite films with optimized grain size and good substrate coverage. Several recent studies report on successful methodologies addressing the morphology engineering aspects, including a variation of the processing and post-treatment conditions, solvent annealing and solvent engineering approaches, gas-assisted deposition methods, use of self-assembled monolayers (SAMs), additive engineering, thermal annealing and some novel combinations. The compact, cohesive and highly crystalline perovskite films obtained with those methods result in enhanced PCE and improved long-term

View Article Online
DOI: 10.1039/D1EE00062D

stability as well as reproducibility of the ensuing PSCs.

4.1 Methods to modify perovskite film morphology

4.1.1 Enlarged grain size using additives. Enlarged perovskite crystal size and preferential orientation of perovskites represent an effective way to increase thin film crystallization, obtain high-quality perovskite films with fewer grains, GBs and trap states, leading to significant enhancement to both efficiency and stability of PSCs. To achieve these goals, various strategies have been intensively investigated in recent years. Precursor additives have been vastly explored as a morphology/crystallinity modifiers as they modify the colloid distribution in the perovskite precursor and the coordination ability of lead cation and iodide anions present in the perovskite matrix through the formation of coordination bonds (i.e. hydrogen bond interactions) as these additives are incorporated within the perovskite lattice. The incorporation of hydrophobic sulfur (S) based ionic materials have been successfully employed in PSCs as morphology modifiers resulting in significant enhancement of the device performance.[240] Moreover, the addition of solid iodine (I_2) as precursor additive in a mixed-halide perovskite solution resulted in achieving large crystalline grain perovskite films with an optimized composition (i.e. homogeneous dispersion of $MAPbCl_3$ and $MAPbI_3$ throughout the film) and in improved efficiencies from 9.83% to 15.58%.[241] Treating perovskite films with various iodide/chloride solutions or incorporating them into the precursor solutions led to different composition perovskite films with large grain sizes.[242-245] For example, MA^+-free FA^+ and Cs^+ mixed-cation perovskite thin films with micrometre-sized grains were fabricated upon treating the perovskite films with fluorinated ammonium iodide {4-fluoro-phenethylammonium iodide (4F-PEAI)} solution. This resulted in the formation of thin 2D $(4F\text{-}PEA)_2PbI_4$ films on the surface with a significant improvement in PL intensity and enhanced

View Article Online
DOI: 10.1039/D1EE00062D

PCEs of 20.6% and 18.5% during reverse and forward scanning, respectively, compared to 18.6% and 17.0% for the untreated devices.[242] Introduction of an optimized 3% concentration of caesium iodide to the precursor solution had a considerable effect on the morphology and optoelectronic properties of $MAPbI_3$-based perovskite films. A high-quality, defect-free, smooth perovskite film with a large grain size of ~1.8 mm was obtained, enabling the demonstration of mesoscopic $MAPbI_3$ PSCs with a PCE of ~19%, negligible hysteresis and enhanced stability under ambient conditions.[243] Addition of guanidinium iodide into the perovskite precursor solution enabled the formation of high-quality perovskite films which endowed the ensuing PSCs with a reproducible photovoltage of 1.20 V. This was attributed to suppression of both non-radiative recombinations and interfacial charge accumulation.[244]

The influence of a chloride-anion based surface treatment using a perovskite precursor (MACl) acetonitrile solution to obtain high quality, homogeneous $MAPbI_3$ films was examined by Uribe *et al*. MACl treatment had a dominant effect on increasing the grain size, passivating defects at GBs, enhancing crystallinity and improving PSC performance.[245] Perovskite film treatment with hydrophobic fluorinated aliphatic amine hydroiodide compounds led to larger perovskite grains, a decreased number of GBs, suppressed carrier recombination and accelerated electron transfer. Thus, PCE of the amine-modified PSCs increased from 12.23% to 13.88%, maintaining this value by ~85% after exposure to 50% RH for 10 days due to the enhanced film hydrophobicity.[246] Addition of hydrohalic acids to the perovskite precursor solution initiated the dissolution of the lead polyhalide colloids present that provided nucleation sites for the perovskite crystallization, critically impacting morphology, crystal quality, and optoelectronic properties of a formamidinium–caesium mixed-cation lead mixed-halide perovskite (**Figure 11 a-d**).[247] Solution ageing time could control colloids' size and dispersion in the precursor solution, whereas highly

View Article Online
DOI: 10.1039/D1EE00062D

ordered, and textured crystals were observed for films prepared from solutions with lower colloidal concentrations. As a result, an increase in the grain size, crystallinity, and texture could be achieved along with a two-fold increase in carrier mobilities leading to a PCE of 18.8%.

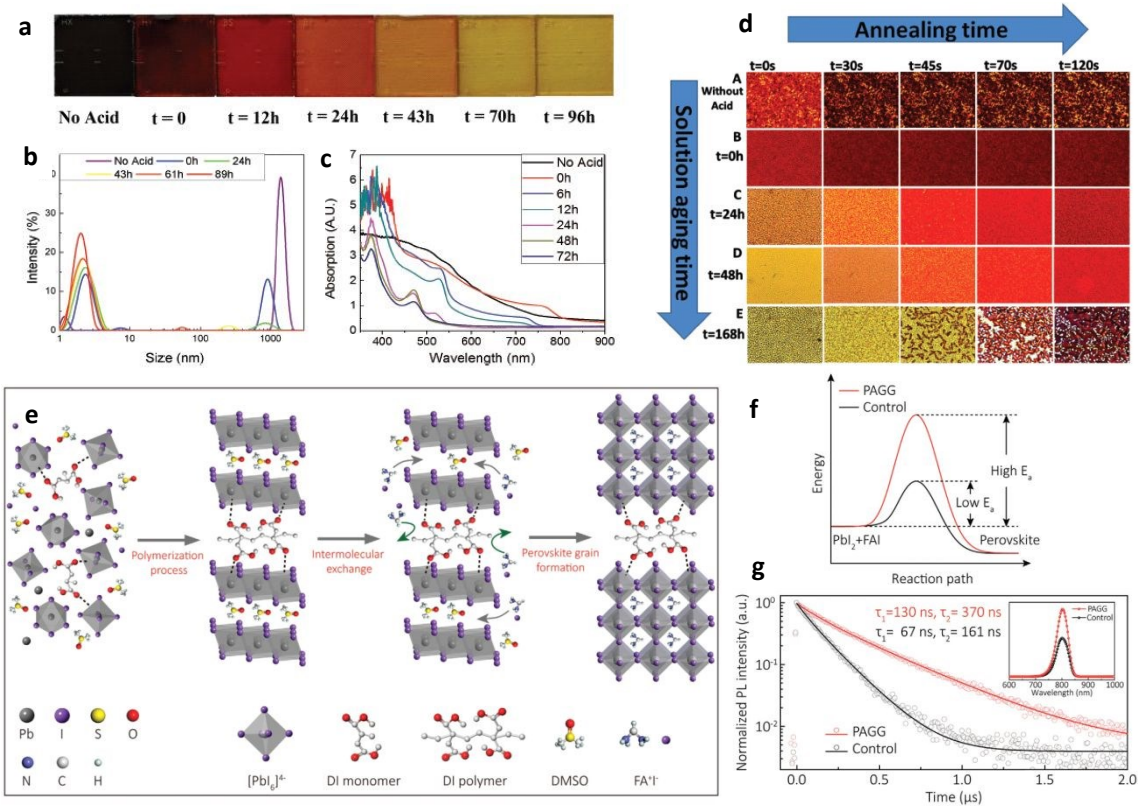

Figure 11. Impact of colloids in the precursor solution on the nucleation stage of the $FA_{0.83}Cs_{0.17}Pb(Br_{0.2}I_{0.8})_3$ perovskite. (a) Photographs of thin films spin-coated and dried at 70 °C under N_2, prepared with solutions aged in an N_2 atmosphere for various periods after the addition of hydrohalic acid. (b) Colloidal hydrodynamic size distribution via dynamic light scattering of different perovskite solutions. (c) Ultraviolet-visible absorbance spectra of pristine and acid-modified perovskite thin films. (d) Growth kinetics of the $FA_{0.83}Cs_{0.17}Pb(Br_{0.2}I_{0.8})_3$ perovskite system with various colloid concentrations. Microscopy images of postnucleation thin films heated at 220 °C in air prepared using precursor solutions aged with acid for a while. (A-E) Precursor solution aged for 0 hours without hydrohalic acids (A), 0 hours with the addition of acids (B), 24 hours (C), 48 hours (D), and 168 hours (E).[247] Copyright 2017, John Wiley and Sons. (e) Schematic illustration of polymerization-assisted grain growth (PAGG) process and the binding energies between additives and PbI_2 molecules. (f) Schematic diagram of perovskite crystallization kinetics of PbI_2 films without (black) and with (red) PAGG process. (g) Time-resolved PL spectra (Inset: steady-state PL spectra) of the perovskite films without (black) and with (red) PAGG process.[249] Copyright 2020, John Wiley and Sons.

View Article Online
DOI: 10.1039/D1EE00062D

In a different approach, glucose was introduced in $MAPbI_3$ to realize high-quality films, decreased defect density, enlarged grain size and a reduced amount of grain boundaries. PCE of inverted planar PSCs increased from 17.53% to 20.15%, accompanied by excellent reproducibility, suppressed hysteresis and enhanced stability in heat, light and moisture conditions.[248] In a drastically different method, the addition of small dimethyl itaconate (DI) monomers into the PbI_2 precursor solution triggered a polymerization-assisted grain growth during the PbI_2 film annealing. During this process the bulkier polymers formed anchored on the GBs, effectively passivating under-coordinated lead ions and reducing the defect density (**Figure 11 e-g**).[249] As a result, a champion PCE of 23.0% was obtained in $FA_{1-x}MA_xPbI_3$ PSCs, together with a longer lifetime where 85.7% and 91.8% of the initial PCE remained after 504 hours continuous illumination and 2,208 hours shelf storage, respectively. Furthermore, aniline[250], benzylamine[144] and phenethylamine[144] additives incorporated into the perovskite solution favour perovskite film quality.[144,251] In that case, the degree of hydrophobicity arising from the aromatic group and the packing of the molecular additive (i.e. formation of *j*-aggregates) was the critical mechanisms for improved overall PSC performance. Another small molecule, pyrrole, was introduced into caesium containing triple cation perovskite precursor solution.[251] It was demonstrated that pyrrole controlled the resulting film crystallinity and surface roughness, improved crystal quality, reduced trap density, and non-radiative recombination. The working mechanism combines its nitrogen atom with the lead-iodine (Pb-I) framework by either coordinating with the Pb ions or forming hydrogen bonds with the perovskite organic cation. Pyrrole-modified PSCs showed a high PCE of 20.07%, stabilized for more than 30 days storage at 10% RH. Recently, Liu *et al.* demonstrated an improved perovskite film quality by adding methylamine (MA) into the precursor solution.[252] MA effectively passivated shallow electronic defects present at GBs, increasing carrier lifetime, upon

View Article Online
DOI: 10.1039/D1EE00062D

molecular cross-linking on the perovskite grains through intense hydrogen bond interactions. Multiple functionalities of MA were unveiled; effective suppression of I_2 impurities, acting as a Lewis base coordinating to Pb(II) to restrict I-rich iodoplumbate complexes, thus avoiding the disturbance of Pb/I stoichiometry, and interference with the film growth, leading to larger grains. Consequently, MA-treated PSCs reached an increased PCE with a peak value of 20.02%. Introduction of the bivalent alkyldiammonium cation ethylenediamine (EDA^{2+}) into the perovskite ($MA_{0.7}FA_{0.3}PbI_3$) film was found to form a triple cation perovskite $(MA_{0.7}FA_{0.3})_{1-2x}EDA_xPbI_3$ as a light absorber.[253] PSCs fabricated with the optimized absorber with the composition $(MA_{0.7}FA_{0.3})_{0.97}EDA_{0.015}PbI_3$ (x = 1.5%) achieved a PCE of 20.01% with negligible hysteresis. More importantly, the devices retained 96% of their initial efficiencies after 25 days of storage in an ambient atmosphere. Conjugated large-volume amines such as 3-phenyl-2-propen-1-amine (PPA) were later introduced in solution in formamidinium tin iodide ($FASnI_3$) perovskite. The corresponding films showed an enlarged grain size, reduced trap density, preferential crystal orientation and enhanced structural stability. Efficient, self-healed, PSCs with negligible hysteresis and highly robust stability (maintaining 92% of the initial PCE after 1440 h) were demonstrated.[253] Incorporation of bilateral alkylamine (BAA) additives and the associated anchoring of monolayer bilateral amino groups also led to surface defect passivation and enhanced stability by exposing the linking hydrophobic alkyl chain.[254] A PCE of 21.5% with a record-small V_{OC} deficit of 0.35 V and an improved device shelf lifetime to >1000 hours and operational stability to >500 hours under light, with 90% of the initial efficiency retained, were achieved.

Hydrogen halogens, such as hydroiodic and hydrobromic acids, have been shown to significantly affect the perovskite morphology by dissolving large perovskite particles into smaller ones with a more uniform distribution.[255] As an example, Heo *et al.*, fabricated uniform perovskite

View Article Online
DOI: 10.1039/D1EE00062D

films by introducing HBr to the precursor solution.[256] Inclusion of HBr aqueous solution in a $MAPbBr_3$ DMF solution retarded the nucleation time during the spin-coating process due to the improved solubility. It resulted in dense perovskite films with higher surface coverage. Accordingly, planar HBr-modified $MAPbBr_3$ PSCs exhibited the highest PCE with decreased hysteresis.

Additive-assisted perovskite crystal growth employing oxalic acid (OA) with two bifacial carboxylic acid groups into the perovskite precursor solution was also successful. It facilitated the crystallisation process's modulation leading to increased grain size, reduced GBs and trap states. Subsequently, OA-modified cells reached an enhanced PCE and demonstrated greatly enhanced thermal stability as they retained 70% of the initial efficiency after 19 hours.[257] Similarly, Huang *et al.* employed hydrobromic acid to assist the crystallization and improve the surface coverage of $MAPbI_{3-x}Cl_x$.[258] As a result, a superior quality perovskite layer with fewer pinholes and lower surface roughness was obtained, which led to improved and stabilized PSC performance.

A series of organic halide salts having different organic cations and halide anions to control the perovskite film morphology and crystallinity were also employed as additives in PSCs. For example, organic halide salts with other bulky aromatic organic cations and halide anions were applied as processing additives in a $MAPbI_{3-x}Cl_x$ perovskite film. It was shown that both the perovskite film's morphology and crystallinity were critically dependent on the organic halide salts' types and concentrations. Among them, tetraphenylphosphonium iodide (TPPI) and chloride (TPPCl) were the most efficient in improving the film crystallinity, and surface coverage I^- and Cl^- anions chelated to the Pb^{2+} cations affected the kinetics of film formation. Consequently, the PCE reached ≈11.5% for the additive-enhanced cells.[259] Upon incorporation of 5 mol.% *n*-propylammonium iodide (PAI) in a $FA_{0.79}MA_{0.16}Cs_{0.05}PbI_{2.5}Br_{0.5}$ perovskite film, a two-

View Article Online
DOI: 10.1039/D1EE00062D

dimensional $(PA)_2PbI_4$ with the Ruddlesden−Popper perovskite was formed through the reaction between PAI and PbI_2.[260] Furthermore, fewer −COOH (carboxyl) groups were present on the perovskite film surface containing $(PA)_2PbI_4$, indicating the suppressed penetration of oxygen and moisture into the perovskite. In contrast, the film also exhibited greatly enhanced hydrophobicity and an upshift of its conduction band minimum by 0.16 eV, leading to a more favourable interfacial energy alignment. Consequently, an improved PCE of up to 17.23% with suppressed hysteresis was obtained in PSCs that retained ~50% of the initial efficiency after 2000 hours in the air under 45% RH.

Tetrabutylammonium bromide (TBAB) addition into the perovskite ($CsPbI_{2.4}Br_{0.6}$) precursor solution also induced a larger grain size and increased crystallinity films.[261] The fabricated PSCs exhibited a PCE of 15.21% while also retained over 93% of this efficiency upon storage in N_2 for 1600 hours. Alternatively, a multifunctional 1,6-diaminohexane dihydrochloride (1,6-DD) additive was introduced into the precursor solution.[262] A small amount of this additive modulated crystallization dynamics and yielded films with enhanced crystallinity and enlarged grain size. Notably, its two terminal $-NH_3^+$ groups passivated the vacancy defects at the perovskite crystal surface, suppressing charge recombination and facilitating charge transport. In contrast, its hydrophobic hexane alkyl chains increased the moisture resistance of the perovskite film. Furthermore, adjacent crystal surfaces were linked through the additive hexane alkyl chain, thus enhancing the interaction between perovskite grains and anchoring the perovskite film's microstructure. The modified cells' PCE was improved by 20%, while the efficiency maintained to above 90% of the initial value after exposure to air for 16 days. Meanwhile, simpler chloride molecules, like $PbCl_2$, MACl, FACl, and CsCl that bear Cl^- anions, also enabled effective passivation or doping of the perovskite material. Chlorine anion was shown to alter thin film morphology and crystallisation, providing larger grains

View Article Online
DOI: 10.1039/D1EE00062D

with smooth discontinuities around them.[263]

Introduction of the lead thiocyanate $Pb(SCN)_2$ additive up to 2 mol% concentration in a DMF precursor solution improved the mixed-cation lead mixed-halide crystallinity $FA_{0.8}Cs_{0.2}PbI_{2.68}Br_{0.32}$ perovskite and, overall, enhanced film quality by increasing grain-size, lowering the number of pinholes, and reducing trap density.[264] $Pb(SCN)_2$-modified PSCs showed a high PCE with reduced hysteresis and remarkably high moisture stability, maintaining ~85 % of their initial efficiency in the ambient environment (~60 % RH) after 45 days. Similarly, $Pb(SCN)_2$ additive combined with DMF annealing markedly increased the grain size of the mixed-cation lead mixed-halide ($FA_{0.8}Cs_{0.2}Pb(I_{0.7}Br_{0.3})_3$) perovskite thin films from 66 nm to 1036 nm with a 3-fold increase in carrier lifetime while avoiding excess PbI_2 formation. As a result, the device exhibited an enhanced as well as stabilized PCE.[265]

Recently, a simple novel approach was proposed by Bai *et al.* regarding the practical use of ionic liquids (ILs) as additives in PSCs for the first time.[266] In particular, incorporating 1-butyl-3-methylimidazolium tetrafluoroborate ($BMIMBF_4$) in a perovskite precursor solution led to the formation of lead halide/imidazolium halide complexes, enhanced crystallinity and reduced defects in the corresponding films. IL-modified p-i-n planar heterojunction $(FA_{0.83}MA_{0.17})_{0.95}Cs_{0.05}Pb(I_{0.9}Br_{0.1})_3$ PSCs exhibited outstanding long-term operational stability, as manifested by a decrease in performance of only ~5% for encapsulated devices under continuous illumination for more than 1800 hours at ~75 °C, and a high PCE of 19.8%. Another promising approach was introducing a stoichiometric amount of tropolone as a chelating agent for the lead, which facilitated the growth of a uniform mixed cation perovskite layer with excellent surface coverage. More specifically, tropolone was found to be present only during the colloidal liquid phase while absent from the perovskite film during its formation due to its unique characteristics

View Article Online
DOI: 10.1039/D1EE00062D

of low melting and boiling temperatures. Devices with a maximum PCE of 20% were demonstrated, a 25% increase concerning the reference cells.[267]

Other highly encouraging approaches include the use of graphene,[268] nanoparticles[269] and polymer-based additives.[270,271] Specifically, the addition of graphene oxide (GO) in the precursor solution led to improved quality $MAIPbI_3$ films.[268] 1 vol.% of GO was found to modulate the perovskite film growth by increasing the grain size and film uniformity and enhance film crystallization with preferential out-of-plane orientation. GO-modified n-i-p planar heterojunction PSCs showed an enhanced PCE with reduced hysteresis. Introduction of $CsPbBr_3$ nanoparticles (NPs) into the chlorobenzene antisolvent allowed them to act as nucleation centres in the $MAPbI_3$ film growth process and considerably improved its quality in terms of film morphology and crystallinity, leading to reduced recombination and improved charge transfer.[269] Furthermore, they induced the formation of a $Cs_{1-y}MA_yPbI_{3-x}Br_x$ passivation layer on top of the perovskite layer, resulting in a much improved device performance with a PCE of 20.46% along with enhanced stability (**Figure 12**).

Nanostructures, such as $BiFeO_3$ (BFO) oxide perovskite one, incorporated as an additive in $MAPbI_3$ during the spin-coating of the precursor solution were shown to serve as heterogeneous nucleation sites during the crystal growth of $MAPbI_3$ film and, as a consequence, increased the perovskite crystal grain size, the film crystallinity and its uniformity.[270] As a result, the trap density decreased, while the charge carrier mobility and electron diffusion length increased, leading to significant enhancement in J_{SC} and the corresponding PCE. Incorporating sulfonated carbon nanotubes (s-CNTs) in the $MAPbI_3$ perovskite precursor solution resulted in several MAI molecules interacting with s-CNTs in the precursor solution and filling of the GBs during the spin-coating process. Upon heating of the film, this was followed by an increase of the grain size due

View Article Online
DOI: 10.1039/D1EE00062D

to the continuous evolution of the perovskite grain growth.[271] Meanwhile, solution-processed electron buffer layers such as PCBM among others could be used to assist in the growth of compact overlayer perovskite thin films. A stabilized PCE of 17.6% at the MPP with a V_{OC} of 1.11 V was obtained for PCBM-modified devices.[272]

On the other hand, polymer modifiers with different coordinating groups, such as poly(4-vinylpyridine) (PVP) were demonstrated to improve the electronic properties of the MAPbI3 films markedly and significantly enhance device PCE from 16.9% to 18.8% with a very high V_{OC} of up to 1.16 V as well as shelf lifetime up to 90 days (retaining 85% of the initial efficiency).[273] The mechanism behind this improvement was the changes of trap states which was highly dependent on the functional groups and their interaction with the perovskite. Pyridine group with high binding energy with Pb^{2+} was more effective in trap-state passivation than the carboxylic group with low coordination energy. Defect states could be effectively passivated by chemical groups that donate electron density, likely by sharing lone electron pairs with the empty 6*p* orbitals of under-coordinated Pb^{2+} sites. Another polymeric additive, namely polycaprolactone (PCL), was highly effective in enhancing the crystal grain size (>400 nm), reducing surface defects, ensuring uniform coverage and promoting the mechanical strength of entirely flexible PSCs.[274] PCL exerted a substantial effect on crystal growth as the carbonyl groups in PCL formed an intermediate adduct with Pb^{2+}. Champion cells exhibited a 38% enhancement in their PCE which was retained to ~90% of the initial value after 300 bending cycles.

A synergistic strategy involved combining two additives, MACl and MAH_2PO_2, in the perovskite precursor solution for practical, synergistic, grain size engineering.[275] MACl could enable preferential grain growth, increase the grain size and produce smoother films, while MAH_2PO_2 complimentarily suppressed non-radiative recombination at GBs. Together, they

View Article Online
DOI: 10.1039/D1EE00062D

promoted grain growth further, lowered trap density and increased carrier recombination lifetime, enabling an enhanced device performance in tandem cells. Furthermore, simultaneous incorporation of fluoride and iodide based additives (SnF_2 and GeI_2) also revealed their strong impact in trap passivation $FA_{0.75}MA_{0.25}Sn_{1-x}Ge_xI_3$ based PSCs by suppressing the oxidation of Sn^{2+} to Sn^{4+} and reducing trap state density, respectively.[276] As a result, a longer charge diffusion length (~1 μm) and lifetime were obtained, coupled with considerable carrier mobility and a PCE of 7.9%.

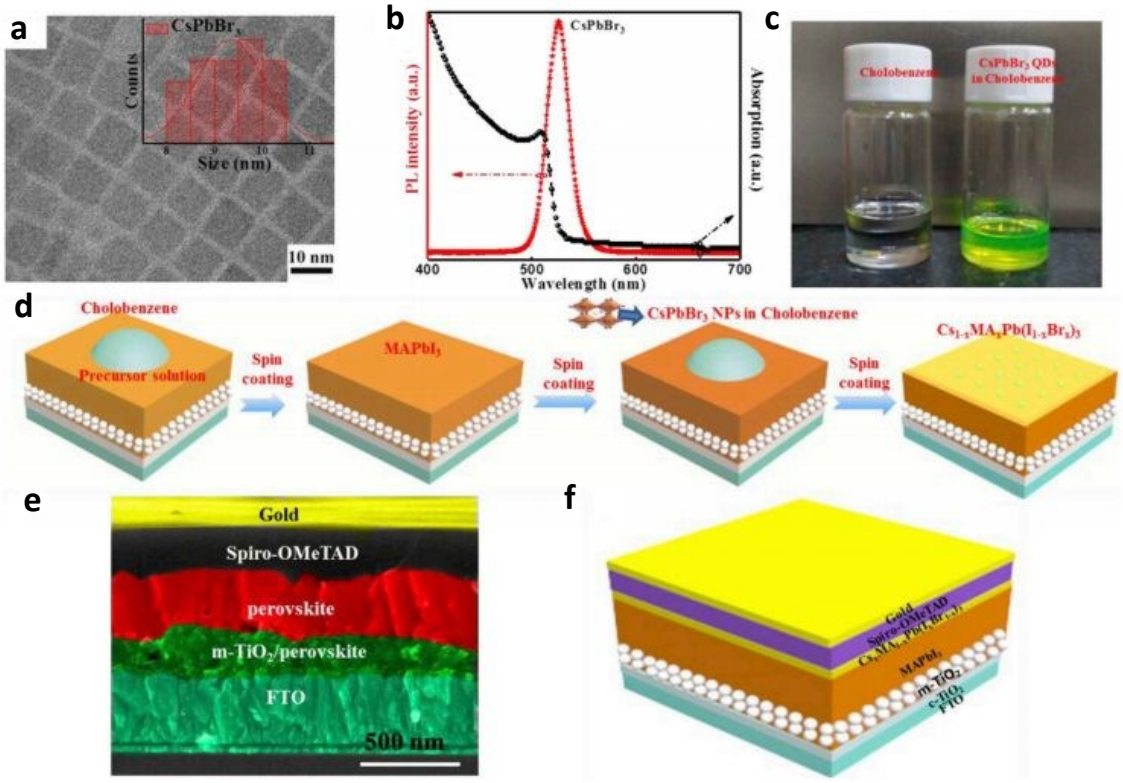

Figure 12. (a) Transmission electron microscopy (TEM) image of $CsPbBr_3$ nanoparticles. The inset shows the size distribution. (b) UV–Vis absorption spectrum (black line) and photoluminescence spectrum of $CsPbBr_3$ nanoparticles. (c) Photographs of the chlorobenzene solution without and with the $CsPbBr_3$ nanoparticles. (d) Schematic of the fabrication procedure of perovskite films incorporated with $CsPbBr_3$ nanoparticles. (e) Cross-sectional scanning electron microscopy (SEM) image and (f) illustration of the complete PSC architecture.[269] Copyright 2019, Elsevier.

View Article Online
DOI: 10.1039/D1EE00062D

4.1.2 Solvent annealing. $MAPbI_3$ grain cluster size can also be tuned via solvent annealing, whereas perovskite film crystallization and the crystal orientation are near related to the substrate's surface chemistry and wettability. Solvent annealing (SA) has been demonstrated as a highly effective passivation method for controlling perovskite defect states and promoting grain growth and crystal size and orientation, as precursor ions may diffuse over long distances presence of solvent during annealing. Hydrophilic surfaces were favourable for the growth of large perovskite grains that showed an order of magnitude lower trap densities than smaller ones. As a result, large cluster sizes led to longer charge recombination lifetimes and higher device V_{OC}.[277] Note that the concentration of the perovskite solution may have a massive impact on the crystallite size and the rotation speed during the spin-coating process can determine the layer coverage of the perovskite film.[278] Exposure of the complete PSCs to ambient air could be essential to obtain the highest PCE as, for example, in the case of methylammonium bismuth iodide (MBI) PSCs. For high-performance PSCs under ambient fabrication conditions, a novel pre-nucleation strategy was recently proposed in order to obtain a compact and uniform perovskite layer. Specifically, a programmed sample spinning and multiple antisolvent dripping methods to continuously form the $PbI_2 \cdot 2DMSO$ and $Pb_2I_4 \cdot 2DMSO$ complexes and thus prolong the nucleation of the intermediates preventing the water-assisted growth into a too large size was employed.[279] Conversion to a high-quality perovskite film could be simply achieved by heating or simply ageing at room temperature. Impressively, these PSCs achieved a highly reproducible PCE of 18.8% (more than a factor of 2 higher than the reference cells).

An organic solvent vapour atmosphere introduced during the spin-coating and formation of the perovskite film was proposed to alter $MAPbI_3$ crystal orientation and the grain size. It was found that 1,2-dichlorobenzene (DCB) and dimethyl sulfoxide (DMSO) vapour atmospheres were

View Article Online
DOI: 10.1039/D1EE00062D

more useful to obtain slightly more extensive and more oriented $MAPbI_3$ grains.[280] Both DCB and DMSO treatment reduced the trap density and oriented the perovskite grains resulting in a longer charge recombination lifetime and high V_{OC}, FF and PCE for PSCs (**Figure 13**).

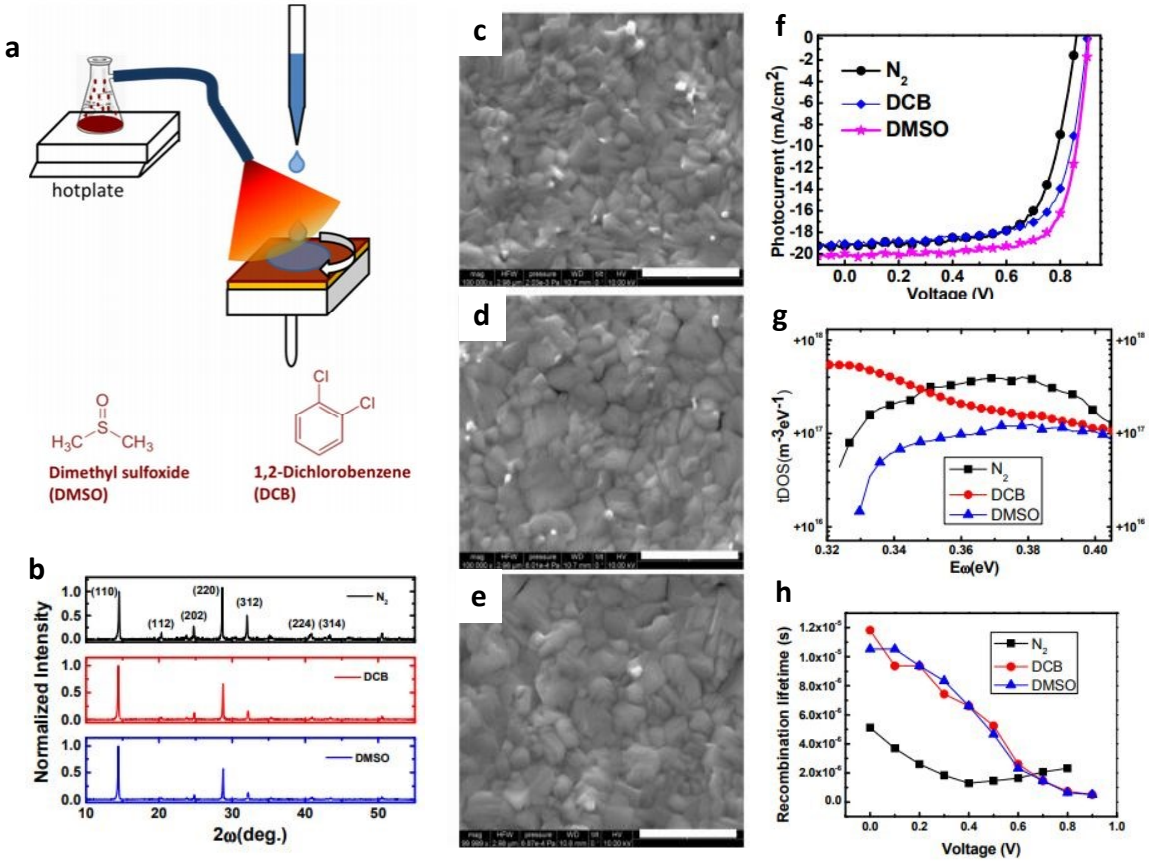

Figure 13. (a) Schematic illustration of the solvent annealing approach: solvent vapour was generated by heating DMSO and DCB solvents were directed by a tube to the film surface during the spin-coating process. The chemical structures of DMSO and DCB solvents are also shown. (b) X-ray diffraction spectra of perovskite films grown in N_2 and using the solvent annealing with DCB, and DMSO, respectively. Scanning electron microscopy (SEM) surface topography of perovskite films fabricated in the atmosphere of (c) N_2, (d) DCB vapour, and (e) DMSO vapour, respectively. The scale bar is 1 µm. (f) J-V characteristics taken under AM 1.5G illumination of PSCs fabricated under an atmosphere of N_2 and DCB, and DMSO vapours, respectively. (g) Trap-density of states measured with thermal admittance spectroscopy and (h) carrier recombination lifetime of the PSCs fabricated under different atmospheres.[280] Copyright 2015. the Royal Society of Chemistry.

Another approach focused on the SA of the PbI_2 precursor to facilitate its conversion to $MAPbI_3$. Only DMSO led to porous PbI2 films from the employed solvents, which aided the

View Article Online
DOI: 10.1039/D1EE00062D

complete conversion to the perovskite film with a larger grain size.[281] On the other hand, DMF, acetone and 2-propanol (IPA) resulted in dense PbI_2 films, which hindered the complete conversion to $MAPbI_3$. Efficiencies of up to 18.5% were obtained for the DMSO-SA films. Mixed solvent vapour annealing was introduced as an alternative method to improve the performance of PSCs. A DMF/CB mixed solvent (1:20, v/v) for 6 min was the optimal treatment to obtain very smooth, crystalline, $MAPbI_{3-x}Cl_x$ films and PSCs with an enhanced PCE combined with high reproducibility and stability.[282] Similarly, a mixed antisolvent (IPA) and solvent (DMF) (100:1,v/v) vapour environment could significantly improve the perovskite film quality, increase the grain size and the film crystallinity and, consequently enhance as well as stabilize the PCE of $MAPbI_3$ based PSCs.[283] The same treatment also led to highly efficient $MAPbI_{3-x}Cl_x$ cells with a PCE of up to 18.9% with improved storage stability. Other high boiling point solvents have also been highly successful in the SA treatment of PSCs. For example, a novel *g*-butyrolactone (GBL) solvent vapour post-annealing treatment on $MAPbI_3$ improved the complete transformation of PbI_2, increasing the crystal grain size and film crystallinity and reducing GBs. This effectively promoted charge dissociation and transport and boosted the performance of mesoporous $MAPbI_3$ PSCs, mainly due to the significant increase of the J_{SC}.[284] Alternatively, *n*-butanol was employed in a mixed MAI/IPA solution. The obtained perovskite films exhibited an enhanced density and absorbance and larger grain size as *n*-butanol prevented the fast solvent evaporation in the MAI/IPA solution. SA-modified $MAPbI_3$ PSCs reached an optimum stabilized PCE of 14.81%.[285] SA has also recently been extended to preparing novel, high-quality 2D perovskite films. For example, enhanced crystallinity 2D $(BA)_2(MA)_3Pb_4I_{13}$ thin films could be produced with denser, larger-crystal grains and increased carrier diffusion lengths, reaching promising device efficiencies.[286]

View Article Online
DOI: 10.1039/D1EE00062D

4.1.3 Template-induced film growth. In a different strategy, appropriate materials were used as templates to control perovskite film nucleation. For example, PMMA was recently used as a useful template to control perovskite nucleation and crystal growth. Polymer-templated heterogeneous nucleation and growth enabled smooth perovskite films of high quality with remarkably long photoluminescence (PL) lifetime to be obtained and stable PSCs with a PCE of 21.6% and excellent reproducibility to be realized.[287] PMMA was found to slow down the perovskite crystal growth by forming an intermediate adduct with PbI_2, allowing the randomly formed nuclei to adjust their orientation to minimize the total Gibbs free energy and grow in the thermodynamically preferred direction.

Wang *et al.* reported a templated growth mechanism of layered perovskites along the out-of-plane direction from 3D-like ones. This growth method enabled the achievement of enhanced carrier transport and improved PSC performance. The method involved incorporating additional ammonium halide salts in the precursor solution to suppress the nucleation of both layered and 3D perovskites inside the solution and force the film formation to start from the solution surface (**Figure 14**).[288] Fast drying of the solvent resulted in 3D-like perovskites which could surprisingly act as templates for the growth and nucleation of layered perovskites, enabled by the periodic corner-sharing octahedra networks on the surface of 3D-like perovskites and the lattice matching between layered perovskites and corner-sharing PbI_6 octahedra chains.

In another approach, addition of semiconducting single-walled carbon nanotubes (SWNTs) to perovskite films as additives functioned simultaneously as crystal growth templates and charge bridges between perovskite grains. SWNTs retarded the crystal growth and functioned as the cross-linker between perovskite grains.[289]

View Article Online
DOI: 10.1039/D1EE00062D

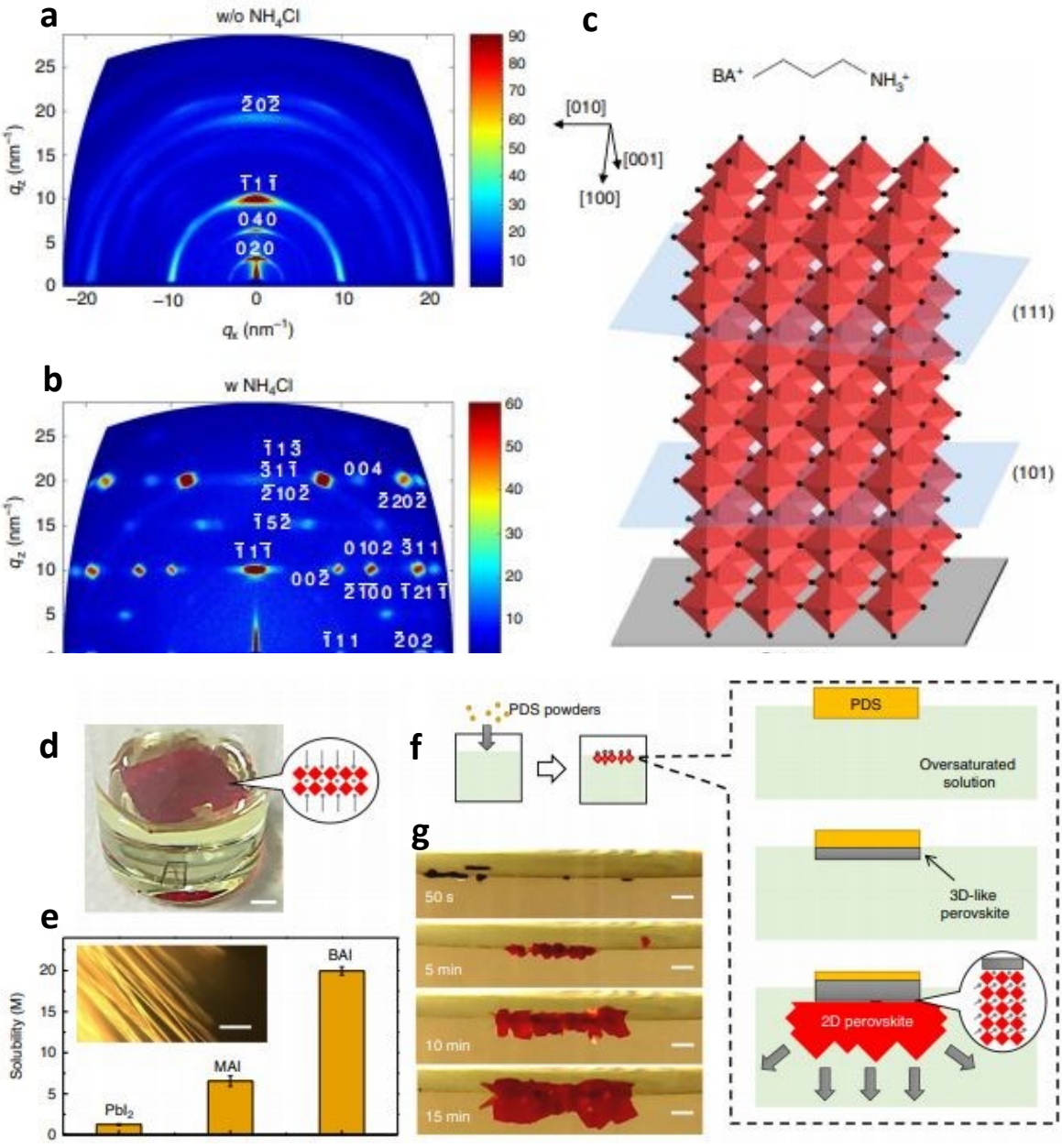

Figure 14. Template-assisted growth of perovskite films: GIWAXS patterns of butylamine (BA)-based perovskite films grown from precursor solution (a) without additive and (b) with NH_4Cl additive (in a molar ratio of NH_4Cl:PbI_2 equal to 1:2). (c) Illustration of the perovskite material in the film with out-of-plane orientation. The BA molecular structure is also shown. (d) Single crystals of $BA_2MAPb_2I_7$ were formed on the air/liquid interface upon slowly cooling the supersaturated solution. (e) Comparison of the solubility of MAI, PbI_2 and BAI in DMF solvent. The inset shows the first precipitation of PbI_2-DMF-contained solvate phases in BA-based perovskite precursor solution upon drying. (f) and (g) Process illustration and optical photos, respectively, of the directional growth of BA-based perovskite crystals upon spreading of PbI_2-DMF powder at the liquid surface of the oversaturated precursor solution. Reproduced with permission from ref. 288. Copyright 2020 Springer Nature.

View Article Online
DOI: 10.1039/D1EE00062D

Also, sodium deoxycholates attached to the SWNTs passivated the GBs by forming Lewis adducts.[290] As a result, more uniform perovskite films with larger crystal grains were obtained, and a high PCE of 19.5% was obtained. A soft template controlled growth method was proposed by introducing (adamantan-1-yl)methanammonium to control the nucleation and growth rate of $CsPbI_3$ crystals. This method produced smooth, pinhole-free, $CsPbI_3$ films with a crystal grain size on a micrometre scale, significantly reduced defect density and non-radiative charge recombination, and yielded PSCs remarkable efficiency of 16.04%, which retained 90% of the initial efficiency after 3000 hours of continuous illumination and heating.

The perovskite layer morphology can be effectively controlled by inserting appropriate interlayers underneath the perovskite absorber. For example, a hydrophilic groups (C-O and C=O) grafted buffer layer (HGGBL) deposited on the non-wetting hole transporting material (HTM) resulted to a significant reduction of the surface potential and surface tension force and found to serve as morphology modifier for the perovskite overlayer, thus facilitating the growth of large perovskite crystals. [291] In addition, the carbonyl groups tightly bonded with perovskite via Lewis base sites, inducing the formation of a compact, smooth, pinhole-free perovskite film with low bulk defect density. As a result, the fabricated inverted planar PSCs' photovoltaic performance was dramatically boosted with their PCE and reproducibility, additional merit of PSCs towards commercialization.

4.1.4. Colloidal engineering. Perovskite precursor solutions are generally colloidal dispersions, with a colloidal size up to the mesoscale, rather than real solutions. The soft colloid is made of a coordination complex in the form, for example, of a Pb polyhalide framework between organic and inorganic components, which can be structurally tuned by the coordination degree. Utilization

View Article Online
DOI: 10.1039/D1EE00062D

of coordination engineering by employing additional MA halide in excess of the stoichiometric ratio for tuning the coordination degree and mode in the initial solution, along with a thermal treatment for the release of excess MA halides, led to conformal coverage, preferential orientation, and high purity perovskite thin films of exceptional quality.[292] Furthermore, an excess organic component reduced the colloidal size and tuned the framework's morphology, whereas partial chlorine substitution accelerated the crystalline nucleation process. Combining colloidal chemistry and coordination engineering, planar PSCs with a PCE as high as 17% with suppressed hysteresis were demonstrated.

A simple treatment of the perovskite surface with various iodide, bromide or chloride-based perovskite solutions is an alternative method for controlling perovskite film quality.[293,294] For example, methylammonium bromide (MABr) solution treatment via spin-coating with an optimized concentration was highly effective in forming large-grain, pinhole-free, $MAPbI_{3-x}Br_x$ thin films, induced by the Br-related lower surface energy of perovskite crystallites facilitating a highly-selective Ostwald ripening process. High-efficiency PSCs based on compact $MAPbI_{3-x}Br_x$ films with a ~ 19% PCE and improved stability could be obtained.[272] Phenyltrimethylammonium bromide (PTABr) post-treatment notably stabilized $CsPbI_3$-based PSC performance by both gradient halide (Br) doping and surface organic cation passivation. The PTABr treatment significantly stabilized the perovskite phase and enhanced the PSC performance combined with improved stability (**Figure 15a**).[294] Surface treatment of β-$CsPbI_3$ films with choline iodide resulted in stable, highly crystalline, films upon surface trap state passivation with increased carrier lifetime and improved energy-level alignment in treated PSCs with stable efficiencies reaching 18.4% under 45°C ambient conditions.[24]

View Article Online
DOI: 10.1039/D1EE00062D

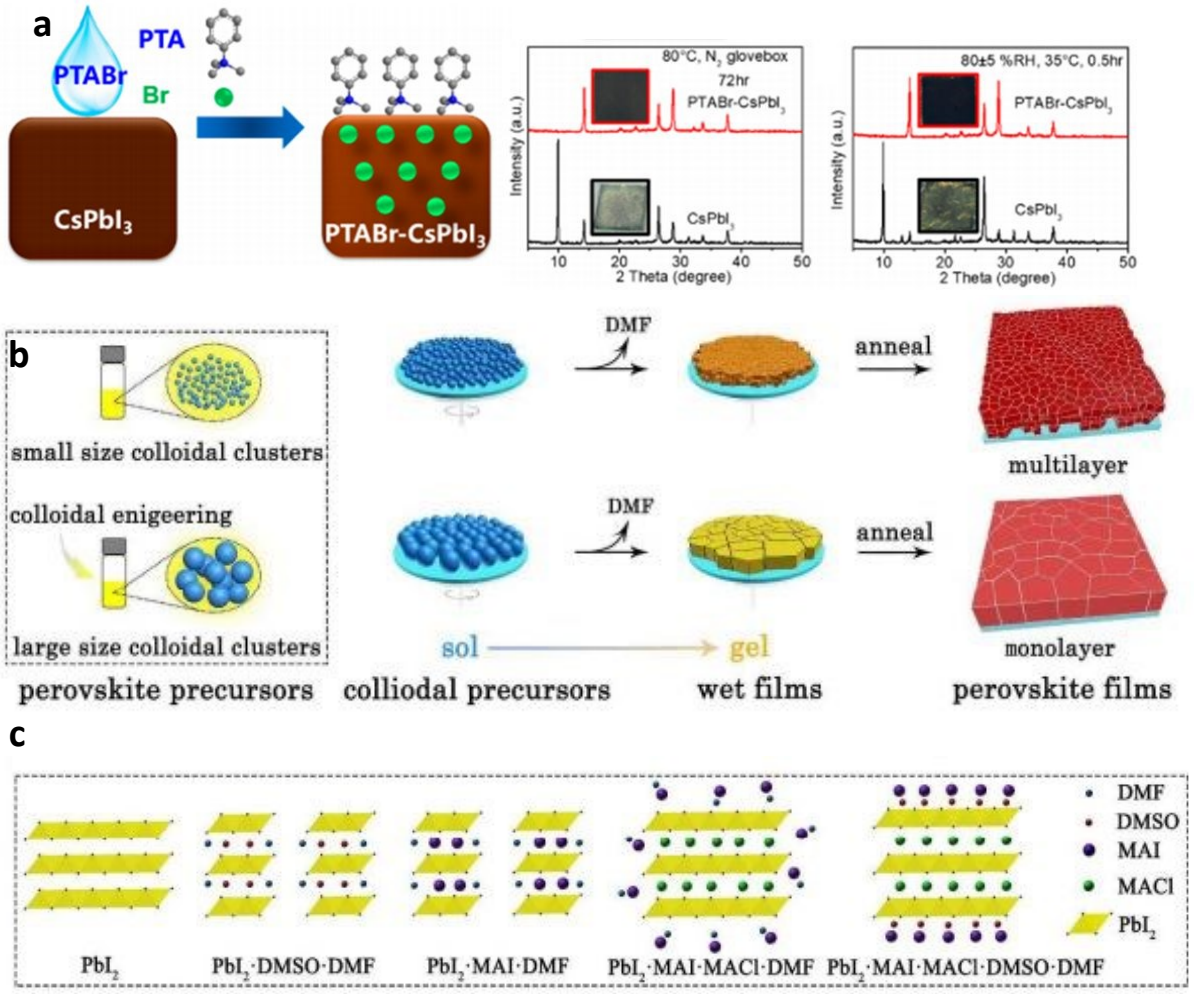

Figure 15. (a) Schematic illustration of gradient Br doping and PTA organic cation surface passivation on $CsPbI_3$ perovskite thin film (up). XRD patterns evolution of $CsPbI_3$ and PTABr-$CsPbI_3$ thin films heated in an N_2 glovebox at 80 °C for 72 hours (down, left) and PTABr-$CsPbI_3$ and $CsPbI_3$ thin films after exposed to 80 ± 5% RH at ~35 °C for 30 min (down, right). The insets show the corresponding photographs.[294] Copyright 2018, American Chemical Society. (b) Schematic illustrations of the formation of perovskite film from precursor solutions containing additives. (c) Scheme of the structures of colloidal clusters in different precursor solutions.[298] Copyright 2017, the Royal Society of Chemistry.

Meanwhile, control of the perovskite film surface chemistry by applying a series of postdeposition ligand treatments on polycrystalline $MAPbI_3$ thin films showed that a variety of Lewis bases acting as electron donors could markedly reduce non-radiative recombination, improve the bulk PLQE and increase the PL lifetime, ⟨τ⟩, with extensive enhancements

View Article Online
DOI: 10.1039/D1EE00062D

concentrated at GBs. Thin-film PLQE as high as 35% and ⟨τ⟩ as long as 8.82 μs at solar equivalent carrier densities using tri-*n*-octylphosphine oxide-treated films were demonstrated.[295] Further improvements have resulted in surface-treated $MAPbI_3$ thin films with excellent passivation, thus reaching a very high quasi-Fermi-level splitting of 97.1% of the radiative limit and an internal PLQE of 91.9% under 1 sun illumination intensity, which sets a benchmark for perovskites.[296] On the other hand, the colloidal clusters act as nucleation centres for growth and crystallization control of the perovskite, hence directly modulating the resultant film crystallization and morphology (**Figure 15b,c**).[297,298] Notably, through careful management of the colloidal precursor, highly reproducible and high performing (PCE >21% in devices based in presynthesized $FAPbI_3$) stable PSCs can be achieved.[299]

4.2 Control of perovskite film crystallinity

Precise control over the perovskite film crystallization process and its kinetics combined with uniform film formation and optimal surface coverage are highly critical factors to reduce trap density and boost fabricated devices' performance. It was previously demonstrated that nanoscale microstructural defects residing within individual grains of solution-processed $MAPbI_3$ thin films are responsible for undesired interfacial recombination. Co-annealing of the as-deposited $MAPbI_3$ layer with PCBM that served as the electron transporting layer (ETL) could markedly eliminate interface defects and improve intragrain crystallinity by facilitating a highly coherent crystallographic orientation within individual grains.[300] Compositional engineering of the perovskite absorber was also proven beneficial in providing superior crystalline quality films with fewer defects and enhanced photostability. For example, Cs incorporation within the efficient lead mixed halide perovskites significantly suppressed the unwanted halide segregation under photo-

View Article Online
DOI: 10.1039/D1EE00062D

illumination, the cause of high PSC photoinstability. Snaith and co-workers optimised the Cs content to obtain perovskite films with high crystalline quality and long charge-carrier lifetimes.[301] They showed that photo-induced halide segregation was significantly suppressed, leading to better device performance and superior photostability of the fabricated solar cells. In the following sections, we summarize recent advances in efficient control of perovskite films crystallinity to boost the overall PSC performance.

4.2.1 Crystallinity control through additives. The insertion of additives into the perovskite precursor solution has been found beneficial in terms of high crystallinity of the resultant perovskite film.[302] Different processing additives, such as 1,8-diiodooctane (DIO)[302] and diiodoperfluoroalkyl-based ones[303] could modulate the crystal growth resulting in the deposition of perovskite films with high crystallinity. A notable example regards bidentate halogenated additives, capable of temporarily chelating with Pb^{2+} ions during crystal growth, thus facilitating homogenous nucleation and altering the kinetics of crystal growth. The ultimate result was much smoother and continuous film surfaces and a high PCE (~19%) was obtained in $MAPbI_{3-x}Cl_x$ PSCs.[304] Addition of NH_4SCN into the perovskite precursor solution also resulted in perovskite films with an increased crystal grain size, lower trap-state density, enhanced crystallinity and carrier transport, leading to PSCs with a champion PCE of 19.36% for triple-cation perovskites.[305]

An effective acetate mediation strategy for significantly retarding the crystallization process and thus the phase transformation in $CsPbI_2Br$ perovskite was demonstrated via the addition of acetate like cobalt(II) acetate ($Co(Ac)_2$) or zinc acetate ($Zn(Ac)_2$).[306] The proposed mechanism involved the growth of the perovskite crystal following the Ostwald ripening mechanism at 270 ℃ annealing temperature, during which the acetate would be left out from GBs.

View Article Online
DOI: 10.1039/D1EE00062D

Both acetates led to forming a flat, dense and defect-free perovskite film and improved the device stabilized efficiency. Sub-micrometre swellable polymer colloid particles (i.e. microgels, MGs) were employed as additives to prepare uniform thin $MAPbI_3$ perovskite films. MGs promoted high quality, pinhole-free, film formation with improved coverage by acting as colloidal sponges, thereby delaying perovskite crystallization.[307] Moreover, Pb coordination by the MGs and passivation of $MAPbI_3$ was also noted, resulting in improved performance $MAPbI_3$ PSCs. A minimal amount (<0.1 wt%) of a non-volatile polymer additive, poly(ethylene glycol) tridecyl ether (PTE), could be incorporated into the perovskite precursor solution to control the film crystallization kinetics.[308] A smoother film surface was obtained, combined with suppressed charge recombination both among free carriers and between trapped and free carriers. These led to an improved PCE and enhanced electrical operational stability for $MAPbI_3$ PSCs. 2D-3D heterojunctions could be formed upon using a small amount of the organic halide salt ($DMEDAI_2$) for perovskite surface functionalization and modulation of crystallization, resulting in the formation of an ultrathin wide-bandgap 2D perovskite layer on top of the 3D $MAPbI_3$. Reduced surface defects and improved crystallinity led to PSCs with an exceptional PCE of ~20.2% and enhanced stability.[309]

Polymers have also been applied as crystallinity modulators/template growth in perovskite films. A thin layer of poly(ethylene oxide) (PEO), a well-known hygroscopic polymer, enabled highly stable PSCs during operation and in a humid atmosphere when coated on top of the perovskite film.[310] It was demonstrated that PEO chemically interacts with undercoordinated Pb ions on the perovskite surface, and thus passivates the corresponsing defect sites. In the presence of PEO, unencalsulated PSCs retained more than 95% of their initial PCE over 15 h illumination in ambient atmosphere. In addition, polymer passivation layers could enhance the device V_{OC}

View Article Online
DOI: 10.1039/D1EE00062D

when inserted at the perovskite–charge transport layer interfaces.[311] Similarly, an optimal amount of insulating polystyrene (PS) inserted in the perovskite precursor solution could also control film crystallization, improve surface coverage and result in smoother and more uniform perovskite thin films with larger grain size. PS-modified PSCs with a PCE exceeding 13% were realized along with improved stability.[312] Different self-doped organic and inorganic components were also found to regulate perovskite film crystallization and electrical properties. Typically, the organic components enhanced conductivity and reduced hysteresis, while the inorganic components could effectively promote crystal growth, reduce GBs and surface defects. However, a critical composition was required to benefit perovskite crystallization with enhanced crystal size and pinhole-free morphology. The corresponding mixed-cation PSCs achieved a high efficiency over 19.14% and good stability.[313] However, the size of perovskite crystallites could be decreased upon the addition of polymers such as polyethylene glycol (PEG), polyethyleneimine (PEI), poly(acrylic acid) (PAA) and polyvinylpyrrolidone (PVP) due to phase separation in the perovskite–polymer mixture.[314] Nevertheless, PAA highly suppressed the formation of hydrate perovskite phases, contributing to an improvement in the stability of perovskite films under humid air and ambient illumination. These results demonstrated that proper material choice to create a polymer-perovskite hybrid phase could significantly prolong the device lifetime.

4.2.2 Substrate controlled crystallization. The crystal growth process may be affected by external parameters, such as the substrate's wettability and roughness.[315] For example, replacing the commonly used TiO_2 bottom ETL in regular planar PSCs with lanthanum (La)-doped barium stannate ($BaSnO_3$) (LBSO) layer which, besides its high electron mobility and appropriate electronic structure, initiated better crystallization of the $MAPbI_3$ perovskite. As a result solar cells

View Article Online
DOI: 10.1039/D1EE00062D

with a steady-state PCE of 21.2% and remarkable photostability (they retained 93% of the initial performance after 1000 hours of full sun illumination) were fabricated.[316] Similarly, Yang *et al*., demonstrated the beneficial growth of $CsPbIBr_2$ films deposited on an indium sulphide (In_2S_3) ETL.[317] The reduced Gibbs free energy of the ETL surface promoted the formation of a compact, smooth and pinhole-free perovskite film with high crystallinity, which enabled good overall device performance. Tian *et al*., modified the surface wetting of the tin oxide (SnO_2) bottom ETL in regular planar PSCs by coating a hydrophobic amino-functionalized polymer film, PN4N, onto its surface.[318] With their method, the number of $CsPbI_2Br$ perovskite nuclei sites was significantly decreased, enabling larger crystals with fewer grain boundaries. The resultant perovskite film exhibited a high degree of crystallinity with low defect density, contributing to significant device performance improvement. Added to the merits, a high photostability was demonstrated for the fabricated cells, which retained more than 90% of the initial efficiency under continuous 1 sun illumination for 400 hours.

Besides altering the underlayer's wetting properties, the morphology and crystalline quality of the perovskite layer can be further controlled through adjustment of the substrate temperature. Zhang et al., demonstrated that by heating the substrate they could influence the crystallization process of a mixed cation mixed halide perovskite (in particular, $(FAPbI_3)_{0.85}(MAPbBr_3)_{0.15}$) through the formation of intermediate phases.[319] Their results showed that elevating the substrate temperature can modify the perovskite film morphology from a pure dendritic to a dendritic/island structure (**Figure 16**). The perovskite films with fewer islands also exhibited lower defect density and better device performance. Regarding more advanced perovskite structures, crystallization in the highly promising quantum well Ruddlesden-Popper phase halide perovskites could be controlled by managing their molecular stacking and crystal

View Article Online
DOI: 10.1039/D1EE00062D

orientation. For example, 2D $BA_2MA_3Pb_4I_{13}$ perovskites depicted an enhanced vertical crystal orientation on a PTAA HTL, resulting in polycrystalline films with suppressed charge recombination and p-i-n PSCs displaying a champion PCE of 14.3% with negligible hysteresis.[320]

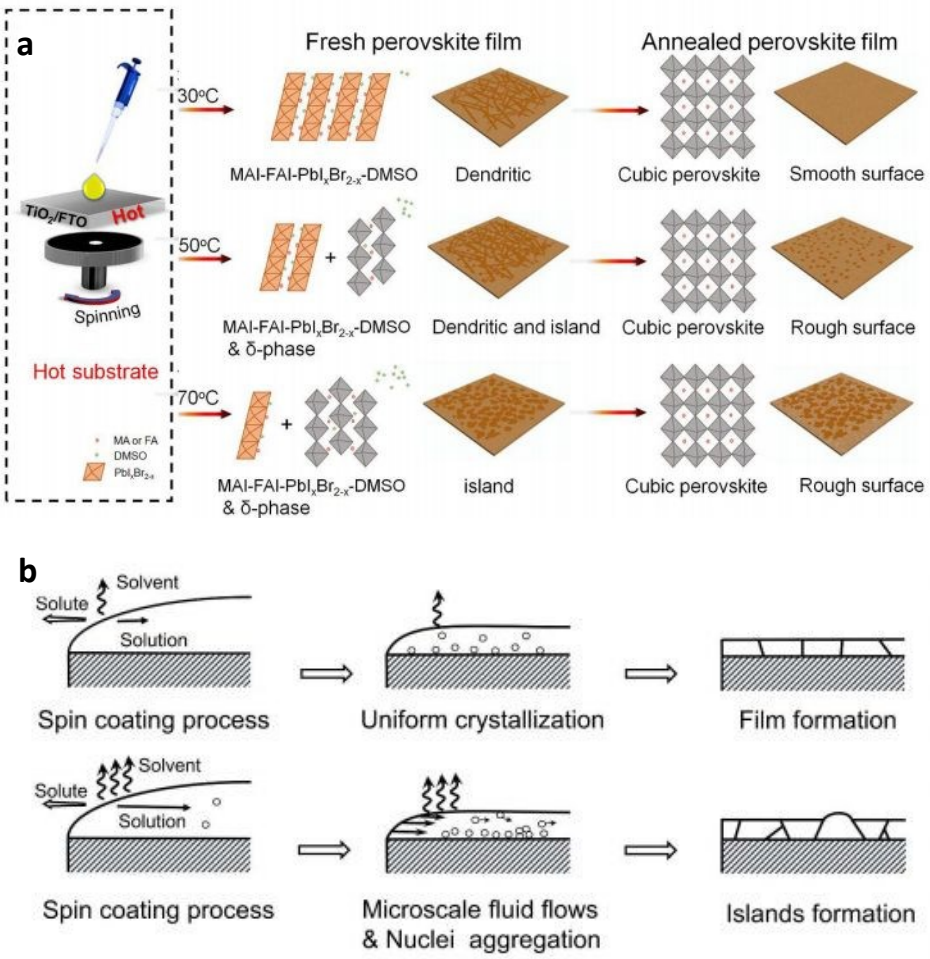

Figure 16. (a) Illustration of the substrate temperature controlled crystallization process of the perovskite films fabricated at different substrate temperature (30 °C, 50 °C and 70 °C). (b) Schematic diagram of the morphology evolution of the perovskite films fabricated at different substrate temperature.[319] Copyright 2019, the Royal Society of Chemistry.

4.2.3 Post-deposition treatments. Post-deposition treatments can also affect crystallization control. For example, the temperature and duration of thermal post-treatment are key factors

View Article Online
DOI: 10.1039/D1EE00062D

influencing the morphology, crystallization and optoelectronic properties of the resultant perovskite film. Post-annealing in a controlled (nitrogen) atmosphere played a decisive role in the crystallization and preferential orientation of perovskite films and improved PCE after optimizing the annealing time. Specifically, as-prepared films underwent a gradual transition from distinct, mainly precursor, crystalline structures into a highly ordered perovskite structure upon ramping the temperature followed by a re-crystallization process.[321] Very recently, an unprecedented low-temperature (<80 °C) and ultrafast microwave (MW) annealing process was employed to yield, upon optimization of the power and the irradiation time, uniform, compact, and crystalline formamidinium-cesium mixed-cation lead mixed halide perovskite films with excellent coverage and micrometre-scale grains.[322]

Another alternative growth method, termed vertical recrystallization, was proposed, which used methylammonium chloride (MACl) to obtain compact mixed-cation formamidinium perovskites with high crystallinity in a vertical orientation, thus minimizing vertical GBs and trap sites.[323] This yielded inverted-structure PSCs with an efficiency of up to 20.6% and light soaking and thermal stability as long as 500 hours. Additionally, a post-deposition reaction between a pre-existing perovskite film and methylamine (MA) gas has recently demonstrated the potential to improve film morphology and increase grain size drastically, boosting PSC performance.[324] Furthermore, Zhang et *al.*, employed a hot-air-flow (HAF) post-treatment method to control the crystallization of a $CsPb_2Br$ perovskite film.[325] They succeeded in uniform rapid heating of the perovskite layer which induced rapid volatilization of dimethyl sulfoxide (DMSO) in the vertical direction. In a different approach, Zai *et al.*, expanded the spin-coating time and were able to enhance precursor mass transport in bothdirections (horizontal and vertical) directions, hence achieving better crystallization of the perovskite $CsPbI_2Br$ film.[326]

View Article Online
DOI: 10.1039/D1EE00062D

4.2.4 Solvent engineering. Solvent engineering is a widely applicable method to control nucleation and crystallization dynamics in perovskite thin films and effectively passivate traps. It is based on the principle that, during film deposition, the excess solvent is not removed. Still, a small quantity remains and assists in forming chemical adducts with the perovskite precursors that regulate nucleation, grain size and film growth. By adjusting the evaporation rate of solvent, the crystallization rate of perovskite could be controlled, and homogeneous pore filling in the mesoscopic structure was successfully achieved, leading to a PCE of 16.26% in ternary-cation based mesoscopic PSCs.[327] A solvent-engineering approach successfully reduced the crystallization temperature of MAPbI3 single-crystal films (<90 °C) and in yielding improved crystalline quality grain-boundary-free, films with longer carrier lifetimes and carrier diffusion lengths. Following this approach, single-crystal inverted PSCs showed a markedly enhanced V_{OC} of 1.15 V and a PCE of up to 21.9%, among the highest reported for $MAPbI_3$-based cells.[328] Applying ethyl acetate (EA) as an environment-friendly solvent treatment led to a dramatic improvement in PSCs' performance, with PCE as high as 18% with good stability. EA improved film morphology and crystallinity and, under optimized conditions, led to the formation of a self-induced textured structure that was highly beneficial for increasing the interface area between the perovskite layer and the HTL, thus enhancing photogenerated current density without affecting interfacial recombination.[329] Similarly, acetic acid (Ac) was employed as an antisolvent in a one-step process to control perovskite crystallization (**Figure 17 a-d**).[330] Ac reduced the film roughness and the amount of residual PbI2 and exerted a chemical passivation effect from the electron-rich carbonyl group (C=O) in Ac, and regulated the perovskite film crystallization kinetics. PCEs of 22% and 23% were demonstrated for formamidinium-caesium mixed-cation lead mixed-halide

View Article Online
DOI: 10.1039/D1EE00062D

PSCs ($Cs_{0.05}FA_{0.80}MA_{0.15}Pb(I_{0.85}Br_{0.15})_3$) and ($Cs_{0.05}FA_{0.90}MA_{0.05}Pb(I_{0.95}Br_{0.05})_3$, respectively, with negligible hysteresis and markedly enhanced device stabilities, maintaining even up to 96% of the initial efficiency after 2400 hours storage in the ambient environment. It has also been recognized that the precursor solution ageing time, before casting into a thin film, is an essential factor that critically affects the crystal formation, surface uniformity, and the trap state density of the perovskite film and overall device performance.[331,332] Specifically, the precursor's progressive ageing for more than 24 hours dramatically promoted the efficient formation of larger crystals after the fast nucleation of smaller crystals. In contrast, hot-casting also led to the formation of perovskite films with superior crystallinity (**Figure 17 e-g**).[331]

The addition of formic acid significantly slowed down the degradation of dimethylformamide (DMF) involved in the precursor perovskite solution upon tuning the pH and hence the solution's colloid concentration.[332] As a result, improved crystallization and optoelectronic quality of the resulting perovskite films with larger domains and more highly oriented crystals occurred, leading to devices with a record low loss in potential from bandgap to V_{OC} of 0.36 V and PCEs of over 18% for $MAPbI_{3-x}Cl_x$ based PSCs and up to 20% for mixed cation, mixed halide PSCs. This study identified a strong correlation between DMF degradation, solution pH, and perovskite crystallization, illustrating a fundamental mechanism that significantly impacted perovskite film crystallization.

View Article Online
DOI: 10.1039/D1EE00062D

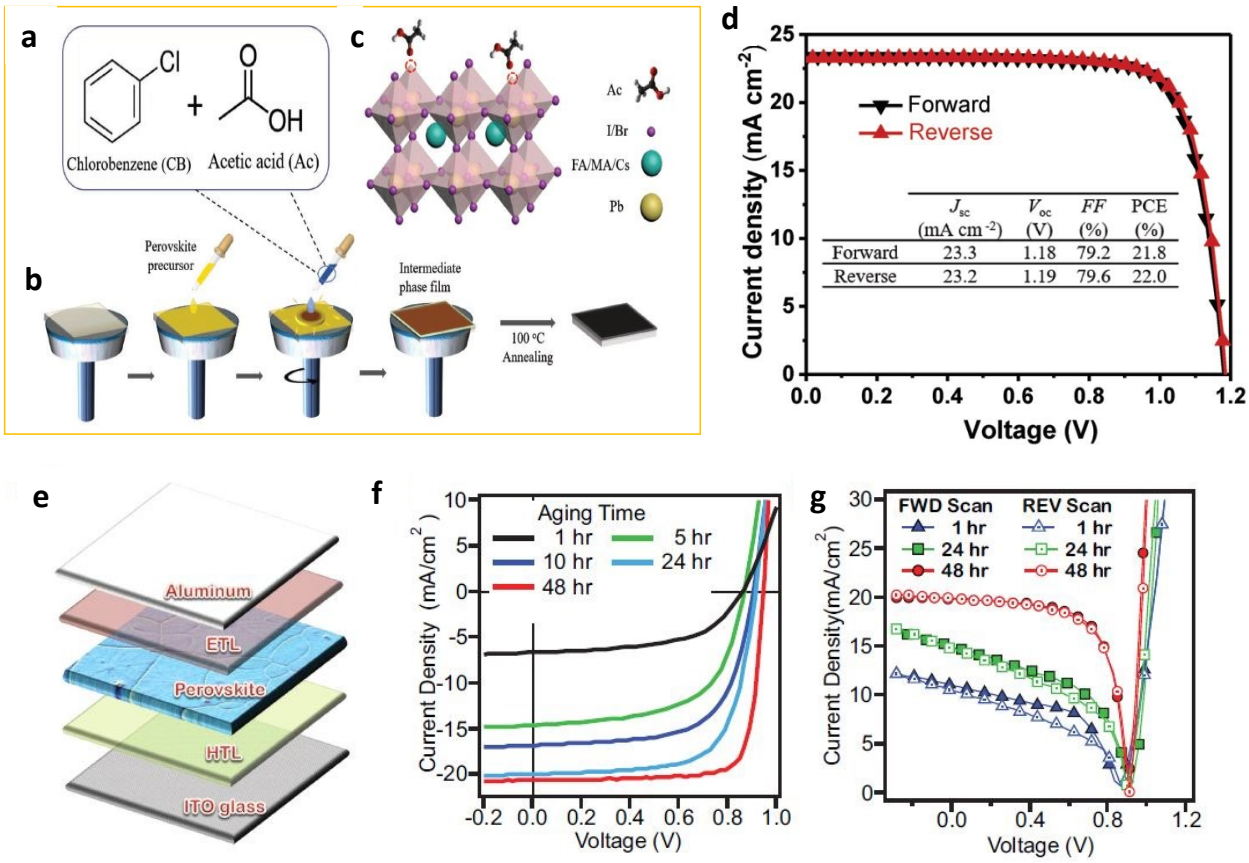

Figure 17. Acetic acid (Ac) assisted perovskite fabrication strategy and PSC performance. (a) Chemical structures of chlorobenzene and acetic acid (Ac). (b) Schematic illustration of the Ac assisted crystallization process. (c) Passivation of dangling bonds by Ac in the perovskite crystalline film. (d) Forward and reverse scan J–V curves of the best $Cs_{0.05}FA_{0.80}MA_{0.15}Pb(I_{0.85}Br_{0.15})_3$ PSCs.[330] Copyright 2020, John Wiley and Sons. Solar cell performance as a function of precursor solution ageing times: (e) Planar architecture of fabricated perovskite solar cells. (f) J–V characteristics and (g) hysteresis test of perovskite solar cells with different ageing times.[331] Copyright 2017, John Wiley and Sons.

Perhaps the most suitable solvent combination includes DMF and DMSO.[333-336] This appropriate binary selection resulted in the formation of dense, compact, pinhole-free films of the mixed halide $MAPb(I_{1-x}Br_x)_3$ (x = 0.1) hybrid perovskite with few GBs and grains with an average size of 450 nm and to the demonstration of PSCs with enhanced PCE.[333] An optimal composition (volume ratio of 3:2) and precursor concentration also led to improved crystallization and pinhole-free film formation of inorganic $CsPbI_2Br$ perovskite, thus achieving improved device

View Article Online
DOI: 10.1039/D1EE00062D

performance and good stability under 100 °C stress and continuous light soaking.[334] Similarly, it was applied to prepare high-performance planar 2D PSCs with efficiencies beyond 10% (up to 11.8%) and outstanding stability.[335] In this method, the crystallization process includes two distinct steps. The first step is forming the flaky capping layer at the air−liquid interface, where heterogeneous nucleation primarily occurs as driven by fast DMF volatilization, with an intermediate product forming that retards crystallization. In the second step, the capping layer serves as a seed layer that forces the subsequent vertically growth and crystallization. Alternatively, acetonitrile/methylamine (ACN/MA) compound solvent system was explored in the precursor salt to deposit smooth, highly crystalline films of wide bandgap $MAPbBr_3$ with the aid of a quaternary ammonium halide salt (choline chloride) as a passivating agent and yield PSCs with a PCE of up to 8.9%.[336]

Upon employing a two-step method, PbI_2 and perovskite films were treated with isopropyl alcohol, acetone, diethyl ether and dichloromethane (**Figure 18a**).[337] Meanwhile, triethylenetetramine (TETA) was introduced as an alternative reagent to remove residual PbI_2 altogether and prepare shiny, dense, pinhole-free films with sufficiently large grain sizes and enhanced crystallinity as well as PSCs with a 55% efficiency increase, compared to the other used solvents, in ambient air. A two-step sequential solvent engineering method including IPA in the first step and a mixed solvent of IPA/cyclohexane in the second step,[338] facilitated the conversion of PbI_2 to a compact $MAPbI_3$ perovskite layer. The efficient and complete conversion of PbI2 to perovskite involving different steps as diffusion, infiltration, contact, and the reaction is crucial, and their simultaneous optimization would facilitate high-quality film formation. As a result, a significant enhancement in device performance and reproducibility with a record PCE value of 14.38% for carbon-based PSCs was obtained owing mainly to the lower trap density, improved

View Article Online
DOI: 10.1039/D1EE00062D

interfacial contact and faster charge transport (**Figure 18b**). Asides from the conventional two-step deposition method, a three-step sequential coating method has been explored to prepare high-quality $MAPbI_3$ layers based on solvent (isopropanol, lPA) substitution instead of annealing treatment. Stonehenge-like PbI_2 films due to the volume expansion with controllable porosity and crystallinity were formed, allowing the complete conversion of PbI_2 to $MAPbI_3$. Consequently, PSCs with high reproducibility and a PCE of 17.78% was achieved.[339]

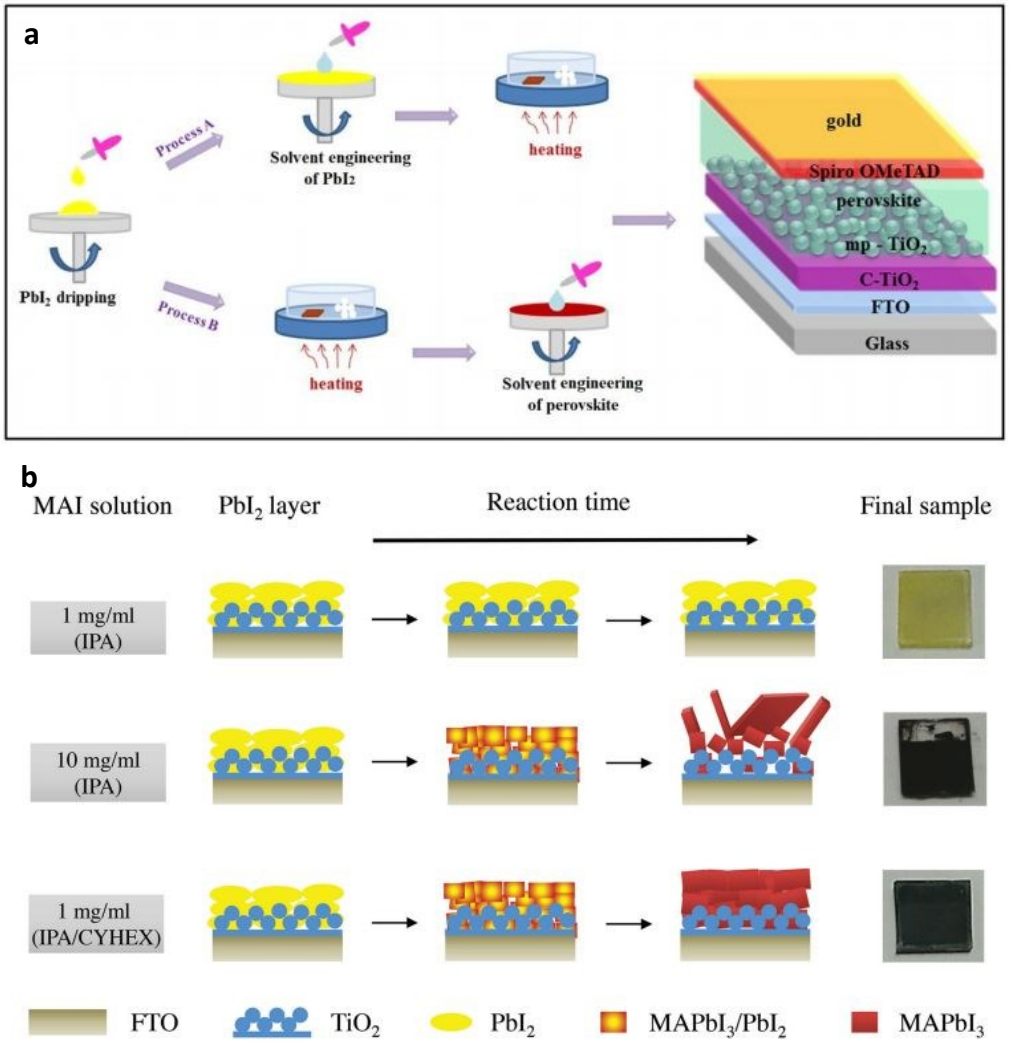

Figure 18. (a) Schematic illustration of the two solvent perovskite deposition method and representation of the mesoscopic PSC structure.[337] Copyright 2019, the Royal Society of Chemistry. (b) Solvent engineering strategy for carbon-based PSCs.[338] Copyright 2017, John Wiley and Sons.

View Article Online
DOI: 10.1039/D1EE00062D

A different approach using solvent complexes in Bi-based perovskites resulted in compact films of methylammonium bismuth iodide (MABI), caesium bismuth iodide (CsBI), and formamidinium bismuth iodide (FABI). The selected complexes, DMF/DMSO and DMF/tBP (4-tert butylpyridine) could increase the solubility of the Bi precursor, followed by a rapid onset of film nucleation via an antisolvent drip, thus effectively controlling growth and resulting in more uniform and dense Bi-based films with lower pinhole density during the spinning stage.[340] Application of MABI as the photoactive component yielded devices with a PCE of 0.71%, the highest report value for MABI-based PSCs. Alternatively, antisolvent treatments can be utilized for the preparation of conformal, improved quality, perovskite films.[341-347] For example, a simple antisolvent washing treatment using iodine modulation could significantly improve the $MAPbI_3$ film quality and uniformity. The upgraded antisolvent enhanced the perovskite crystallization and passivated the under-coordinated Pb^{2+} ions. Modified planar heterojunction n-i-p PSCs showed an exceptional PCE of 21.33%, retaining 91% of its initial value in ambient after 30 days.[341]

An in-situ tin(II) inorganic complex antisolvent process was proposed to tune the film nucleation and crystal growth process markedly. A unique formation of a quasi-core–shell structure of the Pb–Sn perovskite–tin(II) complex and heterojunction perovskite structure was achieved with the core-shell structure covered by a tin(II) complex at the GBs, effectively passivating trap states and suppressing nonradiative recombination.[344] The mixed Pb–Sn low-bandgap PSCs delivered a remarkable PCE of 19.03% with a FF over 80% and outstanding operational stability of up to 560 h. Adjusting the ratio of two solvents in a mixed antisolvent could nicely regulate perovskite crystal quality and reduce surface defects associated with non-radiative recombination losses. For example, a volume ratio of 1:1 for toluene and diethyl ether was optimal for the fabrication of PSCs with a maximum PCE of 16.96%, negligible hysteresis and enhanced

View Article Online
DOI: 10.1039/D1EE00062D

stability as the low boiling point and volatile diethyl ether solvent readily promoted the growth of perovskite grains.[345]

Green, environmentally friendly, solvents have received immense attention to replacing toxic antisolvents used in the fabrication of PSCs.[346,347] In this regard, ethyl acetate (EA) demonstrated the potential to control film morphology in ambient humidity. Upon incorporating $FAPbIBr_2$ into a $MAPbI_3$ matrix, a very large grain size up to ~1.5 μm could be achieved, resulting in reduced trap density and suppression of charge recombination. PCEs of optimized devices reached an impressive value of 20.93% with high stability as manifested by the very similar film morphologies and PCEs obtained under both dry and relatively high RH (50%) conditions due to the exceptional humidity resistance of EA.[346] Another green, nonhalogenated, bifunctional (anti)solvent, methyl benzoate (MB), with a high boiling point and low volatility was developed as both an antisolvent to generate crystal seeds during spin-coating and as a digestive-ripening solvent for the perovskite precursor to prevent the loss of organic components during the thermal-annealing stage and suppress the formation of various lead halide phases (**Figure 19a-d**).[347] As a result, planar n–i–p PSCs achieved an outstanding PCE up to 22.37% with negligible hysteresis and >1300 hours stability. Solvent-antisolvent combination has been explored to exploit their advantages synergistically.[348,349] Ambient processed $MAPbI_{3-x}Cl_x$ thin films with substantial grains (>5 μm), minimal GBs, excellent crystallinity and surface coverage could, for example, be obtained upon using an optimized combination of chlorobenzene and ethanol (3:1 volume ratio) to produce PSCs with a PCE of up to 14.0%.[233] Unique adducts formed between CsI and precursor solvents and antisolvents have been found for the inorganic perovskite $CsPbI_3$ that were not observed for other A-site cation salts.

These adducts, as well as PbI_2–DMSO adducts, controlled nucleation and film

View Article Online
DOI: 10.1039/D1EE00062D

crystallization. In particular, the use of a green solvent, methyl acetate (MeOAc), could promote crystallization by forming a CsI–MeOAc adduct and resulting in PSCs with a PCE of 14.4%[349] In another strategy, non-traditional solvent engineering was introduced for low-temperature perovskite film processing. Solvent coordination was explored by using DMSO as an additive instead of co-solvent and mixed 1-methyl-2-pyrrolidinone (NMP) and dimethylacetamide as the primary solvents for the perovskite precursor (**Figure 19e**).[350] The coordination strength established a trade-off between fast and retarded film crystallization with the mixed solvent with 30% DMSO depicting a uniform, compact perovskite layer and high efficiency of 18.19%. A ternary-mixed-solvent method for the growth of high-quality mixed-cation lead mixed-anion perovskite films was realized by introducing NMP into the precursor solution.[351] NMP was found to readily control the rapid nucleation and slow down crystal growth via the intermediate phase PbI_2-NMP (Lewis acid-base adduct). Consequently, dense, large grain, pinhole-free perovskite films with long carrier lifetime were obtained that yielded PSCs with an outstanding PCE of 19.61% upon optimising the precursor solvent composition.

View Article Online
DOI: 10.1039/D1EE00062D

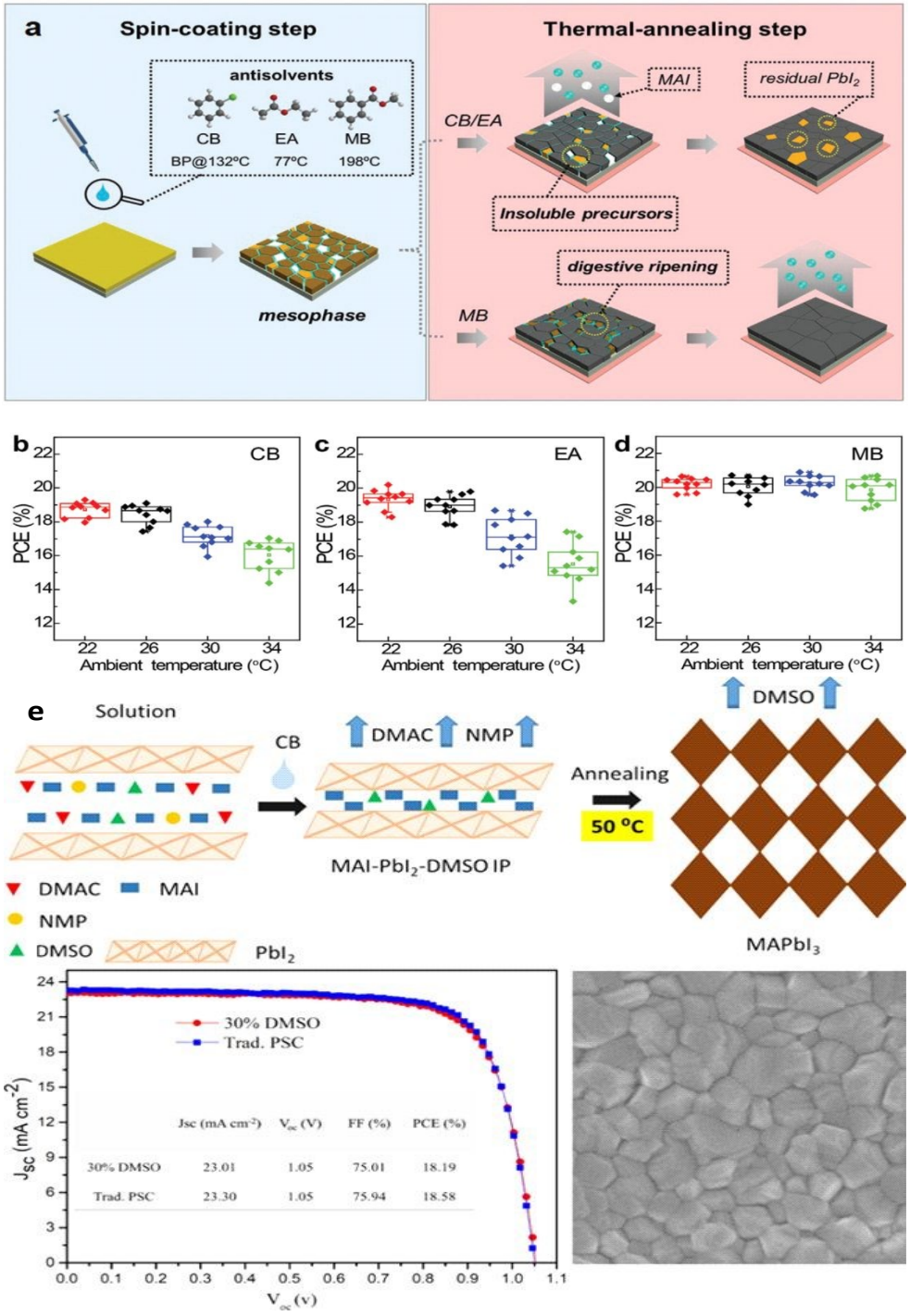

Figure 19. (a) Schematic processing scheme for perovskite films treated by different antisolvents (Chlorobenzene, CB, ethyl acetate, EA, and methyl benzoate, MB). (b) PCE distributions of CB-PSCs, EA-PSCs, and MB-PSCs with different ambient temperatures (22, 26, 30 and 34 °C).[347] Copyright 2020, John Wiley and Sons. (e) Schematic illustration of the evolution mechanism for low-temperature annealed films, J−V curves of devices produced without and with 30% DMSO and top-view SEM images of the perovskite films with 30% DMSO as a fraction of NMP after annealing at 50 °C for 30 min.[350] Copyright 2019, American Chemical Society.

View Article Online
DOI: 10.1039/D1EE00062D

Combining volatile non-coordinating solvents to Pb^{2+} and low-volatile coordinating solvents was recently demonstrated to lead to both fast drying and large perovskite grains with adequate crystallinity at room temperature with good reproducibility. It was successfully employed in the fabrication of blade-coated modules with a PCE of up to 16.4%.[352] 2D perovskites with improved morphology and crystalline quality and more favourable perpendicular orientation were made with a mixed DMF/DMSO solvent and a small amount of hydroiodic acid (HI) additive. Fabricated PSCs exhibited a champion PCE of 12.04% with a high FF of 81.04% and improved environmental stability, benefiting from the hydrophobic behaviour of the organic spacing cation employed.[353] A volatile solid glycolic acid ($HOCH_2COOH$, GA) in a $FA_{0.85}MA_{0.15}PbI_3$ precursor solution was explored as an alternative route to regulate perovskite film quality (**Figure 20**). This could be achieved by sublimating GA before 150 °C in the perovskite film without any residual after annealing. The proposed mechanism involved the strong interaction between GA and Pb^{2+}, thus yielding a champion device PCE as high as 21.32% with excellent stability. On the other hand, the utilization of a non-volatile thioglycolic acid ($HSCH_2COOH$, TGA) with a similar structure to GA also induced large perovskite grains but with pinholes, leading to an increased defect density and a 20% decline in PCE.[354]

View Article Online
DOI: 10.1039/D1EE00062D

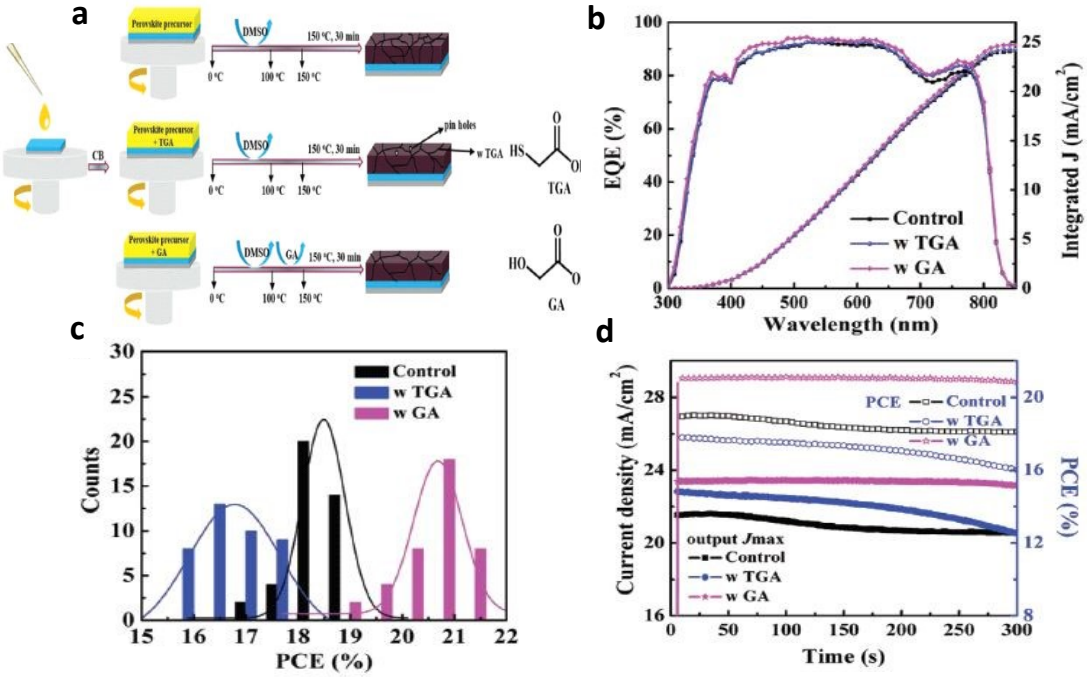

Figure 20. (a) Schematic diagram of perovskite films' preparation process with/without thioglycolic acid ($HSCH_2COOH$, TGA) or glycolic acid ($HOCH_2COOH$, GA) and molecular structures of TGA and GA. (b) incident photon-to-electron conversion efficiency (IPCE), (c) histogram of the PCE of 40 devices, and (d) stable output J_{max} and PCE curves for the optimized pristine and GA- or TGA-modified PSCs.[354] Copyright 2020, John Wiley and Sons.

Thermal annealing (TA) is an alternative route to produce high quality, crystalline, perovskite thin films employed in the fabrication of improved performance PSCs. Critical parameters are the time and temperature of the TA process.[355-358] Alternative methods, such as radiative TA (RTA)[359] and rapid TA using UV light[360,361] have also been proposed as simple, fast, processes for improved PSC performance. For example, rapid TA using intense UV pulsed light (IPL) initiated a radiative thermal response enabled by a suitable alkyl halide (diiodomethane, CH_2I_2) additive to the MAI/PbI_2 precursor.[360] CH_2I_2 dissociated upon UV exposure releasing iodine ions in the film, influencing the perovskite formation and reducing defect states. Optimization of the concentration of CH_2I_2 and the IPL processing parameters led to PSCs with improved film morphology, which increased their efficiencies from 10% to 16.5%, a considerable

View Article Online
DOI: 10.1039/D1EE00062D

improvement compared to previous reports using the IPL method without the additive.[249] IPL was also utilized to quickly fabricate efficient PSCs by annealing of both the SnO_2 ETL and the mixed triple cation perovskite thin films.[361] CH_2I_2 slowed down the film crystallization and improved the surface morphology by only supplying iodine cleaved by UV light during the IPL process. Efficiency for the IPL-modified PSCs reached a maximum of 12.56% when processed in ambient conditions with an RH of 60%. A novel flash infrared annealing method was also recently proposed as a rapid (1.2 s), cost-effective method to fabricate planar heterojunction PSCs with efficiencies exceeding 18% without using antisolvent.[362]

Synergistic solvent-based crystallization with subsequent TA of the PbI_2 precursor could also be applied to prepare high-performance mesoporous PSCs.[363] This method regulated the driving force to the crystallization of PbI_2. It resulted in perovskite films exhibiting voids and spaces that would be highly favourable for efficient infiltration of MAI solution, leading to rapid, complete perovskite conversion, which also showed an enhanced light-harvesting ability. Mesostructured PSCs showed a significant PCE improvement with less hysteresis due to all the photovoltaic parameters' simultaneous enhancement.[363] Moreover, a vacuum-assisted method under room temperature conditions in air,[364] a novel cryogenic process instead of the conventional antisolvent method and treatment of the perovskite film with ammonium iodide isopropanol solution induced a significant enhancement in grain size and crystallinity.[365,366] Performance parameters of representative examples of PSCs employing molecular compounds to control thin film morphology, grain size and crystallinity are summarized in **Table 5**. Description of stability measurements and obtained results in PSCs embedding passivation approached described herein are summarized in **Table 6.**

View Article Online
DOI: 10.1039/D1EE00062D

Table 5. Performance of PSCs employing various inorganic and organic molecular compounds for controlling perovskite crystal growth, grain size, crystallinity and morphology (PCEs denote champion values).

Molecular Compound (Passivation mechanism)	**PSC structure**	**PCE (%) Before/after passivation**	**Section**	**Ref.**
Iodine (I_2) (Control of crystallinity)	ITO/PEDOT:PSS/$MAPbI_xCl_{3-x}$/PCBM/Al	9.83/15.58	4.1.1	241
4F-PEAI (Formation of larger grains)	FTO/$TiCl_4$/$CH[(NH_2)_2]_{0.9}Cs_{0.1}PbI_3$/ 4F-PEAI/Spiro-OMeTAD/Ag	18.60/20.60	4.1.1	242
CsI (Formation of larger grains)	FTO/SnO_2/$MAPbI_3$-CsI/Spiro-MeOTAD/Ag	16.23/18.82	4.1.1	243
MACl (Morphology control)	ITO/NiO_x/$MAPbI_3$-MACl/PCBM/Rhodamine/Ag	8.50/15.40	4.1.1	245
MACl (Assisted vertical recrystallization of perovskite film)	FTO/NiO_x/$FAPbI_3$/MACl/PCBM/TiO_x/Ag	13.24/20.65	4.2.3	323
ChCl (Increased crystallinity)	FTO/SnO_2/$MAPbBr_3$-ChCl/SWCNTs/Spiro-OMeTAD/Au	-/8.90	4.2.4	336
NH_4Cl (Templated growth)	ITO/PEDOT:PSS/$(BA)_2(MA)_3Pb_4I_{13}$-NH_4Cl /PCBM/BCP/Cu	1.00/14.40	4.1.3	288
Glucose (Enhanced morphology of perovskite film)	ITO/P3CT-K/$MAPbI_3$-Glucose/PCBM/ZnO/Al	17.53/20.15	4.1.1	248
$BiFeO_3$ (Morphology control)	ITO/NiO_x/$MAPbI_3$-$BiFeO_3$/PCBM/BCP/Ag	13.80/15.81	4.1.1	270
PCBM (Control of integrain crystallinity)	ITO/PEDOT:PSS/$MAPbI_3$/$PC_{61}BM$/LiF/Al	13.60/17.40	4.2	300
DIO (Facilitate nucleation and modulate the kinetics of crystal growth during crystallization)	ITO/PEDOT:PSS/ $MAPbI_{3-x}Cl_x$:DIO/$PC_{61}BM$/Bis-C_{60}/Ag	7.90/11.80	4.2.1	302
NH_4SCN (Increased grain size)	ITO/SnO_2/CSFAMAPbI_xBr_{3-x}-NH_4SCN/Spiro-OMeTAD/Au	17.24/19.36	4.2.1	305
$Co(Ac)_2$ (Returded crystal	FTO/TiO_2/$CsPbI_2Br$-$Co(Ac)_2$/ Spiro-OMeTAD/Ag/Au	12.83/15.04	4.2.1	306

View Article Online
DOI: 10.1039/D1EE00062D

growth)				
PNVF-NVEE (Delayed perovskite crystallization)	ITO/TiO_2/$MAPbI_3$:PNVF-NVEE/ Spiro-MeOTAD/Au	4.93/9.62	4.2.1	307
PTE (Regulate crystallization kinetics)	ITO/NiO_x/$MAPbI_3$-PTE/PCBM/BCP/Ag	15.50/16.78	4.2.1	308
PC:GBL (Affected the crystallization process)	ITO/PTAA/$MAPbI_3$-PC:GBL/C_{60}/BCP/Cu	21.00/21.90	4.2.4	328
EA (Imrovement of surface quality)	FTO/TiO_2/$MAPbI_3$-EA/Spiro-OMeTAD/Ag	14.90/18.00	4.2.4	329
PTAA (Managing the orientational crystallization)	ITO/PTAA/$BA_2MA_3Pb_4I_{13}$/C_{60}/BCP/Ag	10.72/14.30	4.2.2	320
PEO (Chemical interaction with lead ions)	FTO/TiO_2/C_{60}//$MAPbI_3$-PEO/Spiro-OMeTAD/Au	16.40/16.43	4.2.1	310
$DMEDAI_2$ (Reduction of surface defects)	ITO/SnO_2/$MAPbI_3$:$DMEDAI_2$/Spiro-MeOTAD/Au	18.69/20.18	4.2.1	309
PMMA (Controlled nucleation and crystal growth)	FTO/TiO_2/$(FAI)_{0.81}(PbI_2)_{0.85}(MAPbBr_3)_{0.15}$: PMMA/Spiro-OMeTAD/Au	-/21.60	4.1.3	287
Sulfonate-CNTs (Enhancimg grain size)	FTO/TiO_2/$MAPbI_3$-sCNTs/Spiro-MeOTAD/Ag	10.30/15.10	4.1.1	271
s-SWCNTs (Crystal growth templates)	ITO/SnO_2/$MAPbI_3$:s-SWCNTs/Spiro-MeOTAD/Au	18.10/19.50	4.1.3	289
Adamantan-1-yl)methanammonium (ADMA) (Crystal growth templates)	FTO/NiO_x/$CsPbI_3$-ADMA/ZnO/ITO	10.35/16.04	4.1.3	290
HBr (Improved surface coverage)	FTO/TiO_2/PCBM/$MAPbBr_3$-HBr/PIF8-TAA/Au	-/10.40	4.1.1	256
MA (Reduction of intrinsic defects)	FTO/TiO_2/$MAPbI_3$/Spiro-OMeTAD/Au	16.77/20.02	4.1.1	252
Biuret (Regulate the	FTO/TiO_2/$MAPbI_3$/Spiro-OMeTAD/Au	18.26/21.16	3.2.1	221

View Article Online
DOI: 10.1039/D1EE00062D

crystallization process of perovskite crystals and passivate the defects atGBs)				
TPPI (Interface modification)	ITO/PEDOT:PSS/$MAPbI_{3-x}Cl$/$PC_{61}BM$/TPPI/Al	10.00/13.00	4.1.1	259
PAI (Suppressed penetration of oxygen and moisture into the perovskite material)	FTO/TiO_2/$FA_{0.79}MA_{0.16}Cs_{0.05}PbI_{2.5}Br_{0.5}$/Spiro-OMeTAD/Au	16.86/17.23	4.1.1	260
ITIC-Th (Suppressed the formation of yellow δ-phase)	FTO/TiO_2/$MA_{0.17}FA_{0.83}Pb(I_{0.83}Br_{0.17})_3$-ITIC-Th/Spiro-OMeTAD/Au	18.07/19.20	3.1.1	152
Methyl Benzoate (MB) (Rapidly generates crystal seeds)	FTO/SnO_2/$FA_{0.85}MA_{0.15}Pb(I_{0.85}Br_{0.15})_3$-MB/Spiro-OMeTAD/Au	19.38/22.37	4.2.4	347
DMSO:DMAC:NMP (Formation of high quality perovskite layer)	FTO/TiO_2/$MAPbI_3$-DMSO:DMAC:NMP/ Spiro-OMeTAD/Au	16.19/18.19	4.2.4	350
$CsPbBr_3$ NPs (Improved the film structure, morphology and crystallinity)	FTO/TiO_2/PCBM/$MAPbI_3$-$CsPbBr_3$/Spiro-OMeTAD/Au	18.51/20.46	4.1.1	269
Acetic acid (Ac) (Controlled perovskite crystallization)	ITO/TiO_2/$Cs_{0.05}FA_{0.90}MA_{0.05}Pb(I_{0.95}Br_{0.05})_3$-Ac/Spiro-OMeTAD/Au	19.10/23.00	4.2.4	330
Glycolic Acid ($HOCH_2COOH$, GA) (Regulated perovskite crystallization)	FTO/TiO_2/$FA_{0.85}MA_{0.15}PbI_3$-GA/Spiro-OMeTAD/Au	18.85/21.32	4.2.4	354

View Article Online
DOI: 10.1039/D1EE00062D

Table 6. Stability of PSCs employing passivation agents and/or process engineering approaches.

Molecular Compound	PCE (%)	Description of stability test	Ref.
DBTMT	21.12	PSCs retained 96% of their initial PCE upon storage in nitrogen for 600 h	127
TPA-PEABr	18.15	PSCs retained 80% of their initial PCE after keeping at RT and 40−50% RH for a month	129
$CH_3(CH_2)_{42}$ CH_3 (TTC)	20.05	PSCs retained 87% of the initial PCE after continuous exposure for 200 h in air	130
TPFPB	21.60	PSCs retained 70% of their initial PCE after 750 h of storage at RT and 30% RH	131
Pyrazine (Pyr)	19.63	PSCs retained 90% of initial PCE even after aging for 50 h at 55℃	132
Zinc porphyrin (YD2-o-C8)	20.50	PSCs retained 93% of their initial PCE after storage in ambient air (25–40 °C, 20–40% RH) under dark conditions for 30 days	133
DTA	21.45	PSCs retained 90% of initial PCE even after aging for 50 h at 55℃	134
IPFB	15.70	90% of initial PCE even after aging for 50 h at 55℃53% of its highest value within 720 h	135
MSAPBS	21.18	PSCs tested at 25 °C and RH ≈ 25% exhibit excellent air stability (PCE retention >90% after 700 h). Furthermore, these devices were tested under more severe conditions at 85 °C and RH ≈ 85% according to the international standard IEC 61215	139
tertiary and quaternary alkyl ammonium cations		PSCs tested upon storage (~90% RH) over 30 days	140
SN	20.90	maintained 98.1% of the initial PCE, whereas that of the pristine control decreased to 88.4% after 1000 h full solar light soaking of unsealed devices at 60 °C under Ar gas	142
tBBAI	23.50	PSCs retained 95% of the initial PCE after 500 h continuous solar illumination	143
Phenylalkylamines	19.20	PSCs tested upon storage for >4 months in ambient air	144
TPFP	22.02	Unencapsulated and encapsulated devices retain 63% and 80% of the initial efficiency after 14 days of aging under 75% and 85% RH	150
ITIC-Th	19.20	PSCs tested and declined in efficiency from 19.20% (fresh) to 16.55% (39 d)	152
C_{60}-PyP	19.82	PSCs retain 83% and 80% of the initial efficiency after 14 days of aging under 20 °C and 30% RH	158
PCDTBT1	18.67	PSCs retained 90% of their original PCEs after storage of more than 30 days	160
P4VP	20.02	PSCs showed enhanced moisture stability (60 ± 5% RH) and thermal stability (85 °C)	166
KCl	22.60	PSCs showed >75% retention after more than 200 h when placed in a hot-plate at 70 °C in nitrogen	174
Choline chloride	21.00	PSCs maintained 86% of the initial PCE under 1 sun continuous illumination for 26 h	175
PEA_2PbI_4	18.51	PSCs retained 90% of their initial PCE for more than 1,000 h	183

View Article Online
DOI: 10.1039/D1EE00062D

		of exposure in ambient air	
FPEA	18.03	PSCs showed increased ambient laboratory stability	187
$HA_2MAPb_2I_7$	20.62	PSCs maintained 99% of their initial PCE upon storage for 36 days.	188
Phenethylammonium iodide	22.98	PSCs showed increased stability upon storage for 1000 h	189
TMI	18.93	PSCs maintained 95% of their initial PCE upon storage for 800 days.	190
PZPY	18.10	PSCs retained more than 80% of their photovoltaic performance with temperature cycling process (85 °C, 50% RH)	195
TAPbI3	18.97	PSCs retained 92% of the initial efficiency under ambient conditions in air for 2 months	196
2-Aminoterephthalic acid	21.09	PSCs retained 93% of their initial PCE after 500 h continuous illumination	199
ZnPy-NH_3Br	20.00	PSCs retained 85% of their initial PCE when illuminated for 450 h at 45% RH or heated at 85 °C for 1000 h	200
Ammonium bromides	22.00	PSCs retained 72% of their initial PCE after 360 h constant illumination	201
HOOC–Ph–SH thiol	12.40	Improved device stability under storage and continuous illumination	204
p-SAM	21.00	PSCs were stable under standardized MPP operation at 85 °C in inert atmosphere (ISOS-L-2) for more than 250 h and exhibit superior humidity resilience, maintaining ~95% device performance even if stored in humid air in ambient conditions over months (~3000 h, ISOS-D-1)	206
2PACz	20.9	<3% PCE loss under continuous MPP tracking for the investigated PSCs at simulated 1 sun AM 1.5G illumination without active sample cooling	207
PFA	21.31	PSCs retained 97% of their initial PCE after 2500 h of storage in 70% humidity	216
SY-2	18.96	PSCs retained 92% of their initial PCE after 1000 h storage in Ar atmosphere	217
TC-silane	20.03	PSCs retained 80% of their initial PCE after 800 h at ~75% RH in air and for about 80 h under 85 °C thermal stress	219
PBTI	20.67	PSCs retained 70% of initial PCE after 600 h under illumination	223
TMTA	19.26	PSCs retained 80% of their PCE after continuous illumination for 400 h at the MPP tracking. In addition, retained 90% of their PCE under moisture or thermal (85 °C) conditions after ageing for over 1000 h	226
alkylamine ligands	23.00	Stable operation for 1000 h at MPP	228
4-vinylbenzylammonium	20.40	PSCs retained 90% of their PCE after storage for 2300 h	229
CsI	19.00	enhanced stability under ambient conditions	243
glucose	20.15	enhanced stability in heat, light and moisture	248
dimethyl itaconate (DI)	23.00	PSCs retained 85.7% and 91.8% of the initial PCE after 504 hours continuous illumination and 2208 hours shelf storage	249
dimethyl itaconate	20.07	PSCs showed 20.07% stabilized PCE for more than 30 days	251

View Article Online
DOI: 10.1039/D1EE00062D

(DI)		storage at 10% RH	
EDA^{2+}	20.01	PSCs retained 96% of their initial efficiencies after 25 days of storage in an ambient atmosphere	253
bilateral alkylamine (BAA)	21.50	shelf lifetime to >1000 hours and operational stability to >500 hours under light, with 90% of the initial efficiency	254
oxalic acid (OA)	17.12	retained 70% of the initial efficiency after 19 hours	257
$Pb(SCN)_2$	17.00	~85 % of their initial efficiency in the ambient environment (~60 % RH) after 45 days	264
$BMIMBF_4$	19.80	~95% for encapsulated devices under continuous illumination for more than 1,800 hours at ~75 °C	266
$DMEDAI_2$	20.20	PSCs maintained 73.7% of their initial efficiency when stored under ambient conditions with a RH of 60−80% at RT	309
PEO	16.43	PSCs retained more than 95% of their initial PCE over 15 h illumination in ambient atmosphere.	310
Polymer	21.60	Encapsulated cells retained ~91.7% of their initial efficiency after 1000 hours of damp heat exposure	311
Self-doping	19.14	PSCs were stored in an ambient environment (humidity: 20 RH%) without sealing, and the PCE decreased less than 10% even after 500 h	313
PN4N	16,00	PSCs retained more than 90% of the initial efficiency under continuous 1 sun illumination for 400 hours	318
MACl	20.00	thermal stability as long as 500 hours	323
acetic acid (Ac)	22.00	PSCs retained even up to 96% of the initial efficiency after 2400 hours storage in the ambient environment	330
DMF/DMSO	9.14	Stability under 100 °C stress and continuous light soaking	334
Iodine	21.33	PSCs retained 91% of its initial value in ambient after 30 days	341
Tin(II) complex	19.03	Operational stability of up to 560 h	344
Ethyl acetate (EA)	20.93	Stable PCEs obtained under both dry and relatively high RH (50%) conditions	346
3AMP	12.04	Enhanced air and light stability of 2D perovskite based PSCs	353

View Article Online
DOI: 10.1039/D1EE00062D

5. Conclusions and future perspectives

The perovskite photovoltaics community has recently embarked on an evolutionary race to make high-efficiency solar cells. It feels that progress should be made fast enough to prevent climate change. The advancements in solar cells performance have been remarkable with high efficiencies comparable to silicon counterparts to have been achieved in less than a decade. However, further efficiency enhancement combined with substantially improved environmental long-term stability and photostability under continuous illumination and thermal stress will allow this new technology to gain its market entrance. Although several extrinsic factors influence the device stability upon air exposure, illumination, and thermal stress, such as interfacial layers and encapsulation methods, addressing the intrinsic/structural instability of the perovskite itself is a prerequisite to improve PSCs overall performance and stability. To overcome the limitation of instability issues, several cation and anion optimization strategies have already been explored and opened routes for the optimization of perovskites optoelectronic properties through compositional tuning.[367] To this end, colloidal chemistry proved to be a key aspect as the chemical structure of colloids/clusters in the perovskite precursor solution strongly influences the compositional uniformity and crystallinity in the grown perovskite film and eventually the device performance variation and stability. As such, colloidal chemistry has its discrete and important role in stabilizing the perovskite structure and addressing the challenges of reproducibility.

However, the significant sources of intrinsic instability in perovskites are inherent defects arising from the soft nature of crystal lattice and poor polycrystalline morphology of the resultant films. These issues can be successfully addressed through defect passivation using additives bearing appropriate functional groups, surface and interface modification, solvent engineering, interface and capping layers, or employing suitable methods for controlling the perovskite films'

View Article Online
DOI: 10.1039/D1EE00062D

growth precursor additives, substrate modification, post-treatments and solvent annealing. The detrimental ion migration can also be impeded by applying effective passivation strategies that significantly suppress or even prevent defect formation, hence contributing to prolonged device photostability.

The most successful perovskite passivation approaches centre on additives that target to heal defects at grain boundaries, surfaces, and interfaces of the perovskite film. Additives generally suppress the notorious degradation mechanisms such as ion migration and charge accumulation induced degradation, hydrolysis at grain boundaries, halide segregation etc. They include several types of functional molecules that can be either incorporated within the device structure or removed during the fabrication process. A vast variety of additives have already been integrated with success into the perovskite framework.[368,369] Despite successful results in the obtained effeiciency, to further advance the application of additives as passivation agents a deepen understanding of their function and interaction not only with perovskite defects but also with the charge transporting interfaces besides trial and error studies should be actively pursued. For example, a strong correlation between their molecular structure (i.e. exploration of donor-π-acceptor entities) and properties such as the number of hydrogen-bond donor or acceptor,[370] halogen bond donor or acceptor,[371] the length of alkyl chains, the topological polar surface area of the capping layer forming molecules etc, and the achieved passivation levels is urgently needed. This can be accomplished by extensive theoretical calculations combined with targeted photophysical studies to reveal the underlying passivation mechanism(s). Moreover, whether these additives are homogeneously incorporated into the interior or accumulate at the GBs or even form aggregates needs to be studied and correlated with the device performance data. Appropriate imaging methods, such as time-of-flight secondary ion mass spectrometry (TOF-SIMS) and

View Article Online
DOI: 10.1039/D1EE00062D

energy-dispersive X-ray spectroscopy (EDS) mapping, can reveal the structure-property relationship of perovskite materials before and after the application of additives. Additional effects such as the alteration of perovskites' electronic structrure upon additives inclusion into their lattice should also be extensively investigated. Additive engineering could result in local p- or n-type doping, leading to the formation of lateral homojunctions within each individual grain having tremendous impact on the charge recombination lifetimes. The potential formation of lateral homojunction due to additive-induced doping along grain boundaries should be investigated in parallel to the passivation effects as it greatly enhances the charge carrier diffusion length within perovskite grain and along grain boundaries, thus reducing charge recombination in polycrystalline perovskite film based solar cells.

The above paradigm emphasizes the tremendous role of in-depth exploration of the passivation mechanism and additional effects caused by the inclusion of additives into the perovskite lattice, GBs and surface. Nevertheless, the tremendous role of the chemical structure of the applied passivation agent is undeniable. Materials bearing appropriate functional groups to simultaneously passivate several types of defects, alter the electronic structure, cross-link neighbouring grains, elongate carrier diffusion lengths and induce hydrophobic properties should be designed and come into fruition. More systematic investigations to simultaneous enhance the material composition and impede defect formation are necessary.[368,369] This will become possible through interdisciplinary scientific collaboration and perhaps through input from machine learning,[370] which will provide guidelines for further developments of material and processes aiming to simultaneously achieve the above gols while also stabilize the high performance levels of perovskite solar cells. Machine learning, not only can study the trend of passivation capability, potential reactivity, doping etc., of several types of different molecules but also can create models

View Article Online
DOI: 10.1039/D1EE00062D

according to which prediction and design of novel materials would be possible.[371] It can also outline experiments to identify the impact of degradation factors on the different passivation agents including perovskite compositions and propose paradigms for maximizing long-term performance of perovskite solar cells.[372]

It is noteworthy that besides the development of appropriate passivation materials with multiple functions, which will have been successfully predicted prior to design and verified using a large variety of synergistic methods, the adoption of reliable stability test protocols that researchers should subject their solar cells remains a critical issue.[373] For example, measuring the device PCE upon exposing at 1 sun illumination either on ambient air (at RT) or at 45 ^{o}C represents the most popular test, but more aggressive measuring conditions are probably needed to fully evaluate the degradation parameters. Up to now, scientific publications lack consistency in stability measurement parameters adopted and this prevents the deeper understanding of mechanisms causing the severe device instability. Commonly applicable stability procedures will shed more light in different degradation features and provide important feedback to chemists and engineers that work on the optimization of materials and device fabrication methods. Despite the fact that researchers generally follow a more flexible experimental approach to reveal the degradation mechanism of parameters under study, the development of widely applicable standards for testing the perovskite solar cell stability is imperative. Any photovoltaic technology must pass the IEC 61646 protocol of stability and lifetime in order to become commercially available.[374,375] The testing standards focus on environmental parameters such as thermal cycling tests, freeze tests, illumination tests and damp heat tests. Notably, to guarantee lifetimes of at least 25 years, it is necessary to pass the IEC test multiple times.[374] Apart from these environmental condition requirements, there are also economical and marketing standards to be met such as facile

View Article Online
DOI: 10.1039/D1EE00062D

fabrication using low-cost materials and processes. For the organic photovoltaic devices, these standards are known as ISOS protocols.[376] The same protocols also apply for the perovskite solar cell technology, however, with even stronger requirements due to the high hysteresis and the metastable modification of their properties caused by polarization effects during PSC operation, which might reduce the PCE under short-circuit and open-circuit conditions.[377,378] However, even if efficienct and stable PSCs are fabricated, producing stable modules and panels are the main challenges that need to be faced in order to bring these devices closer to the market. Over the last years, there is a considerable effort to fabricate perovskite modules (mini modules with an area of ~10-200 cm^2, sub-modules ~200-800 cm^2, modules ≥ 800cm^2).[379-380]. Precursor ink formulaton,[381] adhesion of the precursor perovskite ink with the charge transporting underlayer,[382] control over the interfaces,[383] and precursor ink coating methods,[384] are critical for the efficiency and stability of the resultant modules.

Because the control over the perovskite precursor's ink composition and intrinsic defects of the resultant film becomes more difficult in the large production scale, this affects the cost of the assembly besides the efficiency and stability of the modules. To this end, absolute control of stoichiometry, defect density, electronic structure, optoelectronic properties, morphology and crystallinity and establishment of commonly accepted processing protocols in small area devices are necessary as they can provide guidelines for the further development of modules and panels. In brief, further advancements on the perovskite solar cell technology requires strong progress not only in the composition together with colloidal chemistry of the perovskite materials, but also in the development of novel passivation materials and processes assisted by machine learning and theoretical calculations in tandem with extensive stubility studies in both cells and modules according to well-established protocols.

View Article Online
DOI: 10.1039/D1EE00062D

Acknowledgements

We acknowledge the support of this work by the project "Development of Materials and Devices for Industrial, Health, Environmental and Cultural Applications" (MIS 5002567), which is implemented under the "Action for the Strategic Development on the Research and Technological Sector", funded by the Operational Programme "Competitiveness, Entrepreneurship and Innovation" (NSRF 2014-2020) and co-financed by Greece and the European Union (European Regional Development Fund).

REFERENCES

1. Z. Song, C. L. McElvany, A. B. Phillips, I. Celik, P. W. Krantz, S. C. Watthage, G. K. Liyanage, D. Apul and M. J. A. Heben, *Energy Environ. Science,* 2017, **10**, 1297-1305.
2. L. Meng, J. You and Y. Yang, *Nat. Commun.*, 2018, **9**, 5265.
3. Y. Rong, Y. Hu, A. Mei, H. Tan, M. I. Saidaminov, S. I. Seok, M. D. McGehee, E. H. Sargent and H. Han, *Science*, 2018, **361**, eaat8235.
4. Z. Yang, Z. Yu, H. Wei, X. Xiao, Z. Ni, B. Chen, Y. Deng, S. N. Habisreutinger, X. Chen, K. Wang, J. Zhao, P. N. Rudd, J. J. Berry, M. C. Beard and J. Huang,. *Nat. Commun*., 2019, **10**, 4498.
5. T. Leijtens, K. A. Bush, R. Prasanna, M. D. McGehee, *Nat. Energy*, 2018, **3**, 828-838.
6. Y. Li, L. Ji, R. Liu, C. Zhang, C. H. Mak, X. Zou, H.-H. Shen, S.-Y. Leu and H.-Y. Hsu, *J. Mater. Chem. A*, 2018, **6**, 12842-12875.
7. A. Kojima, K. Teshima, Y. Shirai and T. Miyasaka, *J. Am. Chem. Soc.*, 2009**, 131**, 6050-6051.

View Article Online
DOI: 10.1039/D1EE00062D

8. The National Renewable Energy Laboratory, Best Research-Cell Efficiency Chart; www.nrel.gov/pv/cell-efficiency.html.
9. H.-S. Kim, C.-R. Lee, J.-H. Im, K.-B. Lee, T. Moehl, A. Marchioro, S.-J. Moon, R. Humphry-Baker, J.-H. Yum, J. E. Moser, M. Grätzel and N.-G. Park, *Scientific Reports*, 2012, **2** (1), 1-7.
10. M. M. Lee, J. Teuscher, T. Miyasaka, T. N. Murakami and H. J. Snaith, *Science*, 2012, **338**, 643-647.
11. G. Schileo and G. Grancini, *J. Phys. Energy*, 2020, **2**, 021005.
12. C. C. Boyd, R. Cheacharoen, T. Leijtens and M. D. McGehee, *Chem. Rev.*, 2019, **119**, 3418-3451.
13. N.-G. Park, *Adv. Energy Mater.*, 2020, **10**, 1903106.
14. S. Zhang, Z. Liu, W. Zhang, Z. Jiang, W. Chen, R. Chen, Y. Huang, Z. Yang, Y. Zhang, L. Han, W. Chen, *Adv. Energy Mater.*, 2020**, 10**, 2001610.
15. Y. Ying, L. Feiyu, Z. Congtan, C. Tian, M. Shupeng, L. Yuan, Z. Liu and G. Xueyi, *Acta Chim. Sinica* **2020**, *78*, 217-231.
16. B. Parida, S. Yoon, S. M. Jeong, J. S. Cho, J.-K. Kim and D.-W. Kang, *Sol. Energy Mater. Sol. Cells*, 2020, **204**, 110212.
17. Y. Zhou, J. Hu, Y. Wu, R. Qing, C. Zhang, X. Xu and M. Jiang, *J. Photonics Energy*, 2019, **9**, 040901.
18. A. K. Jena, A. Kulkarni and T. Miyasaka, *Chem. Rev*., 2019, **119**, 3036-3103.
19. J. Y. Kim, J.-W. Lee, H. S. Jung, H. Shin and N.-G. Park, *Chem. Rev.*, 2020, **120**, 7867-7918.
20. A. Urbina, *J. Phys.:Energy*, 2020, **2**, 022001.

View Article Online
DOI: 10.1039/D1EE00062D

21. R. Wang, M. Mujahid, Y. Duan, Z.-K. Wang, J. Xue and Y. Yang, *Adv. Funct. Mater.*, 2019, **29**, 1808843.

22. G. Y. Kim, A. Senocrate, T.-Y. Yang, G. Gregori, M. Grätzel and J. Maier, *Nat. Mater.*, 2018, **17**, 445-449.

23. N. Aristidou, C. Eames, I. Sanchez-Molina, X. Bu, J. Kosco, M. S. Islam and S. A. Haque, *Nat. Commun*., 2017, **8**, 15218.

24. K. Domanski, J. P. Correa-Baena, N. Mine, M. K. Nazeeruddin, A. Abate, M. Saliba, W. Tress, A. Hagfeldt and M. Grätzel, *ACS Nano*, 2016, **10**, 6306-6314.

25. C. C. Boyd, R. Cheacharoen, K. A. Bush, R. Prasanna, T. Leijtens and M. D. McGehee, *ACS Energy Lett.*, 2018, **3***,* 1772-1778.

26. J. Zhao, Y. Deng, H. Wei, X. Zheng, Z. Yu, Y. Shao, J. E. Shield and J. Huang, *Sci. Adv*., 2017, **3**, No. eaao5616.

27. E. Aydin, M. De Bastiani and S. De Wolf, *Adv. Mater*., 2019, **31**, 1900428.

28. B. Chen, P. N. Rudd, S. Yang, Y. Yuan and J. Huang, Cells. *Chem. Soc. Rev.*, 2019, **48**, 3842-3867.

29. Y. Zhu, S. Poddar, L. Shu, Y. Fu and Z. Fan, *Adv. Mater. Interfaces*, 2020, **7**, 2000118.

30. K.-G. Lim, S. G. Ji, J. Y. Kim and T.-W. Lee, *Small Methods*, 2020, **4**, 2000065.

31. A.N. Singh, S. Kajal, J. Kim, A. Jana, J. Y. Kim and K. S. Kim, *Adv. Energy Mater.*, 2020, **10**, 2000768.

32. S. Akin, N. Arora, S. M. Zakeeruddin, M. Grätzel, R. H. Friend and M. I. Dar, *Adv. Energy Mater.*, 2020, **10**, 1903090.

33. F. Zhang and K. Zhu, *Adv. Energy Mater.*, 2020, **10**, 1902579.

View Article Online
DOI: 10.1039/D1EE00062D

34. M. Azam, K. Liu, Y. Sun, Z. Wang, G. Liang, S. Qu, P. Fan and Z. Wang, *J. Phys. D: Appl. Phys*., 2020, **53**, 183002.

35. M. Vasilopoulou, A. Fakharuddin, A. G. Coutsolelos, P. Falaras, P. Argitis, A. R. b. M. Yusoff and M. K. Nazeeruddin, *Chem. Soc. Rev.*, 2020, **49**, 4496-4526.

36. S. Wang, A. Wang, X. Deng, L. Xie, A. Xiao, C. Li, Y. Xiang, T. Li, L. Ding and F. Hao, *J. Mater. Chem. A*, 2020, **8**, 12201-12225.

37. C. Yi, J. Luo, S. Meloni, A. Boziki, N. Ashari-Astani, C. Grätzel, S. M. Zakeeruddin, U. Rothlisberger and M. Grätzel, *Energy Environ. Sci*., 2016, **9***,* 656-662.

38. H. Min, M. Kim, S.-U. Lee, H. Kim, G. Kim, K. Choi, J. H. Lee and S. I. Seok, *Science*, 2019, **366**, 749-753.

39. M. R. Filip, G. E. Eperon, H. J. Snaith and F. Giustino, *Nat. Commun.*, 2014**, 5**, 5757.

40. C. C. Stoumpos and M. G. Kanatzidis, *Acc. Chem. Res.*, 2015, **48**, 2791-2802.

41. S. González-Carrero, R. E. Galian and J. Pérez-Prieto, *Part. Part. Syst. Charact.,* 2015, **32**, 709-720.

42. Y. Liu, Z. Yang and S. (F.) Liu, *Adv. Sci.*, 2017, **5**, 1700471.

43. X. Zhang, J.-X Shen and C. G. Van de Walle, *Adv. Energy Mater.,* 2020**, 10**, 1902830.

44. K. Tanaka, T. Takahashi, T. Ban, T. Kondo, K. Uchida and N. Miura, *Solid State Commun.*, 2003**, 127**, 619-623.

45. E. T. Hoke, D. J. Slotcavage, E. R. Dohner, A. R. Bowring, H. I. Karunadasa and M. D. McGehee, *Chem. Sci.*, 2015**, 6**, 613-617.

46. Q. Jiang, D. Rebollar, J. Gong, E. L. Piacentino, C. Zheng and T. Xu, *Angew. Chem. Int. Ed.*, 2015, **54**, 7617-7620.

View Article Online
DOI: 10.1039/D1EE00062D

47. Q. Tai, P. You, H. Sang, Z. Liu, C. Hu, H. L. W. Chan and F. Yan, *Nat. Commun.*, 2016**, 7**, 11105.

48. N. Pellet, P. Gao, G. Gregori, T.-Y. Yang, M. K. Nazeeruddin, J. Maier and M. Grätzel, *Angew. Chem. Int. Ed.*, 2014**, 53**, 3151-3157.

49. G. Kieslich, S. Sun and A. K. Cheetham, *Chem. Sci.*, 2014**, 5**, 4712-4715.

50. V. M. Goldschmidt, *Naturwissenschaften*,1926**, 14**, 477-485.

51. Z. Li, M. Yang, J.-S. Park, S.-H. Wei, J. J. Berry and K. Zhu, *Chem. Mater.* 2016**, 28**, 284-292.

52. W. Ke, M. G. Kanatzidis, *Nat. Commun.*, 2019**, 10**, 965.

53. E. Jokar, C.-H. Chien, C.-M. Tsai, A. Fathi and E. W.-G. Diau, *Adv. Mater.*, 2019, **31**, 1804835.

54. S. Shao, J. Liu, G. Portale, H.-H. Fang, G. R. Blake, G. H. ten Brink, L. J. A. Koster and M. A. Loi, *Adv. Energy Mater.*, 2018, **8**, 1702019.

55. N. K. Noel, S. D. Stranks, A. Abate, C. Wehrenfennig, S. Guarnera, A.-A. Haghighirad, A. Sadhanala, G. E. Eperon, S. K. Pathak, M. B. Johnston, A. Petrozza, L.M. Herz and H. J. Snaith, *Energy Environ. Sci.*, 2014, **7**, 3061-3068.

56. F. Hao, C. C. Stoumpos, D. H. Cao, R. P. H. Chang and M. G. Kanatzidis, *Nat. Photonics*, 2014**, 8**, 489-494.

57. W. Ke, C. C. Stoumpos, I. Spanopoulos, L. Mao, M. Chen, M. R. Wasielewski and M. G. Kanatzidis, *J. Am. Chem. Soc.*, 2017, **139**, 14800-14806.

58. T. Leijtens, R. Prasanna, A. Gold-Parker, M. F. Toney and M. D. McGehee, *ACS Energy Lett.*, 2017**, 2**, 2159-2165.

View Article Online
DOI: 10.1039/D1EE00062D

59. M .Chen, M.-G. Ju, H. F. Garces, A. D. Carl, L. K. Ono, Z. Hawash, Y. Zhang, T. Shen, Y. Qi, R.L. Grimm, D. Pacifici, X. C. Zeng, Y. Zhou and N. P. Padture, *Nat. Commun.*, 2019**, 10**, 16.

60. Z. Guo, A. K. Jena, I. Takei, G. M. Kim, M. A. Kamarudin, Y. Sanehira, A. Ishii, Y. Numata, S. Hayase and T. Miyasaka, *J. Am. Chem. Soc.*, 2020, **142**, 9725-9734.

61. L. Liang and P. Gao, *Adv. Sci.*, 2018, **5**, 1700331.

62. D. Zhao, Y. Yu, C. Wang, W. Liao, N. Shrestha, C. R. Grice, A. J. Cimaroli, L. Guan, R. J. Ellingson, K. Zhu, X. Zhao, R. G. Xiong and Y. Yan, *Nat. Energy*, 2017**, 2**, 17018.

63. G. Han, H. D. Hadi, A. Bruno, S. A. Kulkarni, T. M. Koh, L. H. Wong, C. Soci, N. Mathews, S. Zhang and S. G. Mhaisalkar, *J. Phys. Chem. C*, 2018, **122**, 13884-13893.

64. N. Pellet, P. Gao, G. Gregori, T.-Y. Yang, M. K. Nazeeruddin, J. Maier and M. Grätzel, *Angew. Chem. Int. Ed.*, 2014**, 53**, 3151-3157.

65. J. P. Correa Baena, L. Steier, W. Tress, M. Saliba, S. Neutzner, T. Matsui, F. Giordano, T. J. Jacobsson, A. R. Srimath Kandada, S. M. Zakeeruddin, A. Petrozza, A. Abate, M. K. Nazeeruddin, M. Grätzel and A. Hagfeldt, *Energy Environ. Sci.*, 2015**, 8**, 2928-2934.

66. N. J. Jeon, J. H. Noh, W. S. Yang, Y. C. Kim, S. Ryu, J. Seo and S. I. Seok, *Nature*, 2015, **517**, 476-480.

67. N. J. Jeon, H. Na, E. H. Jung, T.-Y. Yang, Y. G. Lee, G. Kim, H.-W. Shin, S. I. Seok, J. Lee and J. Seo, *Nat. Energy*, 2018, **3**, 682-689.

68. J.-W. Lee, D.-H. Kim, H.-S. Kim, S.-W. Seo, S. M. Cho and N.-G. Park, *Adv. Energy Mater.*, 2015, **5**, 1501310.

69. C. Yi, J. Luo, S. Meloni, A. Boziki, N. Ashari-Astani, C. Grätzel, S. M. Zakeeruddin, U. Röthlisberger and M. Grätzel,. *Energy Environ. Sci.*, 2016, **9**, 656-662.

View Article Online
DOI: 10.1039/D1EE00062D

70. D. P. McMeekin, G. Sadoughi, W. Rehman, G. E. Eperon, M. Saliba, M. T. Hörantner, A. Haghighirad, N. Sakai, L. Korte, B. Rech, M. B. Johnston, L. M. Herz and H. J. A. Snaith, *Science*, 2016, **351**, 151-155.

71. M. Saliba, T. Matsui, J.-Y. Seo, K. Domanski, J.-P. Correa-Baena, M. K. Nazeeruddin, S. M. Zakeeruddin, W. Tress, A. Abate, A. Hagfeldt and M. Grätzel, *Energy Environ. Sci.*, 2016, **9**, 1989-1997.

72. M. Saliba, T. Matsui, K. Domanski, J.-Y. Seo, A. Ummadisingu, S. M. Zakeeruddin, J.-P. Correa-Baena, W. R. Tress, A. Abate, A. Hagfeldt and M. Grätzel, *Science*, 2016, **354**, 206-209.

73. H. X. Dang, K. Wang, M. Ghasemi, M.-C. Tang, M. De Bastiani, E. Aydin, E. Dauzon, D. Barrit, J. Peng, D.-M. Smilgies, S. De Wolf and A. Amassian, *Joule*, 2019, **3**, 1746-1764.

74. C. T. Crespo, *Sol. Energy Mater. Sol. Cells*, 2019, **195**, 269-273.

75. W. Rehman, R. L. Milot, G. E. Eperon, C. Wehrenfennig, J. L. Boland, H. J. Snaith, M. B. Johnston and L. M. Herz, *Adv. Mater.*, 2015, **27**, 7938-7944.

76. M. Liu, M. B. Johnston and H. J. Snaith, *Nature*, 2013, **501**, 395-398.

77. J. H. Noh, S. H. Im, J. H. Heo, T. N. Mandal and S. I. Seok, *Nano Lett.,* 2013, **13**, 1764-1769.

78. M. R. Filip, G. Volonakis, F. Giustino, In *Handbook of Materials Modeling: Applications: Current and Emerging Materials*, eds. W. Andreoni and S. Yip, Springer International Publishing: Cham, 2020, pp 295-324.

79. M. Sendner, P. K. Nayak, D. A. Egger, S. Beck, C. Müller, B. Epding, W. Kowalsky, L. Kronik, H. J. Snaith, A. Pucci and R. Lovrinčić. *Mater. Horiz.*, 2016, **3**, 613-620.

80. K. Tanaka, T. Takahashi, T. Ban, T. Kondo, K. Uchida and N. Miura, *Solid State Commun.*, 2003**, 127**, 619-623.

View Article Online
DOI: 10.1039/D1EE00062D

81. H. Jin, E. Debroye, M. Keshavarz, I. G. Scheblykin, M. B. G. Roeffaers, J. Hofkens and J. A. Steele, *Mater. Horiz.*, 2020, **7**, 397-410.

82. Q. Jiang, D. Rebollar, J. Gong, E. L. Piacentino, C. Zheng and T. Xu, *Angew. Chem. Int. Ed.*, 2015, **54**, 7617-7620.

83. Q. Tai, P. You, H. Sang, Z. Liu, C. Hu, H. L. W. Chan and F. Yan, *Nat. Commun.*, 2016, **7**, 11105.

84. Z. Xiao, W. Meng, B. Saparov, H.-S. Duan, C. Wang, C. Feng, W. Liao, W. Ke, D. Zhao, J. Wang, D. B. Mitzi and Y. Yan, *J. Phys. Chem. Lett.*, 2016, **7**, 1213-1218.

85. J. Yang, B. D. Siempelkamp, D. Liu and T. L. Kelly, *ACS Nano*, 2015, **9**, 1955-1963.

86. R. K. Misra, S. Aharon, B. Li, D. Mogilyansky, I. Visoly-Fisher, L. Etgar, E. A. Katz, *J. Phys. Chem. Lett.*, 2015, **6**, 326-330.

87. B. Conings, J. Drijkoningen, N. Gauquelin, A. Babayigit, J. D'Haen, L. D'Olieslaeger, A. Ethirajan, J. Verbeeck, J. Manca, E. Mosconi, F. D. Angelis and H.-G. Boyen, *Adv. Energy Mater.*, 2015, **5**, 1500477.

88. G. E. Eperon, S. D. Stranks, C. Menelaou, M. B. Johnston, L. M. Herz and H. J. Snaith, *Energy Environ. Sci.*, 2014, **7**, 982-988.

89. C. C. Stoumpos, C. D. Malliakas and M. G. Kanatzidis, *Inorg. Chem.*, 2013, **52**, 9019-9038.

90. C. K. Möller, *Nature*, 1958, **182**, 1436.

91. B. Zhao, S.-F. Jin, S. Huang, N. Liu, J.-Y. Ma, D.-J. Xue, Q. Han, J. Ding, Q.-Q. Ge, Y. Feng and J.-S. Hu, *J. Am. Chem. Soc.*, 2018, **140**, 11716-11725.

92. Y. Wang, M. I. Dar, L. K. Ono, T. Zhang, M. Kan, Y. Li, L. Zhang, X. Wang, Y. Yang, X. Gao, Y. Qi, M. Grätzel and Y. Zhao, *Science*, 2019, **365**, 591-595.

View Article Online
DOI: 10.1039/D1EE00062D

93. N. Onoda-Yamamuro, O. Yamamuro, T. Matsuo and H. Suga. *J. Phys. Chem. Solids*, 1992, **53**, 2, 277-281.

94. L. K. Ono, S. (F.) Liu and Y. Qi, *Angew. Chem. Int. Ed.*, 2020, **59**, 6676-6698.

95. P. Zhao, B. J. Kim and H. S. Jung, *Mater. Today Energy*, 2018, **7**, 267-286.

96. A. J. Knight and L. M. Herz, *Energy Environ. Sci.*, 2020, **13**, 2024-2046.

97. G. Xing, N. Mathews, S. S. Lim, N. Yantara, X. Liu, D. Sabba, M. Grätzel, S. Mhaisalkar and T. C. Sum, *Nat. Mater.*, 2014, **13**, 476-480.

98. F. Yuan, Z. Wu, H. Dong, J. Xi, K. Xi, G. Divitini, B. Jiao, X. Hou, S. Wang and Q. Gong, *J. Phys. Chem. C*, 2017, **121**, 15318-15325.

99. W. Peng, B. Anand, L. Liu, S. Sampat, B. E. Bearden, A. V. Malko and Y. J. Chabal, *Nanoscale*, 2016, **8**, 1627-1634.

100. R. J. Stewart, C. Grieco, A. V. Larsen, G. S. Doucette and J. B. Asbury, *J. Phys. Chem. C*, 2016, **120**, 12392-12402.

101. Y. Shao, Z. Xiao, C. Bi, Y. Yuan and J. Huang, *Nat. Commun.*, 2014, **5**, 5784.

102. Y. Lin, L. Shen, J. Dai, Y. Deng, Y. Wu, Y. Bai, X. Zheng, J. Wang, Y. Fang and H. Wei, *Adv. Mater.*, 2017, **29**, 1604545.

103. D. Yang, X. Zhou, R. Yang, Z. Yang, W. Yu, X. Wang, C. Li, S. F. Liu and R. P. Chang, *Energy Environ. Sci.*, 2016, **9**, 3071-3078.

104. A. Baumann, S. Vath, P. Rieder, M. C. Heiber, K. Tvingstedt and V. Dyakonov, *J. Phys. Chem. Lett.*, 2015, **6**, 2350-2354.

105. Z. Ni, C. Bao, Y. Liu, Q. Jiang, W.-Q. Wu, S. Chen, X. Dai, B. Chen, B. Hartweg, Z. Yu, Z. Holman and J. Huang, *Science*, 2020, **367**, 1352-1358.

View Article Online
DOI: 10.1039/D1EE00062D

106. W. S. Yang, B.-W. Park, E. H. Jung, N. J. Jeon, Y. C. Kim, D. U. Lee, S. S. Shin, J. Seo, E. K. Kim and J. H. Noh, *Science*, 2017, **356**, 1376-1379.

107. J. Yuan, L. Zhang, C. Bi, M. Wang and J. Tian, *Sol. RRL*, 2018, **2**, 1800188.

108. G. Yin, H. Zhao, H. Jiang, S. Yuan, T. Niu, K. Zhao, Z. Liu and S. Liu, *Adv. Funct. Mater.*, 2018, **28**, 1803269.

109. D. Bai, J. Zhang, Z. Jin, H. Bian, K. Wang, H. Wang, L. Liang, Q. Wang and S. F. Liu, *ACS Energy Lett.*, 2018, **3**, 970-978.

110. N. Ito, M. A. Kamarudin, D. Hirotani, Y. Zhang, Q. Shen, Y. Ogomi, S. Iikubo, T. Minemoto, K. Yoshino and S. Hayase, *J. Phys. Chem. Lett.*, 2018, **9**, 1682-1688.

111. C. H. Ng, K. Nishimura, N. Ito, K. Hamada, D. Hirotani, Z. Wang, F. Yang, S. Likubo, Q. Shen, K. Yoshino, T. Minemoto and S. Hayase, *Nano Energy*, 2019, **58**, 130-137.

112. C. H. Ng, K. Hamada, G. Kapil, M. A. Kamarudin, Z. Wang, S. likubo, Q. Shen, K. Yoshino, T. Minemoto and S. Hayase, *J. Mater. Chem. A*, 2020, **8**, 2962-2968.

113. G. Namkoong, A. A. Mamun, T. T. Ava, K. Zhang and H. Baumgart, *Org. Electron.*, 2017, **42**, 228-233.

114. Y. Shi, J. Xi, T. Lei, F. Yuan, J. Dai, C. Ran, H. Dong, B. Jiao, X. Hou and Z. Wu, *ACS Appl. Mater. Interfaces*, 2018, **10**, 9849-9857.

115. J. M. Ball and A. Petrozza, *Nat. Energy*, 2016, **1**, 16149.

116. A. Walsh and A. Zunger, *Nat. Mater.*, 2017, **16**, 964-967.

117. J. Kim, A. Ho-Baillie and S. Huang, *Sol. RRL* 2019, **3**, 1800302.

118. D. W. de Quilettes, S. M. Vorpahl, S. D. Stranks, H. Nagaoka, G. E. Eperon, M. E. Ziffer, H. J. Snaith and D. S. Ginger, *Science*, 2015, **348**, 683-686.

119. G. Wang, S. Bai, W. Tress, A. Hagfeldt and F. Gao, *npj Flexible Electron.*, 2018, **2**, 22.

View Article Online
DOI: 10.1039/D1EE00062D

120. E. Aydin, M. De Bastiani and S. De Wolf, *Adv. Mater.*, 2019, **31**, 1900428.

121. M. Jung, S.-G. Ji, G. Kim and Sang Il Seok, *Chem. Soc. Rev.*, 2019, **48**, 2011-2038.

122. C. Liu, Y.-B. Cheng and Z. Ge, *Chem. Soc. Rev.*, 2020, **49**, 1653-1687.

123. W. A. Dunlap-Shohl, Y. Zhou, N.P. Padture and D. B. Mitzi**,** *Chem. Rev.*, 2019, **119**, 5, 3193-3295.

124. T. Wu, Y. Wang, X. Li, Y. Wu, X. Meng, D. Cui, X. Yang and L. Han, *Adv. Energy Mater.*, 2019, **9**, 1803766.

125. D. Xin, S. Tie, R. Yuan, X. Zheng, J. Zhu and W.-H. Zhang, *ACS Appl. Mater. Interfaces*, 2019, **11**, 44233-44240.

126. L. Guan, N. Jiao and Y. Guo, *J. Phys. Chem. C*, 2019, **123**, 14223-14228.

127. J. Zhang, Q. Sun, Q. Chen, Y. Wang, Y. Zhou, B. Song, X. Jia, Y. Zhu, S. Zhang, N. Yuan, J. Ding and Y. Li, *Solar RRL*, 2020, **4**, 1900421.

128. W. Feng, C. Zhang, J.-X. Zhong, L. Ding and W.-Q. Wu, *Chem. Commun.*, 2020, **56**, 5006-5009.

129. B. Zhao, X. Yan, T. Zhang, X. Ma, C. Liu, H. Liu, K. Yan, Y. Chen and X. Li, *ACS Appl. Mater. Interfaces*, 2020, **12**, 9300-9306.

130. Z. Li, J. Dong, C. Liu, J. Guo, L. Shen and W. Guo, *Nano-Micro Lett.*, 2019, **11**, 50.

131. F. Qian, S. Yuan, Y. Cai, Y. Han, H. Zhao, J. Sun, Z. Liu and S. (F.) Liu, *Sol. RRL*, 2019, **3**, 1900072.

132. M.-S. Lee, S. Sarwar, S. Park, U. Asmat, D. T. Thuy, C.-h. Han, S. Ahn, I. Jeong and S. Hong, *Sustainable Energy Fuels*, 2020, **4**, 3318-3325.

133. Y. Zhou, H. Zhong, J. Han, M. Tai, X. Yin, M. Zhang, Z. Wu and H. Lin, *J. Mater. Chem. A*, 2019, **7**, 26334-26341.

View Article Online
DOI: 10.1039/D1EE00062D

134. K. Chen, J. Wu, Y. Wang, Q. Guo, Q. Chen, T. Cao, X. Guo, Y. Zhou, N. Chen, M. Zhang and Y. Li, *J. Mater. Chem. A*, 2019, **7**, 21140-21148.

135. Y. Z. Zheng, X.-T. Li, E.-F. Zhao, X. D. Lv, F. L. Meng, C. Peng, X.-S. Lai, M. Huang, G. Cao, X. Tao and J.-F. Chen, *J. Power Sources*, 2018, **377**, 103-109.

136. A. Abate, M. Saliba, D. J. Hollman, S. D. Stranks, K. Wojciechowski, R. Avolio, G. Grancini, A. Petrozza and H. J. Snaith, *Nano Lett.*, 2014, **14**, 3247-3254.

137. X. Wu, L. Zhang, Z. Xu, S. Olthof, X. R. Y. Liu, D. Yang, F. Gao and S. (F.) Liu, *J. Mater. Chem. A*, 2020, **8**, 8313-8322.

138. H. Si, C. Xu, Y. Ou, G. Zhang, W. Fan, Z. Xiong, A. Kausar, Q. Liao, Z. Zhang, A. Sattar, Z. Kang and Y. Zhang, *Nano Energy*, 2020, **68**, 104320.

139. D. Zheng, R. Peng, G. Wang, J. L. Logsdon, B. Wang, X. Hu, Y. Chen, V. P. Dravid, M. R. Wasielewski, J. Yu, W. Huang, Z. Ge, T. J. Marks and A. Facchetti, *Adv. Mater.*, 2019, **31**, 1903239.

140. S. Yang, Y. Wang, P. Liu, Y.-B. Cheng, H. J. Zhao and H. G. Yang, *Nat. Energy*, 2016, **1**, 15016.

141. F. Palazon, D. Pérez-del-Rey, S. Marras, M. Prato, M. Sessolo, H. J. Bolink and L. Manna, *ACS Energy Lett.*, 2018, **3**, 835-839.

142. D. Bi, X. Li, J. V. Milić, D. J. Kubicki, N. Pellet, J. Luo, T. LaGrange, P. Mettraux, L. Emsley, S. M. Zakeeruddin and M. Grätzel, *Nat. Commun.*, 2018, **9**, 4482.

143. H. Zhu, Y. Liu, F.T. Eickemeyer, L. Pan, D. Ren, M. A. Ruiz-Preciado, B. Carlsen, B. Yang, X. Dong, Z. Wang, H. Liu, S. Wang, S. M. Zakeeruddin, A. Hagfeldt, M. Ibrahim Dar, X. Li and M. Grätzel, *Adv. Mater.,* 2020, **32**, 1907757.

View Article Online
DOI: 10.1039/D1EE00062D

144. F. Wang, W. Geng, Y. Zhou, H.-H. Fang, C.-J. Tong, M. A. Loi, L.-M. Liu and N. Zhao, *Adv. Mater.*, 2016, **28**, 9986-9992.

145. S. Yang, J. Dai, Z. Yu, Y. Shao, Y. Zhou, X. Xiao, X. C. Zeng and J. Huang, *J. Am. Chem. Soc.*, 2019, **141**, 5781-5787.

146. R. Wang, J. Xue, K.-L. Wang, Z.-K. Wang, Y. Luo, D. Fenning, G. Xu, S. Nuryyeva, T. Huang, Y. Zhao, J. L. Yang, J. Zhu, M. Wang, S. Tan, I. Yavuz, K. N. Houk and Y. Yang, *Science*, 2019, **366**, 1509-1513.

147. Z. Huang, M. Wei, Y.-K. Wang, E.-H. Jung, T. G. Allen, E. Van Kerschaver, F. Pelayo García de Arquer, M. I. Saidaminov, S. Hoogland, S. De Wolf and E. H. Sargent, *Nat. Commun.*, 2020, **11**, 1257.

148. L. Yang, Y. Xiao, G. Han, Y. Chang, Y. Zhang, W. Hou, J.-Y. Lin and H. Li, *Org. Electron.* 2020, **81**, 105681.

149. J. Wang, J. Zhang, Y. Zhou, H. Liu, Q. Xue, X. Li, C.-C. Chueh, H.-L. Yip, Z. Zhu and A. K. Y. Jen, *Nat. Commun.*, 2020, **11**, 177.

150. Z. Yang, J. Dou, S. Kou, J. Dang, Y. Ji, G. Yang, W.-Q. Wu, D.-B. Kuang and M. Wang, *Adv. Funct. Mater.*, 2020, **30**, 1910710.

151. F. Liu, Y. Zhang, C. Ding, S. Kobayashi, T. Izuishi, N. Nakazawa, T. Toyoda, T. Ohta, S. Hayase, T. Minemoto, K. Yoshino, S. Dai and Q. Shen, *ACS Nano*, 2017, **11**, 10373-10383.

152. M. Qin, J. Cao, T. Zhang, J. Mai, T.-K. Lau, S. Zhou, Y. Zhou, J. Wang, Y.-J. Hsu, N. Zhao, J. Xu, X. Zhan and X. Lu, *Adv. Energy Mater.*, 2018, **8**, 1703399.

153. M. Li, Y.-H. Chao, T. Kang, Z.-K. Wang, Y.-G. Yang, S.-L. Feng, Y. Hu, X.-Y. Gao, L.-S. Liao and C.-S. Hsu, *J. Mater. Chem. A*, 2016, **4**, 15088-15094.

154. C.-H. Chiang and C.-G. Wu, *Nat. Photonics*, 2016, **10**, 196-200.

View Article Online
DOI: 10.1039/D1EE00062D

155. J. Xu, A. Buin, A. H. Ip, W. Li, O. Voznyy, R. Comin, M. Yuan, S. Jeon, Z. Ning, J. J. McDowell, P. Kanjanaboos, J.-P. Sun, X. Lan, L. N. Quan, D. H. Kim, I. G. Hill, P. Maksymovych and E. H. Sargent, *Nat. Commun.*, 2015, **6**, 7081.

156. Q. Dong, C. H. Y. Ho, H. Yu, A. Salehi and F. So, *Chem. Mater.* 2019, **31**, 6833-6840.

157. Q. Chen, W. Wang, S. Xiao, Y. Cheng, F. Huang and W. Xiang, *ACS Appl. Mater. Interfaces*, 2019, **11**, 27145-27152.

158. J. Zhen, W. Zhou, M. Chen, B. Li, L. Jia, M. Wang and S. Yang, *J. Mater. Chem. A*, 2019, **7**, 2754-2763.

159. P.-P. Cheng, Y.-W. Zhang, J.-M. Liang, W.-Y. Tan, X. Chen, Y. Liu and Y. Min, *Sol. Energy*, 2019, **190**, 264-271.

160. F. Cai, J. Cai, L. Yang, W. Li, R. S. Gurney, H. Yi, A. Iraqi, D. Liu and T. Wang, *Nano Energy*, 2018, **45**, 28-36.

161. C. C. Zhang, M. Li, Z.-K. Wang, Y.-R. Jiang, H.-R. Liu, Y.-G. Yang, X.-Y. Gao and H. Ma, *J. Mater. Chem. A*, 2017, **5**, 2572-2579.

162. C.-Y. Chang and C.-C. Wang, *J. Mater. Chem. A*, 2020, **8**, 8593-8604.

163. Q. Zeng, X. Zhang, X. Feng, S. Lu, Z. Chen, X. Yong, S. A. T. Redfern, H. Wei, H. Wang, H. Shen, W. Zhang, W. Zheng, H. Zhang, J. S. Tse and B. Yang, *Adv. Mater.*, 2018, **30**, 1705393.

164. F. Tan, H. Tan, M. I. Saidaminov, M. Wei, M. Liu, A. Mei, P. Li, B. Zhang, C.-S. Tan, X. Gong, Y. Zhao, A. R. Kirmani, Z. Huang, J. Z. Fan, R. Quintero-Bermudez, J. Kim, Y. Zhao, O. Voznyy, Y. Gao, F. Zhang, L. J. Richter, Z.-H. Lu, W. Zhang and E. H. Sargent, *Adv. Mater.*, 2019, **31**, 1807435.

165. B. Li, Y. Zhang, L. Fu, T. Yu, S. Zhou, L. Zhang and L. Yin, *Nat. Commun.*, 2018, **9**, 1076.

View Article Online
DOI: 10.1039/D1EE00062D

166. Q. Zhang, S. Xiong, J. Ali, K. Qian, Y. Li, W. Feng, H. Wu, J. Song and F. Liu, *J. Mater. Chem. C*, 2020, **8**, 5467-5475.

167. Y. Moriya, R. Ishikawa, S. Akiyama, K. Ueno and H. Shirai, *Chem. Lett.*, 2020, **49**, 87-90.

168. T. Wang, S. Abbasi, X. Wang, Y. Wang, Z. Cheng, J. Wang, H. Liu and W. Shen, *Chem. Commun.*, 2019, **55**, 14996-14999.

169. J. Peng, Y. Wu, W. Ye, D. A. Jacobs, H. Shen, X. Fu, Y. Wan, T. Duong, N. Wu, C. Barugkin, H. T. Nguyen, D. Zhong, J. Li, T. Lu, Y. Liu, M. N. Lockrey, K. J. Weber, K. R. Catchpole and T. P. White, *Energy Environ. Sci.*, 2017, **10**, 1792-1800.

170. H. Chen, T. Liu, P. Zhou, S. Li, J. Ren, H. He, J. Wang, N. Wang and S. Guo, *Adv. Mater.*, 2019, **32**, 1905661.

171. W. Li, X. Lai, F. Meng, G. Li, K. Wang, A. K. K. Kyaw and X. W. Sun, *Sol. Energy Mater. Sol. Cells*, 2020, **211**, 110527.

172. C. Hanmandlu, S. Swamy, A. Singh, H.-A. Chen, C.-C. Liu, C.-S. Lai, A. Mohapatra, C.-W. Pao, P. Chen and C.-W. Chua, *J. Mater. Chem. A*, 2020, **8**, 5263-5274.

173. S.-C. Liu, Z. Li, Y. Yang, X. Wang, Y.-X. Chen, D.-J. Xue and J.-S. Hu, *J. Am. Chem. Soc.*, 2019, **141**, 18075-18082.

174. R. Azmi, N. Nurrosyid, S.-H. Lee, M. Al Mubarok, W. Lee, S. Hwang, W. Yin, T. K. Ahn, T.-W. Kim, D. Y. Ryu, Y. R. Do and S.-Y. Jang, *ACS Energy Lett.*, 2020, **5**, 1396-1403.

175. X. Zheng, B. Chen, J. Dai, Y. Fang, Y. Bai, Y. Lin, H. Wei, X. C. Zeng and J. Huang, *Nat. Energy*, 2017, **2**, 17102.

176. X. Liu, Y. Zhang, L. Shi, Z. Liu, J. Huang, J. S. Yun, Y. Zeng, A. Pu, K. Sun, Z. Hameiri, J. A. Stride, J. Seidel, M. A. Green and X. Hao, *Adv. Energy Mater.*, 2018, **8**, 1800138.

View Article Online
DOI: 10.1039/D1EE00062D

177. H. Si, C. Xu, Y. Ou, G. Zhang, W. Fan, Z. Xiong, A. Kausar, Q. Liao, Z. Zhang, A. Sattar, Z. Kang and Y. Zhang, *Nano Energy*, 2020, **68**, 104320.

178. J. Seo, S. Park, Y. Chan Kim, N. J. Jeon, J. H. Noh, S. C. Yoon and S. I. Seok, *Energy Environ. Sci.*, 2014, **7**, 2642-2646.

179. K. Sun, J. Chang, F. H. Isikgor, P. Li and J. Ouyang, *Nanoscale*, 2015,**7**, 896-900.

180. A. A. Sutanto, N. Drigo, V. I. E. Queloz, I. Garcia-Benito, A. R. Kirmani, L. J. Richter, P. A. Schouwink, K. T. Cho, S. P. Paek, M. K. Nazeeruddin and G. Grancini, *J. Mater. Chem. A*, 2020, **8**, 2343-2348.

181. M. A. Mahmud, T. Duong, Y. Yin, H. T. Pham, D. Walter, J. Peng, Y. Wu, L. Li, H. Shen, N. Wu, N. Mozaffari, G. Andersson, K. R. Catchpole, K. J. Weber and T. P. White, *Adv. Funct. Mater.*, 2019, **30**, 1907962.

182. L. Yang, Y. Li, Y. Pei, J. Wang, H. Lin and X. Li, *J. Mater. Chem. A*, 2020, **8**, 7808-7818.

183. P. Chen, Y. Bai, S. Wang, M. Lyu, J.-H. Yun and L. Wang. *Adv. Funct. Mater*., 2018, **28**, 1706923.

184. S. Gharibzadeh, B. A. Nejand, M. Jakoby, T. Abzieher, D. Hauschild, S. Moghadamzadeh, J. A. Schwenzer, P. Brenner, R. Schmager, A. A. Haghighirad, L. Weinhardt, U. Lemmer, B. S. Richards, I. A. Howard and U. W. Paetzold. *Adv. Energy Mater.*, 2019, **9**, 1803699.

185. Q. Jiang, Y. Zhao, X. Zhang, X. Yang, Y. Chen, Z. Chu, Q. Ye, X. Li, Z. Yin and J. You, *Nat. Photonics*, 2019, **13**, 460-466**.**

186. G. Liu, H. Zheng, H. Xu, L. Zhang, X. Xu, S. Xu, X. Pan, *Nano Energy* 2020, **73**, 104753.

187. V. E. Madhavan, I. Zimmerman, A. A. B. Baloch, A. Manekkathodi, A. Belaidi, N. Tabet and M. K. Nazeeruddin, *ACS Appl. Energy Mater.*, 2020, **3**, 114-121.

View Article Online
DOI: 10.1039/D1EE00062D

188. Q. Zhou, L. Liang, J. Hu, B. Cao, L. Yang, T. Wu, X. Li, B. Zhang and P. Gao, *Adv. Energy Mater.*, 2019, **9**, 1802595.

189. J. Zhuang, P. Mao, Y. Luan, X. Yi, Z. Tu, Y. Zhang, Y. Yi, Y. Wei, N. Chen, T. Lin, F. Wang, C. Li and J. Wang, *ACS Energy Lett.*, 2019, **4**, 2913-2921.

190. Y. Lv, X. Song, Y. Yin, Y. Feng, H. Ma, C. Hao, S. Jin and Y. Shi, *ACS Appl. Mater. Interfaces*, 2020, **12**, 698-705.

191. T. Bu, J. Li, Q. Lin, D. P. McMeekin, J. Sun, M. Wang, W. Chen, X. Wen, W. Mao, C. R. McNeill, W. Huang, X.-L. Zhan, J. Zhong, Y.-B. Chengab, U. Bach and F. Huang, *Nano Energy*, 2020, **75**, 104917.

192. M. Salado, M. Andresini, P. Huang, M. Taukeer Khan, F. Ciriaco, S. Kazim and S. Ahmad, *Adv. Funct. Mater.*, 2020, **30**, 1910561.

193. Y. Chen, Y. Sun, J. Peng, W. Zhang, X. Su, K. Zheng, T. Pullerits and T. Liang, *Adv. Energy Mater.*, 2017, **7**, 1700162.

194. J.-W. Lee, Z. Dai, T.-H. Han, C. Choi, S.-Y. Chang, S.-J. Lee, N. De Marco, H. Zhao, P. Sun, T. Huang and Y. Yang, *Nat. Commun.*, 2018, **9**, 3021.

195. J. Fan, Y. Ma, C. Zhang, C. Liu, W. Li, R. E. I. Schropp and Y. Mai, *Adv. Energy Mater.*, 2018, **8**, 1703421.

196. L. Gao, I. Spanopoulos, W. Ke, S. Huang, I. Hadar, L. Chen, X. Li, G. Yang and M. G. Kanatzidis, *ACS Energy Lett.*, 2019, **4**, 1763-1769.

197. M. M. Elsenety, M. Antoniadou, N. Balis, A. Kaltzoglou, L. Sygellou, A. Stergiou, N. Tagmatarchis and P. Falaras, *ACS Appl. Energy Mater.*, 2020, **3**, 2465-2477.

198. B. Kim and S. I. Seok, *Energy Environ. Sci.*, 2020, **13**, 805-820.

View Article Online
DOI: 10.1039/D1EE00062D

199. X. Wang, Y. Wang, T. Zhang, X. Liu and Y. Zhao, *Angew. Chem. Intern. Edit.*, 2020, **59**, 1469-1473.

200. X.-X. Feng, X.-D. Lv, Q. Liang, J. Cao and Y. Tang, *ACS Appl. Mater. Interfaces*, 2020, **12**, 16236-26242.

201. H. Wang, Z. Wang, Z. Yang, Y. Xu, Y. Ding, L. Tan, C. Yi, Z. Zhang, K. Meng, G. Chen, Y. Zhao, Y. Luo, X. Zhang, A. Hagfeldt and J. Luo, *Adv. Mater.*, 2020, **22**, 2000865.

202. S. M. Park, A. Abtahi, A. M. Boehm and K. R. Graham, *ACS Energy Lett.*, 2020, **5**, 799-806.

203. O. Y. Gong, Y. Kim, D. H. Kim, G. S. Han, S. Jeong and H. S. Jung, *ACS Energy Lett.*, 2020, **5**, 1032-1034.

204. J. Cao, J. Yin, S. Yuan, Y. Zhao, J. Li and N. Zheng, *Nanoscale*, 2015, **7**, 9443-9447.

205. A. Magomedov, A. Al-Ashouri, E. Kasparavičius, S. Strazdaite, G. Niaura, M. Jošt, T. Malinauskas, S. Albrecht and V. Getautis, *Adv. Energy Mater.*, 2018, **8**, 1801892.

206. C. M. Wolff, L. Canil, C. Rehermann, N. L. Nguyen, F. Zu, M. Ralaiarisoa, P. Caprioglio, L. Fiedler, M. Stolterfoht, S. Kogikoski Jr., I. Bald, N. Koch, E. L. Unger, T. Dittrich, A. Abate and D. Neher, *ACS Nano*, 2020, **14**, 1445-1456.

207. A. Al-Ashouri, A. Magomedov, M. Roß, M. Jošt, M. Talaikis, G. Chistiakova, T. Bertram, J. A. Márquez, E. Köhnen, E. Kasparavičius, S. Levcenco, L. Gil-Escrig, C. J. Hages, R. Schlatmann, B. Rech, T. Malinauskas, T. Unold, C. A. Kaufmann, L. Korte, G. Niaura, V. Getautis and S. Albrecht, *Energy Environ. Sci.*, 2019, **12**, 3356-3369.

208. Z. Gu, L. Zuo, T. T. Larsen-Olsen, T. Ye, G. Wu, F. C. Krebs and H. Chen, *J. Mater. Chem. A*, 2015, **3**, 24254-24260.

View Article Online
DOI: 10.1039/D1EE00062D

209. A. Abrusci, S. D. Stranks, P. Docampo, H.-L. Yip, A.-K. Y. Jen and H. J. Snaith, *Nano Lett.*, 2013, **13**, 3124-3128.

210. T. Niu, J. Lu, R. Munir, J. Li, D. Barrit, X. Zhang, H. Hu, Z. Yang, A. Amassian, K. Zhao and S. (F.) Liu, *Adv. Mater.*, 2018, **30**, 1706576.

211. Z. Liu, F. Cao, M. Wang, M. Wang and L. Li, *Angew. Chem*., 2020, **132**, 4190-4196.

212. X. Huang, Q. Cui, W. Bi, L. Li, P. Jia, T. Hou, Y. Hu, Z. Lou and F. Teng, *RSC Adv.*, 2019, 9, 7984-79910.

213. Y. Chen, J. Shia, X. Li, S. Li, X. Lv, X. Sun, Y.-Z. Zheng and X. Tao, *J. Mater. Chem. A*, 2020, **8**, 6349-6359.

214. Y. Yang, L. Wu, X. Hao, Z. Tang, H. Lai, J. Zhang, W. Wang and L. Feng, *RSC Adv.*, 2019, **9**, 28561-28568.

215. H. Yoon, S. M. Kang, J.-K. Lee and M. Choi, *Energy Environ. Sci.*, 2016, **9**, 2262-2262.

216. P. Guo, Q. Ye, X. Yang, J. Zhang, F. Xu, D. Shchukin, B. Wei and H. Wang, *J. Mater. Chem. A*, 2019, **7**, 2497-2506.

217. S.-Y. Wang, C.-P. Chen, C.-L. Chung, C.-W. Hsu, H.-L. Hsu, T.-H. Wu, J.-Y. Zhuang, C. J. Chang, H. M. Chen and Y. J. Chang, *ACS Appl. Mater. Interfaces*, 2019, **11**, 40050-40061.

218. Z. Wang, A. Pradhan, M. A. Kamarudin, M. Pandey, S. S. Pandey, P. Zhang, C. Ng, A. S. M. Tripathi, T. Ma and S. Hayase, *ACS Appl. Mater. Interfaces*, 2019, **11**, 10012-10020.

219. S. Zhao, M. Qin, Y. Xiang, H. Wang, J. Xie, L. Gong, J. Chen, X. Lu, J. Song, J. Qu, J. Xu and K. Yan, *ACS Appl. Energy Mater.*, 2020, **3**, 3302-3309.

220. J.-W. Lee, S.-H. Bae, Y.-T. Hsieh, N. De Marco, M. Wang, P. Sun and Y. Yang, *Chem*, 2017, **3**, 290-302.

View Article Online
DOI: 10.1039/D1EE00062D

221. X. Shi, Y. Wu, J. Chen, M. Cai, Y. Yang, X. Liu, Y. Tao, M. Guli, Y. Ding and S. Dai, *J. Mater. Chem. A*, 2020, **8**, 7205-7213.

222. Z. Liu, L. K. Ono and Y. Qi, J. *of Energy Chemistry*, 2020, **46**, 215-228.

223. W. Chen, Y. Wang, G. Pang, C. W. Koh, A. B. Djurišic´, Y. Wu, B. Tu, F.-Z. Liu, R. Chen, H. Y. Woo, X. Guo and Z. He, *Adv. Funct. Mater.*, 2019, **29**, 1808855.

224. W. Kim, J. B. Park, H. Kim, K. Kim, J. Park, S. Cho, H. Lee, Y. Pak and G. Y. Jung, *J. Mater. Chem. A*, 2019, **7**, 20832-20839.

225. T.-H. Han, J.-W. Lee, C. Choi, S. Tan, C. Lee, Y. Zhao, Z. Dai, N. De Marco, S.-J. Lee, S.-H. Bae, Y. Yuan, H. M. Lee, Y. Huang and Y. Yang, *Nat. Commun.*, 2019, **10**, 520.

226. X. Li, W. Zhang, Y.-C. Wang, W. Zhang, H.-Q. Wang and J. Fang, *Nat. Commun.*, 2018, **9**, 3806.

227. S.-C. Yun, S. Ma, H.-C. Kwon, K. Kim, G. Jang, H. Yang and J. Moon, *Nano Energy*, 2019, **59**, 481-491.

228. X. Zheng, Y. Hou, C. Bao, J. Yin, F. Yuan, Z. Huang, K. Song, J. Liu, J. Troughton, N. Gasparini, C. Zhou, Y. Lin, D.-J. Xue, B. Chen, A. K. Johnston, N. Wei, M. N. Hedhili, M. Mei, A. Y. Alsalloum, P. Maity, B. Turedi, C. Yang, D. Baran, T. D. Anthopoulos, Y. Han, Z.-H. Lu, O. F. Mohammed, F. Gao, E. H. Sargent and O. M. Bakr, *Nat. Energy*, 2020, **5**, 131-140.

229. A. H. Proppe, M. Wei, B. Chen, R. Quintero-Bermudez, S. O. Kelley and E. H. Sargent, *J. Am. Chem. Soc.*, 2019, **141**, 14180-14189.

230. J. Peng, J. I. Khan, W. Liu, E. Ugur, T. Duong, Y. Wu, H. Shen, K. Wang, H. Dang, E. Aydin, X. Yang, Y. Wan, K. J. Weber, K. R. Catchpole, F. Laquai, S. De Wolf and T. P. White, *Adv. Energy Mater.*, 2018, **8**, 1801208.

View Article Online
DOI: 10.1039/D1EE00062D

231. Y. Li, W. Sun, F. Gu, D. Ouyang, Z. Bian, Z. Liu, W. C. H. Choy and T. L. Kelly, *Adv. Mater. Interfaces*, 2019, **6**, 1900474.

232. J. Xia, K. Xi, A. Sadhanal, K. H. L. Zhang, G. Li, H. Dong, T. Lei, F. Yuan, C. Ran, B. Jiao, P. R. Coxon, C. J. Harris, X. Hou, R. Vasant Kumar and Z. Wu, *Nano Energy*, **2019**, *56*, 741-750.

233. L. Liu, S. Huang, Y. Lu, P. Liu, Y. Zhao, C. Shi, S. Zhang, J. Wu, H. Zhong, M. Sui, H. Zhou, H. Jin, Y. Li and Q. Chen, *Adv. Mater.*, 2018, **30**, 1800544.

234. N. D. Pham, V. T. Tiong, D. Yao, W. Martens, A. Guerrero, J. Bisquert and H. Wang, *Nano Energy*, 2017, **41**, 476-487.

235. P. Zhu, S. Gu, X. Luo, Y. Gao, S. Li, J. Zhu and H. Tan, *Adv. Energy Mater.*, 2020, **10**, 1903083.

236. X. Cheng, S. Yang, B. Cao, X. Tao and Z. Chen, *Adv. Funct. Mater.*, 2020, **30**, 1905021.

237. H.-S. Rao, B.-X. Chen, X.-D. Wang, D.-B. Kuang and C.-Y. Su, *Chem. Commun.*, 2017, **53**, 5163.

238. J. Schlipf, A. M. Askar, F. Pantle, B. D. Wiltshire, A. Sura, P. Schneider, L. Huber, K. Shankar and P. Müller-Buschbaum, *Sci. Rep.*, 2018, **8**, 4906.

239. Y. Wang, X. Sun, Z. Chen, Y.-Y. Sun, S. Zhang, T.-M. Lu, E. Wertz and J. Shi, *Adv. Mater.*, 2017, **29**, 1702643.

240. H. Min, G. Kim, M. J. Paik, S. Lee, W. S. Yang, M. Jung and S. I. Seok, *Adv. Energy Mater.*, 2019, **9**, 1803476.

241. H. Tsai, W. Nie, P. Cheruku, N. H. Mack, P. Xu, G. Gupta, A. D. Mohite and H.-L. Wang, *Chem. Mater.*, 2015, **27**, 5570-5576.

242. R. Ishikawa, K. Ueno and H. Shirai, *Org. Electron.*, 2020, **78**, 105596.

View Article Online
DOI: 10.1039/D1EE00062D

243. S. Sidhik, A. C. Pasarán, C. R. Pérez, T. López-Luke and E. De la Rosa, *J. Mater. Chem. C*, 2018, **6**, 7880-7889.

244. E. A. Alharbi, M. I. Dar, N. Arora, M. H. Alotaibi, Y. A. Alzhrani, P. Yadav, W. Tress, A. Alyamani, A. Albadri, S. M. Zakeeruddin and M. Grätzel, *AAAS Research*, 2019, **2019**, 8474698.

245. J. L. Uribe, J. Ciro, J. F. Montoya, J. Osorio and F. Jaramillo, *ACS Appl. Energy Mater.*, 2018, **1**, 1047-1052.

246. S. Zhao, B. Zhao, Y. Chen, G. Yang and X. Li, *ACS Appl. Energy Mater.*, 2019, **2**, 6230-6236.

247. D. P. McMeekin, A. Wang, W. Rehman, F. Pulvirenti, J. B. Patel, N. K. Noel, M. B. Johnston, S. R. Marder, L. M. Herz and H. J. Snaith, *Adv. Mater.*, 2017, **29**, 1607039.

248. Y. Zhang, S. Chen, H. Chen, G. Zhang, M. Zhao, C. Zhao, W. Guo, W. Ji, Z. Shi and T. Jiub, *J. Mater. Chem. C*, 2020, **8**, 5894-5903.

249. Y. Zhao, P. Zhu, M. Wang, S. Huang, Z. Zhao, S. Tan, T.-H. Han, J.-W. Lee, T. Huang, R. Wang, J. Xue, D. Meng, Y. Huang, J. Marian, J. Zhu and Y. Yang, *Adv. Mater.*, 2020, **32**, 1907769.

250. Y. Wang, T. Li, Z. Li, S. Wang and X. Deng, *Adv. Funct. Mater.*, 2019, **29**, 1903330.

251. X. Liu, J. Wu, Q. Guo, Y. Yang, H. Luo, Q. Liu, X. Wang, X. He, M. Huang and Z. Lan, *J. Mater. Chem. A*, 2019, **7**, 11764-11770.

252. Z. Liu, J. Hu, H. Jiao, L. Li, G. Zheng, Y. Chen, Y. Huang, Q. Zhang, C. Shen, Q. Chen and H. Zhou, *Adv. Mater.*, 2017, **29**, 1606774.

253. Z. Chen, X. Zheng, F. Yao, J. Ma, C. Tao and G. Fang, *J. Mater. Chem. A*, 2018, **6**, 17625-17632.

View Article Online
DOI: 10.1039/D1EE00062D

254. W.-Q. Wu, Z. Yang, P. N. Rudd, Y. Shao, X. Dai, H. Wei, J. Zhao, Y. Fang, Q. Wang, Y. Liu, Y. Deng, X. Xiao, Y. Feng and J. Huang, *Sci. Adv.*, 2019**, 5**, eaav8925.

255. F. Haque, M. Wright, M. A. Mahmud, H. Yi, D. Wang, L. Duan, C. Xu, M. B. Upama and A. Uddin, *ACS Omega*, 2018, **3**, 11937-11944.

256. J. H. Heo, D. H. Song and S. H. Im, *Adv. Mater.*, 2014, **26**, 8179-8183.

257. M. A. Afroz, N. Ghimire, K. M. Reza, B. Bahrami, R. S. Bobba, A. Gurung, A. H. Chowdhury, P. K. Iyer and Q. Qiao, *ACS Appl. Energy Mater.*, 2020, **3**, 2432-2439.

258. J. Huang, M. Wang, L. Ding, Z. Yang and K. Zhang, *RSC. Adv.*, 2016, **6**, 55720-55725.

259. C. Sun, Q. Xue, Z. Hu, Z. Chen, F. Huang, H.-L Yip and Y. Cao, *Small*, 2015, **11**, 3344-3350.

260. D. Yao, C. Zhang, S. Zhang, Y. Yang, A. Du, E. Waclawik, X. Yu, G. J. Wilson and H. Wang, *ACS Appl. Mater. Interfaces* 2019, **11**, 29753-29764.

261. X. Jia, L. Liu and Z. Fang, *J. Mater. Chem. C*, 2019, **7**, 7207-7211.

262. Y. Wang, S. Liu, Q. Zeng, R. Wang, W. Qin, H. Cao, L. Yang, L. Lia, S. Yin and F. Zhang, *Sol. Energy Mater. Sol. Cells*, 2018, **188**, 140-148.

263. L .Fan, Y. Ding, J. Luo, B. Shi, X. Yao, C. Wei, D. Zhang, G. Wang, Y. Sheng, Y. Chen, A. Hagfeldt, Y. Zhao and X. Zhang, *J. Mater. Chem. A*, 2017, **5**, 7423-7432.

264. Y. Cai, S. Wang, M. Sun, X. Li and Y. Xiao, *Org. Electron.*, 2018, **53**, 249-255.

265. Y. Yu, C. Wang, C. R. Grice, N. Shrestha, D. Zhao, W. Liao, L. Guan, R. A. Awni, W. Meng, A. J. Cimaroli, K. Zhu, R. J. Ellingson and Y. Yan, *ACS Energy Lett.*, 2017, **2**, 1177-1182.

View Article Online
DOI: 10.1039/D1EE00062D

266. S. Bai, P. Da, C. Li, Z. Wang, Z. Yuan, F. Fu, M. Kawecki, X. Liu, N. Sakai, J. T.-W. Wang, S. Huettner, S. Buecheler, M. Fahlman, F. Gao and H. J. Snaith, *Nature*, 2019, **571**, 245-250.

267. S. Masi, N. Sestu, V. Valenzano, T. Higashino, H. Imahori, M. Saba, G. Bongiovanni, V. Armenise, A. Milella, G. Gigli, A. Rizzo, S. Colella and A. Listorti, *ACS Appl. Mater. Interfaces,* 2020, **12**, 18431-18436.

268. X. Zhang, G. Ji, D. Xiong, Z. Su, B. Zhao, K. Shen, Y. Yang and X. Gao, *RSC Adv.*, 2018, **8**, 987-993.

269. Y. Gao, Y. Wu, H. Lu, C. Chen, Y. Liu, X. Bai, L. Yang, W. W. Yu, Q. Dai and Y. Zhang, *Nano Energy*, 2019, **59**, 517-526.

270. H. Xu, H. Zhang, Y. Ma, M. Jiang, Y. Zhang, Y. Wu, H. Zhang, R. Xia, Q. Niu, X. Li and W. Huang, *Sci. Rep.*, 2019, **9**, 15441.

271. Y. Zhang, L. Tan, Q. Fu, L. Chen, T. Ji, X. Hua and Y. Chen, *Chem. Commun.*, 2016, **52**, 5674-5677.

272. C. Tao, S. Neutzner, L. Colella, S. Marras, A. R. S. Kandada, M. Gandini, M. De Bastiani, G. Pace, L. Manna, M. Caironi, C. Bertarellia and A. Petrozza, *Energy Environ. Sci.*, 2015, **8**, 2365-2370.

273. L. Zuo, H. Guo, D. W. deQuilettes, S. Jariwala, N. De Marco, S. Dong, R. DeBlock, D. S. Ginger, B. Dunn, M. Wang and Y. Yang, *Sci. Adv.*, 2017, **3**, e1700106.

274. Y. Lan, Y. Wang and Y. Song, *Flexible Printed Electron.*, 2020, **5**, 014001.

275. B. Chen, Z. Yu, K. Liu, X. Zheng, Y. Liu, J. Shi, D. Spronk, P. N. Rudd, Z. Holman and J. Huang, *Joule*, 2019, **3**, 177-190.

View Article Online
DOI: 10.1039/D1EE00062D

276. C. H. Ng, K. Nishimura, N. Ito, K. Hamada, D. Hirotani, Z. Wang, F. Yang, S. Iikubo, Q. Shen, K. Yoshino, T. Minemoto and S. Hayase, *Nano Energy*, 2019, **58**, 130-137.

277. X. Lin, A. S. R. Chesman, S. R. Raga, A. D. Scully, L. Jiang, B. Tan, J. Lu, Y.-B. Cheng and U. Bach, *Adv. Funct. Mater.*, 2018, **28**, 1805098.

278. S. Sanders, D. Stümmler, P. Pfeiffer, N. Ackermann, F. Schimkat, G. Simkus, M. Heuken, P. K. Baumann, A. Vescan and H. Kalisch, *Phys. Status Solidi A*, 2018, **215**, 1800409.

279. K. Zhang, Z. Wang, G. Wang, J. Wang, Y. Li, W. Qian, S. Zheng, S. Xiao and S. Yang, *Nat. Commun.*, 2020, **11**, 1006.

280. J. Lian, Q. Wang, Y. Yuan, Y. Shao and J. Huang, *J. Mater. Chem. A*, 2015, **3**, 9146-9151.

281. Y. Wang, S. Li, P. Zhang, D. Liu, X. Gu, H. Sarvari, Z. Yea, J. Wu, Z. Wang and Z. D. Chen, *Nanoscale* 2016, **8**, 19654-19661.

282. H. Yu, X. Liu, Y. Xia, Q. Dong, K. Zhang, Z. Wang, Y. Zhou, B. Song and Y. Li, *J. Mater. Chem. A* 2016, **4**, 321-326.

283. X. Sun, C. Zhang, J. Chang, H. Yang, H. Xi, G. Lu, D. Chen, Z. Lin, X. Lu, J. Zhang and Y. Hao, *Nano Energy* 2016, **28**, 417-425.

284. J. Luo, R. Z. Qiu, Z. S. Yang, Y. X. Wang and Q. F. Zhang, *RSC Adv.* 2018, **8**, 724-731.

285. J. Mou, J. Song, M. Che, Y. Liu, Y. Qin, H. Liu, L. Zhu, Y. Zhao and Y. Qiang, *J. Mater. Sci.:Mater. Electron.*, 2019, **30**, 746-752.

286. Z.-H. Zheng, H.-B. Lan, Z.-H. Su, H.-X. Peng, J.-T. Luo, G.-X. Liang and P. Fan, *Sci. Rep.* 2019, **9**, 17422.

287. D. Bi, C. Yi, J. Luo, J.-D. Décoppet, F. Zhang, S. M. Zakeeruddin, X. Li, A. Hagfeldt and M. Grätzel, *Nat. Energy*, 2016, **1**, 16142.

View Article Online
DOI: 10.1039/D1EE00062D

288. J. Wang, S. Luo, Y. Lin, Y. Chen, Y. Deng, Z. Li, K. Meng, G. Chen, T. Huang, S. Xiao, H. Huang, C. Zhou, L. Ding, J. He, J. Huang and Y. Yuan, *Nat. Commun.*, 2020, **11**, 582.

289. S. Seo, I. Jeon, R. Xiang, C. Lee, H. Zhang, T. Tanaka, J.-W. Lee, D. Suh, T. Ogamoto, R. Nishikubo, A. Saeki, S. Chiashi, J. Shiomi, H. Kataura, H. M. Lee, Y. Yang, Y. Matsuo and S. Maruyama, *J. Mater. Chem. A*, 2019, **7**, 12987-12992.

290. C. Liu, Y. Yang, X. Xia, Y. Ding, Z. Arain, S. An, X. Liu, R. C. Cristina, S. Dai and M. K. Nazeeruddin, *Adv. Energy Mater.*, 2020, **10**, 1903751.

291. X. Liu, Y. Cheng, C. Liu, T. Zhang, N. Zhang, S. Zhang, J. Chen, Q. Xu, J. Ouyang and H. Gong, *Energy Environ. Sci.*, 2019, **12**, 1622-1633.

292. K. Yan, M. Long, T. Zhang, Z. Wei, H. Chen, S. Yang and J. Xu, *J. Am. Chem. Soc.*, 2015, **137**, 4460-4468.

293. M. Yang, T. Zhang, P. Schulz, Z. Li, G. Li, D. H. Kim, N. Guo, J. J. Berry, K. Zhu and Y. Zhao, *Nat. Commun.*, 2016, **7**, 12305.

294. Y. Wang, T. Zhang, M. Kan and Y. Zhao, *J. Am. Chem. Soc.*, 2018, **140**, 12345-12348.

295. D. W. deQuilettes, S. Koch, S. Burke, R. K. Paranji, A. J. Shropshire, M. E. Ziffer and D. S. Ginger, *ACS Energy Lett.*, 2016, **1**, 438-444.

296. I. L. Braly, D. W. deQuilettes, L. M. Pazos-Outón, S. Burke, M. E. Ziffer, D. S. Ginger and H. W. Hillhouse, *Nat. Photonics*, 2018, **12**, 355-361.

297. F. Zhang and K. Zhu, *Adv. Energy Mater.*, 2019, **10**, 1902579.

298. B. Li, M. Li, C. Fei, G. Cao and J. Tian, *J. Mater. Chem. A*, 2017, **5**, 24168-24177.

299. Y. Zhang, S. Seo, S. Y. Lim, Y. Kim, S.-G. Kim, D.-K. Lee, S.-H. Lee, H. Shin, H. Cheong and N. G. Park, A*CS Energy Lett.*, 2020, **5**, 360-366.

View Article Online
DOI: 10.1039/D1EE00062D

300. T. Du, C. H. Burgess, C.-T. Lin, F. Eisner, J. Kim, S. Xu, H. Kang, J. R. Durrant and M. A. McLachlan, *Adv. Funct. Mater.*, 2018, **28**, 1803943.

301. W. Rehman, D. P. McMeekin, J. B. Patel, R. L. Milot, M. B. Johnston, H. J. Snaith and L. M. Herz, *Energy Environ. Sci.*, 2017, **10**, 361-369.

302. P.-W. Liang, C.-Y. Liao, C.-C. Chueh, F. Zuo, S. T. Williams, X.-K. Xin, J. Lin and A. K.-Y. Jen, *Adv. Mater.*, 2014, **26**, 3748-3754.

303. S. Bi, H. Wang, J. Zhou, S. You, Y. Zhang, X. Shi, Z. Tang and H. Zhou, *J. Mater. Chem. A*, 2019, **7**, 6840-6848.

304. G. Fu, L. Hou, Y. Wang, X. Liu, J. Wang, H. Li, Y. Cui, D. Liu, X. Lia and S. Yang, *Sol. Energy Mater. Sol. Cells*, 2017, **165**, 36-44.

305. Z. Liu, D. Liu, H. Chen, L. Ji, H. Zheng, Y. Gu, F. Wang, Z. Chen and S. Li, *Nanoscale Res. Lett.*, 2019, **14**, 304.

306. L. Ye, H. Wang, Y. Wei, P. Guo, X. Yang, Q. Ye and H. Wang, *ACS Appl. Energy Mater.*, 2020, **3**, 658-665.

307. C. Dokkhan, M. Z. Mokhtar, C.-R. Ke, A. S. Walton, Q. Chen, N. W. Hodson, Q. Lian and B. R. Saunders, *ACS Appl. Energy Mater.*, 2019, **2**, 6624-6633.

308. J. Hong, H. Kim and I. Hwang, *Org. Electron.*, 2019, **73**, 87-93.

309. Q. He, M. Worku, L. Xu, C. Zhou, H. Lin, A. Robb, K. Hanson, Y. Xin and B. Ma, *ACS Appl. Mater. Interfaces*, 2020, **12**, 1159-1168.

310. M. Kim, S. G. Motti, R. Sorrentino and A. Petrozza, *Energy Environ. Sci.*, 2018, **11**, 2609-2619.

311. J. Peng, D. Walter, Y. Ren, M. Tebyetekerwa, Y. Wu, T. Duong, Q. Lin, J. Li, T. Lu, M. A. Mahmud, O. L. C. Lem, S. Zhao, W. Liu, Y. Liu, H. Shen, L. Li, F. Kremer, H. T. Nguyen,

View Article Online
DOI: 10.1039/D1EE00062D

D.-Y. Choi, K. J. Weber, K. R. Catchpole and T. P. White, *Science*, 2021, **371**, 390-395.

312. H. P. Kim, A. R. B. M. Yusoff and J. Jang, *Nanoscale Adv.*, 2019, **1**, 76-85.

313. T. Bu, X. Liu, R. Chen, Z. Liu, K. Li, W. Li, Y. Peng, Z. Ku, F. Huang, Y.-B. Cheng and J. Zhong, *J. Mater. Chem. A*, 2018, **6**, 6319-6326.

314. D. J. Fairfield, H. Sai, A. Narayanan, J. V. Passarelli, M. Chen, J. Palasz, L. C. Palmer, M. R. Wasielewski and S. I. Stupp, *J. Mater. Chem. A*, 2019, **7**, 1687-1699.

315. W. Chen, X. Li, Y. Li and Y. Li, *Energy Environ. Sci*., 2020, **13**, 1971-1996.

316. S. Shin, E. J. Yeom, W. S. Yang, S. Hur, M. G. Kim, J. Im, J. Seo, J. H. Noh and S. I. Seok, *Science*, 2017, **356**, 167-171.

317. B. Yang, M. Wang, X. Hu, T. Zhou and Z. Zang, *Nano Energy*, 2019, **57**, 718-727.

318. J. Tian, Q. Xue, X. Tang, Y. Chen, N. Li, Z. Hu, T. Shi, X. Wang, F. Huang, C. J. Brabec, H.-L. Yip and Y. Cao, *Adv. Mater*., 2019, **31**, 1901152.

319. H. Zhang, C. Zhao, D. Li, H. Guo, F. Liao, W. Cao, X. Niu and Y. Zhao, *J. Mater. Chem. A*, 2019, **7**, 2804-2811.

320. G. Wu, J. Zhou, J. Zhang, R. Meng, B. Wang, B. Xue, X. Leng, D. Zhang, X. Zhang, S. Bi, Q. Zhou, Z. Wei, H. Zhou and Y. Zhang, *Nano Energy*, 2019, **58**, 706-714.

321. Y. Yang, S. Feng, M. Li, W. Xu, G. Yin, Z. Wang, B. Sun and X. Gao, *Sci. Rep.*, 2017, **7**, 46724.

322. M. J. Brites, M. A. Barreiros, V. Corregidor, L. C. Alves, J. V. Pinto, M. J. Mendes, E. Fortunato, R. Martins and J. Mascarenhas, *ACS Appl. Energy Mater.*, 2019, **2**, 1844-1853.

323. F. Xie, C.-C. Chen, Y. Wu, X. Li, M. Cai, X. Liu, X. Yang and L. Han, *Energy Environ. Sci.*, 2017, **10**, 1942-1949.

View Article Online
DOI: 10.1039/D1EE00062D

324. T. Seewald, E. R. Schütz, C. Ebenhoch and L. Schmidt-Mende, *J. Phys.: Energy*, 2020, **2**, 021001.

325. L. Zhang, B. Li, J. Yuan, M. Wang, T. Shen, F. Huang, W. Wen, G. Cao and J. Tian, *J. Phys. Chem. Lett*., 2018, **9**, 3646-3653.

326. H. Zai, D. Zhang, L. Liang, C. Zhu, S. Ma, Y. Zhao, Z. Zhao, C. Chen, H. Zhou, Y. Li and Q. Chen, *J. Mater. Chem. A*, 2018, **6**, 23602-23609.

327. Q. Wang, W. Zhang, Z. Zhang, S. Liu, J. Wu, Y. Guan, A. Mei, Y. Rong, Y. Hu and H. Han, *Adv. Energy Mater.*, 2019, **10**, 1903092.

328. A. Y. Y. Alsalloum, B. Turedi, X. Zheng, S. Mitra, A. A. Zhumekenov, K. Lee, P. Maity, I. Gereige, A. Alsaggaf, I. S. Roqan, O. F. Mohammed and O. M. Bakr, *ACS Energy Lett.*, 2020, **5**, 657-662.

329. W. Zhang, Y. Jiang, Y. Ding, M. Zheng, S. Wu, X. Lu, X. Gao, Q. Wang, G. Zhou, J. Liu, M. J. Naughton, K. Kempa and J. Gao, *Opt. Mater. Express*, 2017, **7**, 2150-2160.

330. Y. Li, J. Shi, J. Zheng, J. Bing, J. Yuan, Y. Cho, S. Tang, M. Zhang, Y. Yao, C. F. J. Lau, D. S. Lee, C. Liao, M. A. Green, S. Huang, W. Ma and A. W. Y. Ho-Baillie, *Adv. Sci.*, 2020, **7**, 1903368.

331. H. Tsai, W. Nie, Y.-H. Lin, J. B. Blancon, S. Tretiak, J. Even, G. Gupta, P. M. Ajayan and A. D. Mohite, *Adv. Energy Mater.*, 2017, **7**, 1602159.

332. N. K. Noel, M. Congiu, A. J. Ramadan, S. Fearn, D. P. McMeekin, J. B. Patel, M. B. Johnston, B. Wenger and H. J. Snaith, *Joule*, 2017, **1**, 328-343.

333. J. V. Patil, S. S. Mali, J. S. Shaikh, A. P. Patil, P. S. Patil and C. K. Hong, *Dyes Pigm.*, 2019, **168**, 311-316.

View Article Online
DOI: 10.1039/D1EE00062D

334. S. Zhang, S. Wu, W. Chen, H. Zhu, Z. Xiong, Z. Yang, C. Chen, R. Chen, L. Han and W. Chen, *Mater. Today Energy*, 2018, **8**, 125-133.

335. J. Zhang, L. Zhang, X. Li, X. Zhu, J. Yu and K. Fan, *ACS Sustainable Chem. Eng.*, 2019, **7**, 3487-3495.

336. N. K. Noel, B. Wenger, S. N. Habisreutinger, J. B. Patel, T. Crothers, Z. Wang, R. J. Nicholas, M. B. Johnston, L. M. Herz and H. J. Snaith, *ACS Energy Lett.*, 2018, **3**, 1233-1240.

337. N. Timasi, S. Tafazoli, E. Nouri, M. R. Mohammadi and Y. Li, *Photochem. Photobiol. Sci.* 2019, **18**, 1228-1234.

338. H. Chen, Z. Wei, H. He, X. Zheng, K. S. Wong and S. Yang, *Adv. Energy Mater.*, 2016, **6**, 1502087.

339. Y. Tu, J. Wu, X. He, P. Guo, T. Wu, H. Luo, Q. Liu, K. Wang, J. Lin, M. Huang, Y. Huang, Z. Lan and S. Li, *J. Mater. Chem. A*, 2017, **5**, 4376-4383.

340. S. S. Shin, J.-P. Correa-Baena, R. C. Kurchin, A. Polizzotti, J. J. Yoo, S. Wieghold, M. G. Bawendi and T. Buonassisi, *Chem. Mater.*, 2018, **30**, 336-343.

341. F. Wang, M. Yang, S. Yang, X. Qu, L. Yang, L. Fan, J. Yang and F. Rosei, *Nano Energy*, 2020, **67**, 104224.

342. H. Tan, A. Jain, O. Voznyy, X. Lan, F. P. G. de Arquer, J. Z. Fan, R. Quintero-Bermudez, M. Yuan, B. Zhang, Y. Zhao, F. Fan, P. Li, L. N. Quan, Y. Zhao, Z.-H. Lu, Z. Yang, S. Hoogland and E. H. Sargent. *Science*, 2017, **355**, 722-726.

343. X. Liu, Z. Yu, T. Wang, K. L. Chiu, F. Lin, H. Gong, L. Ding and Y. Cheng. *Advanced Energy Mater.*, 2020, **10**, 2001958.

344. C. Li, R. Ma, X. He, T. Yang, Z. Zhou, S. Yang, Y. Liang, X. W. Sun, J. Wang, Y. Yan and W. C. H. Choy, *Adv. Energy Mater.*, 2020, **10**, 1903013.

View Article Online
DOI: 10.1039/D1EE00062D

345. H. Yan, H. Wang, J. Zhang, J. Chang and C. Zhang, *Coatings*, 2019, **9**, 766.

346. S. Kim, I. Jeong, C. Park, G. Kang, I. K. Han, W. Kim and M. Park, *Sol. Energy Mater. Sol. Cells*, 2019, **203**, 110197.

347. Y. Yun, F. Wang, H. Huang, Y. Fang, S. Liu, W. Huang, Z. Cheng, Y. Liu, Y. Cao, M. Gao, L. Zhu, L. Wang, T. Qin and W. Huang, *Adv. Mater.*, 2020, **32**, 1907123.

348. D. Gedamu, I. M. Asuo, D. Benetti, M. Basti, I. Ka, S. G. Cloutier, F. Rosei and R. Nechache, *Sci. Rep.*, 2018, **8**, 12885.

349. T. Moot, A. R. Marshall, L. M. Wheeler, S. N. Habisreutinger, T. H. Schloemer, C. C. Boyd, D. R. Dikova, G. F. Pach, A. Hazarika, M. D. McGehee, H. J. Snaith and J. M. Luther, *Adv. Energy Mater.*, 2020, **10**, 1903365.

350. Z. Arain, C. Liu, Y. Ren, Y. Yang, M. Mateen, X. Liu, Y. Ding, Z. Ali, X. Liu, S. Dai, T. Hayat and A. Alsaedi, *ACS Appl. Mater. Interfaces*, 2019, **11**, 16704-16712.

351. T. Wu, J. Wu, Y. Tu, X. He, Z. Lan, M. Huang and J Lin, *J. Power Sources*, 2017, **365**, 1-6.

352. Y. Deng, C. H. Van Brackle, X, Dai, J. Zhao, B. Chen and J. Huang, *Sci. Adv.*, 2019, **5**, eaax7537.

353. W. Ke, L. Mao, C. C. Stoumpos, J. Hoffman, I. Spanopoulos, A. D. Mohite and M. G. Kanatzidis, *Adv. Energy Mater.*, 2019, **9**, 1803384.

354. G. Wu, H. Li, J. Cui, Y. Zhang, S. Olthof, S. Chen, Z. Liu, D. Wang and S. (F.) Liu, *Adv. Sci.*, 2020, **7**, 1903250.

355. J. J. Van Franeker, K. H. Hendriks, B. J. Bruijnaers, M. W. G. M. Verhoeven, M. M. Wienk and R. A. J. Janssen, *Adv. Energy Mater.*, 2016, **7**, 1601822.

View Article Online
DOI: 10.1039/D1EE00062D

356. T. Hwang, A. J. Yun, J. Kim, D. Cho, S. Kim, S. Hong and B. Park, *ACS Appl. Mater. Interfaces*, 2019, **11**, 6907-6917.

357. X. Cao, L. Zhi, Y. Jia, Y. Li, X. Cui, K. Zhao, L. Ci, K. Ding and J. Wei, *J. Colloid Interface Sci.*, 2018, **524**, 483-489.

358. Y. Jiang, L. Pan, D. Wei, W. Li, S. Li, S.-E. Yang, Z. Shi, H. Guo, T. Xia, J. Zang and Y. Chen, *Sol. Energy*, 2018, **174**, 218-224.

359. V. L. Pool, B. Dou, D. G. Van Campen, T. R. Klein-Stockert, F.S. Barnes, S. E. Shaheen, M. I. Ahmad, M. F. A. M. van Hest and M. F. Toney, *Nat. Commun.*, 2017, **8**, 14075.

360. K. Ankireddy, A. H. Ghahremani, B. Martin, G. Gupta and T. Druffel, *J. Mater. Chem. A*, 2018, **6**, 9378-9383.

361. A. H. Ghahremani, B. Martin, A. Gupta, J. Bahadur, K. Ankireddy and T. Druffel, *Mater. Des.*, 2020, **185**, 108237.

362. S. Sánchez, M. Vallés-Pelarda, J.-A Alberola-Borràs, R. Vidal, J. J. Jerónimo-Rendón, M. Saliba, P. P. Boix and I. Mora-Seró, *Mater. Today*, 2019, **31**, 39-46.

363. F. Jia, Y. Guo, L. Che, Z. Liu, Z. Zeng and C. Cai, *Mater. Res. Express*, 2018, **5**, 066404.

364. D. Liu, C. Yang, M. Bates and R. R. Lunt, *iScience*, 2018, **6**, 272-279.

365. A. Ng, Z. Ren, H. Hu, P. W. K. Fong, Q. Shen, S. H. Cheung, P. Qin, J.-W. Lee, A. B. Djurišić, S. K. So, G. Li, Y. Yang and C. A. Surya, *Adv. Mater.*, 2018, **30**, 1804402.

366. D. Luo, W. Yang, Z. Wang, A. Sadhanala, Q. Hu, R. Su, R. Shivanna, G. F. Trindade, J. F. Watts, Z. Xu, T. Liu, K. Chen, F. Ye, P. Wu, L. Zhao, J. Wu, Y. Tu, Y. Zhang, X. Yang, W. Zhang, R. F. Friend, Q. Gong, H. J. Snaith and R. Zhu, *Science*, 2018, **360**, 1442-1446.

367. N. J. Jeon, J. H. Noh, Y.C. Kim, W. S. Yang, S. Ryu and S. I. Seok, *Nature Mater.*, 2014**,** **13**, 897-903.

View Article Online
DOI: 10.1039/D1EE00062D

368. L. Meng, J. You and Y. Yang, *Nat. Commun.*, 2018, **9**, 5265.

369. J.-W. Lee and N.-G. Park, *Adv. Energy Mater*., **2019**, *10,* 1903249.

370. N. T. P. Hartono, J. Thapa, A. Tiihonen, F. Oviedo, C. Batali, J. J. Yoo, Z. Liu, R. Li, D. F. Marrón, M. G. Bawendi, T. Buonassisi and S. Sun, *Nat. Commun.*, 2020, **11,** 4172.

371. Y. Yu, X. Tan, S. Ning and Y. Wu, *ACS Energy Lett.,* 2019, **4**, 2, 397–404.

372. J. M. Howard, E. M. Tennyson, B. R. A. Neves and M. S. Leite, *Joule*, **3**, 2019, 325-337.

373. L. Fu, H. Li, L. Wang, R. Yin, B. Li, L. Yin, *Energy Environ. Sci.*, 2020, **13**, 4017-4056.

374. F. Holzhey and M. Saliba, *J. Mater. Chem. A*, 2018,**6**, 21794-21808.

375. M. V. Khenkin, E. K. Katz, A. Abate, G. Bardizza, J. J. Berry, C. Brabec, F. Brunetti, V. Bulović, Q. Burlingame, A. Di Carlo, R. Cheacharoen, Y.-B. Cheng, A. Colsmann, S. Cros, K. Domanski, M. Dusza, C. J. Fell, S. R. Forrest, Y. Galagan, D. Di Girolamo, M. Grätzel, A. Hagfeldt, E. von Hauff, H. Hoppe, J. Kettle, H. Köbler, M. S. Leite, S. (F.) Liu, Y.-L. Loo, J. M. Luther, C.-Q. Ma, M. Madsen, M.;Manceau, M. Matheron, M. McGehee, R. Meitzner, M. K. Nazeeruddin, A. F. Nogueira, C. Odabaşı, A. Osherov, N.-G. Park, M. O. Reese, F. De Rossi, M. Saliba, U. S. Schubert, H. J. Snaith, S. D. Stranks, W. Tress, P. A. Troshin, V. Turkovic, S. Veenstra, I. Visoly-Fisher, A. Walsh, T. Watson, H. Xie, R. Yıldırım, S. M. Zakeeruddin, K. Zhu and M. Lira-Cantu, *Nat. Energy*, 2020, **5**, 35-49.

376. M. O. Reese, S. A. Gevorgyan, M. Jørgensen, E. Bundgaard, S. R. Kurtz, D. S. Ginley, D. C. Olson, M. T. Lloyd, P. Morvillo, E. A. Katz, A. Elschner, *Sol. Energy Mater. Sol. Cells*, 2011, **95**, 1253.

377. X. Yang, X. Yan, W. Wang, X. Zhu, H. Li, W. C. Ma, *Org. Electron.*, 2016, **34**, 79.

378. Y. Liu, C. Xie, W. Tan, X. Liu, Y. Yuan, Q. Xie, Y. Li, Y. Gao, *Org. Electron.*, 2019, **71**, 123.

View Article Online
DOI: 10.1039/D1EE00062D

379. Y. Galagan, F. Di Giacomo, H. Gorter, G. Kirchner, I. de Vries, R. Andriessen, P. Groen, *Adv. Energy Mater.*, 2018, **8**, 1801935.

380. X. Dai, Y. Deng, C. H. Van, S. Chen, P. N. Rudd, X. Xiao, Y. Lin, B. Chen, J. Huang, *Adv. Energy Mater.*, 2020, **10**, 1903108.

381. M.Yang, Z, Li, M. O. Reese, O. G. Reid, D.Hoe Kim, S. Siol, T. R. Klein, Y. Yan, J. J. Berry, M. F. A. M. van Hest and K. Zhu, *Nature Energy*, 2017, **2**, 17038.

382. Y. Deng, X. Zheng, Y. Bai, Q. Wang, J. Zhao and J. Huang. *Nat Energy*, 2018, **3,** 560–566.

383. Z. Liu, L. Qiu, L. K. Ono, S. He, Z. Hu, M. Jiang, G. Tong, Z. Wu, Y. Jiang, D.-Y. Son, Y. Dang, S. Kazaoui and Y. Qi, *Nature Energy*, 2020, **5**, 596–604.

384. N.-G. Park and K. Zhu, *Nature Reviews Materials*, 2020, **5**, 333–350.